Jordan Journal of
PHYSICS
An International Peer-Reviewed Research Journal

Volume 5, No. 1, 2012, 1433 H

Jordan Journal of Physics (*JJP*): An International Peer-Reviewed Research Journal established by the Higher Research Committee, Ministry of Higher Education & Scientific Research, Jordan, and published quarterly by the Deanship of Research & Graduate Studies, Yarmouk University, Irbid, Jordan.

Manuscripts should be submitted to:

Prof. Ibrahim O. Abu Al-Jarayesh
Editor-in-Chief, Jordan Journal of Physics
Deanship of Research and Graduate Studies
Yarmouk University-Irbid-Jordan
Tel. 00 962 2 7211111 Ext. 2075
E-mail: *jjp@yu.edu.jo*
Website: *http://Journals.yu.edu.jo/jjp*

Jordan Journal of
PHYSICS
An International Peer-Reviewed Research Journal

Volume 5, No. 1, 2012, 1433 H

The Hashemite Kingdom of Jordan

Yarmouk University

Jordan Journal of PHYSICS

An International Peer-Reviewed Research Journal

Special Issue

Volume 5, No. 1, 2012, 1433 H

Instructions to Authors

Instructions to authors concerning manuscript organization and format apply to hardcopy submission by mail, and also to electronic online submission via the Journal homepage website (http://jjp.yu.edu.jo).

Manuscript Submission

1- **Hardcopy**: The original and three copies of the manuscript, together with a covering letter from the corresponding author, should be submitted to the Editor-in-Chief:

Professor Ibrahim O. Abu Al-Jarayesh
Editor-in-Chief, Jordan Journal of Physics
Deanship of Scientific Research and Graduate Studies
Yarmouk University, Irbid, Jordan.
Tel: 00962-2-7211111, Ext. 2075
Fax: 00962-2-7211121
E-mail: jjp@yu.edu.jo

2- **Online**: Follow the instructions at the journal homepage website.

Original *Research Articles*, *Communications* and *Technical Notes* are subject to critical review by minimum of two competent referees. Authors are encouraged to suggest names of competent reviewers. *Feature Articles* in active Physics research fields, in which the author's own contribution and its relationship to other work in the field constitute the main body of the article, appear as a result of an invitation from the Editorial Board, and will be so designated. The author of a *Feature Article* will be asked to provide a clear, concise and critical status report of the field as an introduction to the article. *Review Articles* on active and rapidly changing Physics research fields will also be published. Authors of *Review Articles* are encouraged to submit two-page proposals to the Editor-in-Chief for approval. Manuscripts submitted in *Arabic* should be accompanied by an Abstract and Keywords in English.

Organization of the Manuscript

Manuscripts should be typed double spaced on one side of A4 sheets (21.6 x 27.9 cm) with 3.71 cm margins, using Microsoft Word 2000 or a later version thereof. The author should adhere to the following order of presentation: Article Title, Author(s), Full Address and E-mail, Abstract, PACS and Keywords, Main Text, Acknowledgment. Only the first letters of words in the Title, Headings and Subheadings are capitalized. Headings should be in **bold** while subheadings in *italic* fonts.

Title Page: Includes the title of the article, authors' first names, middle initials and surnames and affiliations. The affiliation should comprise the department, institution (university or company), city, zip code and state and should be typed as a footnote to the author's name. The name and complete mailing address, telephone and fax numbers, and e-mail address of the author responsible for correspondence (designated with an asterisk) should also be included for official use. The title should be carefully, concisely and clearly constructed to highlight the emphasis and content of the manuscript, which is very important for information retrieval.

Abstract: A one paragraph abstract not exceeding 200 words is required, which should be arranged to highlight the purpose, methods used, results and major findings**.**

Keywords: A list of 4-6 keywords, which expresses the precise content of the manuscript for indexing purposes, should follow the abstract.

PACS: Authors should supply one or more relevant PACS-2006 classification codes, (available at http://www.aip.org/pacs/pacs06/pacs06-toc.html)

Introduction: Should present the purpose of the submitted work and its relationship to earlier work in the field, but it should not be an extensive review of the literature (e.g., should not exceed 1 ½ typed pages).

Experimental Methods: Should be sufficiently informative to allow competent reproduction of the experimental procedures presented; yet concise enough not to be repetitive of earlier published procedures.

Results: should present the results clearly and concisely.

Discussion: Should be concise and focus on the interpretation of the results.

Conclusion: Should be a brief account of the major findings of the study not exceeding one typed page.

Acknowledgments: Including those for grant and financial support if any, should be typed in one paragraph directly preceding the References.

References: References should be typed double spaced and numbered sequentially in the order in which they are cited in the text. References should be cited in the text by the appropriate Arabic numerals, enclosed in square brackets. Titles of journals are abbreviated according to list of scientific periodicals. The style and punctuation should conform to the following examples:

1. Journal Article:

a) Heisenberg, W., Z. Phys. 49 (1928) 619.
b) Bednorz, J. G. and Müller, K. A., Z. Phys. B64 (1986) 189
c) Bardeen, J., Cooper, L.N. and Schrieffer, J. R., Phys. Rev. 106 (1957) 162.
d) Asad, J. H., Hijjawi, R. S., Sakaji, A. and Khalifeh, J. M., Int. J. Theor. Phys. 44(4) (2005), 3977.

2. Books with Authors, but no Editors:

a) Kittel, C., "Introduction to Solid State Physics", 8th Ed. (John Wiley and Sons, New York, 2005), chapter 16.
b) Chikazumi, S., C. D. Graham, JR, "Physics of Ferromagnetism", 2nd Ed. (Oxford University Press, Oxford, 1997).

3. Books with Authors and Editors:

a) Allen, P. B. "Dynamical Properties of Solids", Ed. (1), G. K. Horton and A. A. Maradudin (North-Holland, Amsterdam, 1980), p137.
b) Chantrell, R. W. and O'Grady, K., "Magnetic Properities of Fine Particles" Eds. J. L. Dormann and D. Fiorani (North-Holland, Amsterdam, 1992), p103.

4. Technical Report:

Purcell, J. "The Superconducting Magnet System for the 12-Foot Bubble Chamber", report ANL/HEP6813, Argonne Natt. Lab., Argonne, III, (1968).

5. Patent:

Bigham, C. B., Schneider, H. R., US patent 3 925 676 (1975).

6. Thesis:

Mahmood, S. H., Ph.D. Thesis, Michigan State University, (1986), USA (Unpublished).

7. Conference or Symposium Proceedings:

Blandin, A. and Lederer, P. Proc. Intern. Conf. on Magnetism, Nottingham (1964), P.71.

8. Internet Source:

Should include authors' names (if any), title, internet website, URL, and date of access.

9. Prepublication online articles (already accepted for publication):

Should include authors' names (if any), title of digital database, database website, URL, and date of access.

For other types of referenced works, provide sufficient information to enable readers to access them.

Tables: Tables should be numbered with Arabic numerals and referred to by number in the Text (e.g., Table 1). Each table should be typed on a separate page with the legend above the table, while explanatory footnotes, which are indicated by superscript lowercase letters, should be typed below the table.

Illustrations: Figures, drawings, diagrams, charts and photographs are to be numbered in a consecutive series of Arabic numerals in the order in which they are cited in the text. Computer-generated illustrations and good-quality digital photographic prints are accepted. They should be black and white originals (not photocopies) provided on separate pages and identified with their corresponding numbers. Actual size graphics should be provided, which need no further manipulation, with lettering (Arial or Helvetica) not smaller than 8 points, lines no thinner than 0.5 point, and each of uniform density. All colors should be removed from graphics except for those graphics to be considered for publication in color. If graphics are to be submitted digitally, they should conform to the following minimum resolution requirements: 1200 dpi for black and white line art, 600 dpi for grayscale art, and 300 dpi for color art. All graphic files must be saved as TIFF images, and all illustrations must be submitted in the actual size at which they should appear in the journal. Note that good quality hardcopy original illustrations are required for both online and mail submissions of manuscripts.

Text Footnotes: The use of text footnotes is to be avoided. When their use is absolutely necessary, they should be typed at the bottom of the page to which they refer, and should be cited in the text by a superscript asterisk or multiples thereof. Place a line above the footnote, so that it is set off from the text.

Supplementary Material: Authors are encouraged to provide all supplementary materials that may facilitate the review process, including any detailed mathematical derivations that may not appear in whole in the manuscript.

Revised Manuscript and Computer Disks

Following the acceptance of a manuscript for publication and the incorporation of all required revisions, authors should submit an original and one more copy of the final disk containing the complete manuscript typed double spaced in Microsoft Word for Windows 2000 or a later version thereof. All graphic files must be saved as PDF, JPG, or TIFF images.

Allen, P.B., "…….", in: Horton, G.K., and Muradudin, A. A., (eds.), "Dynamical…….", (North……..), pp….

Reprints

Twenty (20) reprints free of charge are provided to the corresponding author. For orders of more reprints, a reprint order form and prices will be sent with the article proofs, which should be returned directly to the Editor for processing.

Copyright

Disclaimer

Indexing

JJP is currently applying for indexing and abstracting to all related International Services.

Jordan Journal of
PHYSICS
An International Peer-Reviewed Research Journal

Volume 5, No. 1, 2012, 1433 H

Editorial Preface

This special issue of Jordan Journal of Physics (JJP) presents 7 selected papers of the second International Conference of Materials in Jordan. These papers were subjected to standard refereeing of JJP.

Jordan Journal of
PHYSICS
An International Peer-Reviewed Research Journal

Volume 5, No. 1, 2012, 1433 H

The International Conference on Materials in Jordan Humboldt Kolleg 9-11 April 2011

Conference Preface

The 1st International Conference on Materials in Jordan (ICMJ) was held in Amman between 4-6 March 2009 following the successful "Materials Workshop" organized by the Jordanian Club of Humboldt Fellows (JCHF) at Goethe Institute/Amman on 12.4.2008. The 2nd Materials Int. Workshop (Humboldt Kolleg) took place in Amman between 10-12 April 2010. Like other Kollegs, the 2nd Int Conf. on Materials in Jordan (Humboldt Kolleg) was held between 9-11 April 2011 with the main co-hosting universities being the GJU and PSUT.

This ICMJ was mainly organized by the JCHF in addition to a large body of national organizers involved: Jordan Atomic Energy Commission (JAEC), German-Jordanian University (GJU), Mu'tah University (MU), Yarmouk University (YU), Jordan University of Science and Technology (JUST), Al al-Bayt University (AaBU), University of Jordan (UJ), Hashemite University (HY). This participation reflects the interest and belief for the achievements to be an outcome of these activities. As a product of this conference and workshops several of our Ph.D. students are completing their studies abroad and scientists are enjoying joint research projects with Int. researchers.

The executive committee of the JCHF that organized the Conference consists of:

Prof. Dr Yaseen Al-Soud / Al al-Bayt University; Secretary General

Prof. Dr. Ahmad Al Ajlouni / JUST; Vice President

Prof. Dr. Marwan S. Mousa / Mu'tah University, President of JCHF

The leadership and guidance by HE Prof Dr. Khaled Toukan, Minister of Energy and Mineral Resources and chairman of the conference, valuable assistance by the GJU, scientific guidance by Dr Nelli Wanderka from Berlin, full support by HE the ambassador of Germany in Jordan Dr. Joachim Heidorn and the First Secretary and the Cultural Attachee of the Embassy Mr Carsten Fischer were all valuable for the success of the conference.

Prof. Dr. Wajih M. Owais Minister of Higher Education and Scientific Research (MoHESR) gave great support to the conference. The financial support by King Abdullah II for Development, Jordan Kuwait Bank, Jordan Ahli Bank, Abdul Hameed Shoman Foundation in addition to the crucial financial support from the Alexander von Humboldt Foundation in Germany enabled us to cover most of the financial expenses for the event. The conference co-hosting by PSUT and the support extended by its president were important to achieve goals of the conference.

The conference was patronized and opened by HE Prof. Dr. Wajih M. Owais MoHESR. The sessions were held at PSUT with attendance of 365 people. HE Prof. Dr. Khaled Toukan the chairman of the conference emphasized the importance that the conf. aims to open avenues of cooperation between academic research institutions, industry, scientific societies and governmental agencies.

Following the opening of the conference the Key Note Speaker Dr. Nelli Wanderka gave a scientific talk about the joint scientific work between Germany and Jordan titled “Modification of Mo-Si alloy microstructure by small additions of Zr”. This was followed by 11 sessions of talks and a poster session. The talks concentrated on modern techniques by Americans, Germans and other participating scientists. Geopolymers session was very interesting in addition to presentations on materials like Uranium, Zeolite, Kaoline, Zircon, Oil Shale, Potassium Chloride from the Dead Sea, natural materials in German industry, nanowire arrays, electron sources development, limestone Ash Mortars of castles in Jordan.

A full day of research on Pharmacy and Pharmaceutical materials was held with the Humboldtian Prof. Luay Rashan organizing that highly exciting day with wide participation from scientists coming from several countries like Jordan, Iraq, Czec, Germany, France Egypt, and Morocco.

The Jordanian National TV gave coverage of the opening, talks and Humboldt Kolleg. Most of the Jordanian newspapers and Petra News Agency covered the conference with articles, pictures and interviews.

It was an honor to the kolleg by dedicating the Conference to Dr. Gisella Janetzke, ex-deputy Secretary General of AvH Foundation after dedicated 30 years of service towards world friendship, cooperation and academic exchange. Dr

Janetzke gave a talk about the foundation and held a session with scientists to explain means and ways to apply for the AvH fellowships. A fruitful working meeting was held on April 10th at the Marriot hotel Amman prior to the conference banquet, discussed means of strengthening cooperation. The meeting was attended by Dr. Janteske, Ms. Dine Hayat, Minister Prof. Wajih Owais, Minister Prof. Khaled Toukan, JCHF, DAAD, German Scientists, Germany Embassy, Presidents and Vice Presidents of Jordanian Public Universities. Following the conference, visits were arranged for delegations interested in joint collaborations with various Jordanian universities.

Prof. Dr. Marwan S. Mousa
Director of 2 ICMJ (Humboldt Kolleg)
President of the Jordanian Club of Humboldt Fellows
President of Jordanian Physics Society
Prof. of Materials
Dept. of Physics
Mu'tah University
Al-Karak, Jordan
email: mmousa@mutah.edu.jo, marwansmousa@yahoo.com

Jordan Journal of
PHYSICS
An International Peer-Reviewed Research Journal

Volume 5, No. 1, 2012, 1433 H

The International Conference on Materials in Jordan
9-11 April 2011
Princess Sumaya University for Technology
Amman, Jordan

Conference Organizing Committee:

1- HE Prof. Dr. Khalid Toukan, Minister of Energy and Mineral Resources, Chairman of the Jordanian Atomic Energy Commission (Chairman of the Conference)
2- Prof. Dr. Labib Khadra, President of German Jordanian University GJU (Co-Chairman of the Conference).
3- Prof. Dr. Marwan S. Mousa, President of Jordanian Club of Humboldt Fellows (Director of the Conference)
4- Dr. Nelia Wanderka, Helmholtz-Center Berlin for Materials and Energy

Conference Advisory Committee:

1- Prof. Dr. Sultan Abu Orabi, President of Yarmouk Univ. (YU) (Humboldt Fellow)
2- Prof. Dr. Abdelrahim Hunaiti, President of Mu'tah Univ. (MU) (Humboldt Fellow)
3- Prof. Dr. Nabil Shawagfeh, President of Al al Bayt Univ. (AABU)
4- Prof. Dr. Issa Batarseh, President of Princess Sumaya Univ. for Technology (PSUT)
5- Dr. Khaled Shreideh, Sec. General of Higher Council for Science and Technology (HCST)
6- Prof. Dr. Abdul Rahim Hamdan, Vice President of Hashemite Univ. (HU)
7- Prof. Dr. Ziad Al-Saad, General Director of Jordan Dept. of Antiquaties (Humboldt Fellow)
8- Prof. Dr. Abdelhadi Soudi, President of Magreb Club of Humboldt Fellows, Rabat, Morocco (Humboldt Fellow)
9- Eng. Samir Abdul Rahim, Assistant GM – Plants Operational Manager, Jordan Abyad Fertilizers & Chemicals

Proceedings Guest Editors:

1- Prof. Dr. Marwan S Mousa (Mu'tah University) : marwansmousa@yahoo.com
2- Prof. Dr. Hani Nicola Khouri (Jordan University) : khouryhn@yu.edu.jo
3- Prof. Dr. Abdul Rahim Hamdan (Hashemite University): hamdan@hu.edu

Conference Scientific Committee:

1- Prof. Dr. Marwan S Mousa (Mu'tah University)
2- Prof. Dr. Hani Nicola Khouri (Jordan University)
3- Prof. Dr. Abdul Rahim Hamdan (Hashemite University)
4- Prof. Dr. Nizar Abu Jaber (German-Jordanian University)
5- Prof. Dr. Ibrahim Abu Al-Jarayesh (Yarmouk University)
6- Prof. Dr. Abdul Haleem Wreikat (Jordanian Atomic Energy Commission)
7- Dr. Ned Xoubi (Jordanian Atomic Energy Commission)
8- Prof. Dr. Awni Hallak (Jordanian Atomic Energy Commission)
9- Prof. Dr. Khaled Khleifat (Mu'tah University)
10- Prof. Dr. Ahmad M Al-Ajlouni, Jordan University of Science and Technology
11- Prof. Dr. Yaseen Al-Sou'd (Al al-Bayt University)
12- Prof. Dr. Sami Mahmood Jordan University)
13- Prof. Dr. Eqab Rabei (Al al-Bayt University)
14- Prof. Dr. Sawsan Al-Oran (Jordan University)
15- Prof. Dr. Laila Abu Hassan (Jordan University)
16- Prof. Dr. Mahmoud Alawi (Jordan University)
17- Dr Yaser Yousef (Yarmouk University)
18- Dr Amjad Fahoum (Yarmouk University)
19- Dr. Khaldoun Tarawneh (Princess Sumaya Univ. for Technology)
20- Dr. Hussein Allaboun (Jordanian Atomic Energy Commission)
21- Dr. Laith Darabee (Jordanian Atomic Energy Commission)
22- Prof. Dr. Saed Dabaneh (Al Balqa Applied University and JNRC)
23- Prof. Dr. Tayel El-Hasan (Mu'tah University)
24- Prof. Dr. Mousa Abu Arabai (Jordan University of Science and Technology)
25- Prof. Dr. Mohammad El-Khateeb (Jordan University of Science and Technology)
26- Prof. Dr. Issa Makhlouf (Hashemite University)
27- Prof. Dr. Luay Rashan (Applied Science University)
28- Dr. Mousa Gougazeh, Tafila Technical University)
29- Dr Jamal Alali (Aqaba Petroleum for Oil Shale)
30- Dr Khalid Al-Nawayseh, Arab Potash Co.
31- Eng. Zeid Matouk (Abyad Fertilizers & Chemicals Co.)
32- Prof. Dr. Mufeed Batarseh (Mu'tah University)
33- Prof. Dr. Mahmoud Ajour (Philadelphia University)
34- Dr Lamia El-Khouri (Yarmouk University)
35- Dr. Sherin Sarayreh (Al-Hussein Bin Talal University)
36- Dr. Bothina Hamad (Jordan University)
37- Prof. Dr. Mohamed AlShare (Mu'tah University)
38- Dr. Khaled Nawafleh (Mu'tah University)
39- Dr. Andreas Fischer (Feodor Lynen Research Fellow, Mu'tah University)
40- Mr. Cyrus Salimi Asl (DAAD Coordination Office in Jordan)

Conference Int. Scientific Committee:

1- Nelia Wanderka, Helmholtz-Center Berlin for Materials and Energy
2- Prof. Dr. Thomas Kelly (Cameca, Madison, Wisconsin, USA)
3- Prof. Dr. Simon Ringer (University of Sydney, Australia)
4- Prof. Dr. Gregory Thomson (University of Alabama, USA)
5- Prof. Dr. Jan Wastiels (Vrije Univ. Brussel, Belgium)
6- Prof. Dr. peter langer (University of Rostock, Germany)
7- Prof. Dr. Frederic Danoix (University of Rouen, France)
8- Prof. Dr. Majda Sekkal-Rahal (University Sidi Bel Abbas, Algeria)
9- Prof. Dr. Mohamed Ellouze (Sfax University, Tunis)
10- Prof. Dr. Fawzi Lakrad (University Hassan II Casablanca, Morocco)
11- Prof. Dr. Hadef redjem (University Oum El Bouaghi, Algeria)
12- Prof. Dr. Marian Jaskula (Jagiellonian University, Cracow, Poland)
13- Prof. Dr. Ibrahim Zeid (Monoufia University, Egypt)
14- Prof. Dr. Abdelaziz Khlaifat (Weatherford Oil Tool ME Ltd, Dubai, UAE)

Jordan Journal of
PHYSICS
An International Peer-Reviewed Research Journal

Volume 5, No. 1, 2012, 1433 H

Table of Contents:

Volume 5, Number 1, 2012. pp. 1-7

Jordan Journal of Physics

ARTICLE

Electrochemical Method of Preparing Metallic, Polymeric and Organic-Inorganic Hybrid Nanowires inside Porous Anodic Alumina Templates

K. Hnida[a], **A. Brzózka**[b] and **M. Jaskuła**[c]

[a] *PhD student, Department of Physical Chemistry and Electrochemistry, Jagiellonian University, Ingardena 3, 30-060 Krakow, Poland.*

[b] *PhD student, Faculty of Non-Ferrous Metals, AGH University of Science and Technology, Al. Mickiewicza 30, Krakow 30-059, Poland.*

[c] *Department of Physical Chemistry and Electrochemistry, Jagiellonian University, Ingardena 3, 30-060 Krakow, Poland.*

Received on: 12/6/2011; Accepted on: 8/1/2012

Abstract: The fabrication of free standing silver, polypyrrole (PPy) and hybrid PPy–Ag nanowire arrays was reported. Silver, PPy and PPy–Ag nanowires were produced by electrochemical deposition/polymerization of metal/polymer in anodic aluminum oxide (AAO) templates. The home–made AAO templates were fabricated by two–step anodization of aluminum performed in oxalic acid, sulfuric acid and phosphoric acid at the anodizing potentials of 25 V, 45 V and 195 V, respectively. Silver nanowires with a diameter of ~40, 80 and 300 nm were synthesized by DC electrode position from a commercially available plating bath. PPy nanowires, ~80 nm in diameter, were synthesized by electropolymerization of a monomer in a solution containing pyrrole (Py) and $NaClO_4$ by applying a constant potential. The hybrid PPy–Ag nanowires, ~80 nm in diameter, were synthesized by a simple simultaneous cathodic electropolymerization of pyrrole and metal deposition in a solution containing HNO_3, $NaNO_3$, pyrrole (Py) and $AgNO_3$ by applying a constant potential. After the electrochemical deposition, free standing Ag, PPy and PPy–Ag nanowire arrays were obtained by a subsequent chemical etching of the AAO template in an aqueous NaOH solution. The morphology and structural characterization of fabricated nanowires were performed by FE–SEM and EDAX analyses.

Keywords: AAO templates; Electrodeposition; Electropolymerization; Nanowires.

Introduction

From a material viewpoint, the advancement of science and technology provides the smaller and smaller dimensions with higher precision and enhanced performance. The widespread interest in nanostructured materials is observed mainly due to the fact that their properties, such as: optical, electrical and mechanical, are usually different from those of the bulk materials. Different methodologies for conventional and unconventional fabrication of nanomaterials, such as photolithography, imprinting, molding and methods based on self–organization, have been developed in the past [1]. For nanotechnological applications of materials, a high order of obtained nanostructures and reproducibility of fabrication method are very important. It is not insignificant that the method of fabricating nanomaterials should be of low cost, and easily performed. Most of the methods listed above, are expensive and time–consuming and thus, difficult for adaptation in the industry [2].

Different methods have been used for preparing 1D nanomaterials [2]. Among these

Corresponding Author: M. Jaskuła. **Email**: jaskula@chemia.uj.edu.pl

methods, a template–based synthesis is one of the most simple and low–cost fabricating ways. This method of fabrication of metallic or polymer nanotubes, nanowires and nanofibers is very promising. The template–assisted method, using porous AAO membranes, allows to control precisely the morphology and dimensions of nanowires.

Porous anodic aluminum oxide (AAO) can be fabricated electrochemically through anodic oxidation of aluminum [3]. AAO membranes have a wide range of applications in both the macro– and nano–world. For example, AAO in the macro–world, can be used as a protective and decorative cover, and in the nano–word in molecular filtration, template synthesis, catalysis, sensing, electronics, photonics, energy storage and drug delivery [4]. However, the most important application of AAO, from the perspective of nanotechnology, is its utilization as a matrix to produce a number of nanomaterials: metal nanostructures (nanodots, nanowires, nanorods and nanotubes), oxide nanostructures (nanodots, nanotubes and nanowires), semiconductor nanostructures (nanodots, nanowires and nanopores), polymer nanostructures (organic and inorganic nanowires and nanotubes) [2]. AAO formed by self–organized anodization of aluminum in acidic electrolytes consists of regularly arranged hexagonal cells with nanopores at their centers (Figure 1) [2]. Depending on the used electrolyte and anodizing conditions, this simple electrochemical process results in nanoporous structures with a pore diameter ranging from about 10 to over 300 nm and the interpore distance ranging from about 35 to 500 nm.

In this study, porous anodic alumina membranes with different pore diameters and interpore distances were fabricated by self–organized process occurring during the anodization of aluminum in sulfuric, oxalic and phosphoric acids.

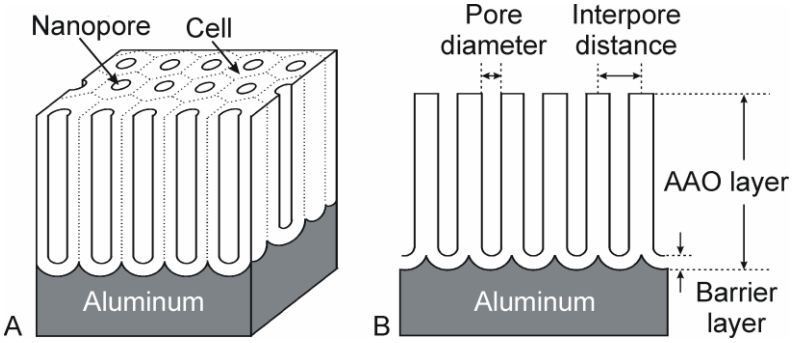

FIG. 1: Idealized structure of anodic porous alumina (A) and cross-sectional view of the anodized layer (B) [2].

It is noteworthy that nanofibers and nanowires have shown higher conductivity and strength over conventional bulk forms. As one of the most promising 1D nanomaterials, silver and polypyrrole nanowires have exhibited many interesting properties that can be exploited in various fields of science and engineering.

Silver nanoparticles are of special interest, because they are potential electrocatalysts for fuel cells [3] and reduction of organic halides [4, 5]. They also can be used in surface plasmon resonance (SPR) [6, 7] and surface–enhanced Raman scattering (SERS) [8, 9], as well as in chemical and biological sensing [10]. Conducting polymers, such as PPy, combining the advantages of organic polymers and the electronic properties of semiconductors, are attractive materials for use in data storage and photovoltaic cells. They also can be used as electrochromic devices, chemical sensors and biosensors, logic or switching elements and supercapacitors [11]. PPy nanostructures could also be utilized as a matrix for the formation of metal–polymer hybrid electrodes [12, 13 and 14], metal oxide–polymer composite nanowires [15, 16] and for embedding or dispersing of metal particles with electrocatalytic properties [17, 18 and 19].

Methodology

In general, the electropolymerization of a monomer and electrode position of metal have been performed at nanochannels of lab–made AAO templates with an average pore diameter of about 40, 80 or 300 nm. The AAO templates were prepared by two–step anodizing as described previously [2], in operating conditions collected in Table 1. Due to a relationship between the pore diameter of AAO and the type of electrolyte used for anodization [2], three

types of templates with different pore diameters were fabricated in sulfuric acid (0.3 M), oxalic acid (0.3 M) and phosphoric acid (2 wt.% in CH_3OH water system 1:4 vol.) solutions at different anodic voltages. A high purity (99.999%) aluminum foil was used as a starting material. After degreasing in ethanol and electropolishing in a mixture of perchloric acid (60 wt.%) and ethanol (1:4 vol.), performed at the constant current density of 0.5 $A \cdot cm^{-2}$ for 1 min at 10 °C, aluminum sheet (25 × 5 × 0.5 mm) was first anodized at a constant voltage. Then, the formed AAO was removed by a wet chemical etching in a mixture of phosphoric acid (6 wt.%) and chromic acid (1.5 wt.%) at 45 °C for about 12 h. After that, the samples were anodized again at the same conditions as during the first anodization. After anodization, the remaining aluminum substrate was chemically removed by immersion in a saturated $HgCl_2$ solution. Subsequently, alumina barrier layer at the pore bottoms was removed in a 5% H_3PO_4 solution at 45 °C. In order to fabricate Ag, PPy and PPy–Ag nanowires, a thin Au conducting layer was sputtered at the bottom side of through–hole AAO membranes.

TABLE 1. Anodizing conditions together with structural features of AAO membranes obtained by two-step anodization in different electrolytes.

Electrolyte	Anodizing voltage [V]	Temperature [^oC]	Duration of the first/second anodization [h]	Pore diameter [nm]	Interpore distante [nm]	Oxide layer thickness [μm]
0.3 M H_2SO_4	25	1	8/10	40	~60	~40
0.3 M $H_2C_2O_4$	45	25	1/4	80	~108	~36
2 % H_3PO_4 in CH_3OH – water system (1:4 vol.)	195	0	8/30	~300	~390	~50

Silver nanowires with different diameters (40, 80 and 300 nm) have been successfully fabricated into the anodic alumina oxide (AAO) membranes by a direct–current electro deposition from a commercially available plating solution with a metal content of 28.7 g/dm^3. Polymer nanowires with a diameter of 80 nm have been synthesized by electropolymerization of a monomer in a solution containing 0.1 M $NaClO_4$ and 0.05 M pyrrole by applying a constant potential of 1.5 V vs. the saturated calomel electrode (SCE). The hybrid PPy–Ag nanowires were synthesized by a simple simultaneous cathodic electropolymerization of pyrrole and metal deposition in a solution containing 0.4 M HNO_3, 0.5 M $NaNO_3$, 0.2 M pyrrole (Py) and 0.1 M $AgNO_3$ by applying a constant potential of –0.625 V vs. the saturated calomel electrode (SCE). With prolonged electrodeposition time, the AAO template changed the color from gold to brown.

To obtain free–standing silver and polypyrrole nanowire arrays, the AAO templates were dissolved by chemical etching in a 1 M NaOH solution. The structural characterization and morphology of silver and polypyrrole nanowires were performed by FE–SEM and EDAX analyses.

Results and discussion

All structural features of porous anodic alumina layers, such as: oxide layer thickness, pore diameter, interpore distance, “barrier layer” thickness as well as the regularity of pore arrangement strongly depend on anodizing conditions, especially chosen electrolyte, anodizing voltage and duration of the process. A self-organized process of aluminum anodization is usually performed in sulfuric, oxalic or phosphoric acid solutions. Figure 2 shows FE–SEM micrographs of AAO templates synthesized in different electrolytes with different pore diameter and interpore distance. Self-organized anodizing of aluminum in acidic electrolytes can result in an almost perfectly ordered nanopore array. The regular nanohole arrangement can be obtained only in the narrow range of anodizing potentials and this potential window varies between 15 and 25 V for sulfuric acid, 30 and 80 V for oxalic acid and 100 and 200 for phosphoric acid, respectively. The structural features of prepared AAO templates are collected in Table 1.

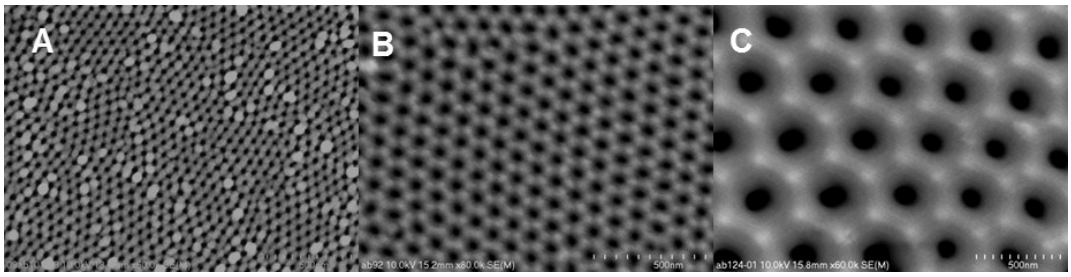

FIG. 2: FE-SEM images of porous alumina templates obtained by anodization of aluminum in sulfuric acid at 25 V (A), oxalic acid at 45 V (B) and phosphoric acid at 195 V (C).

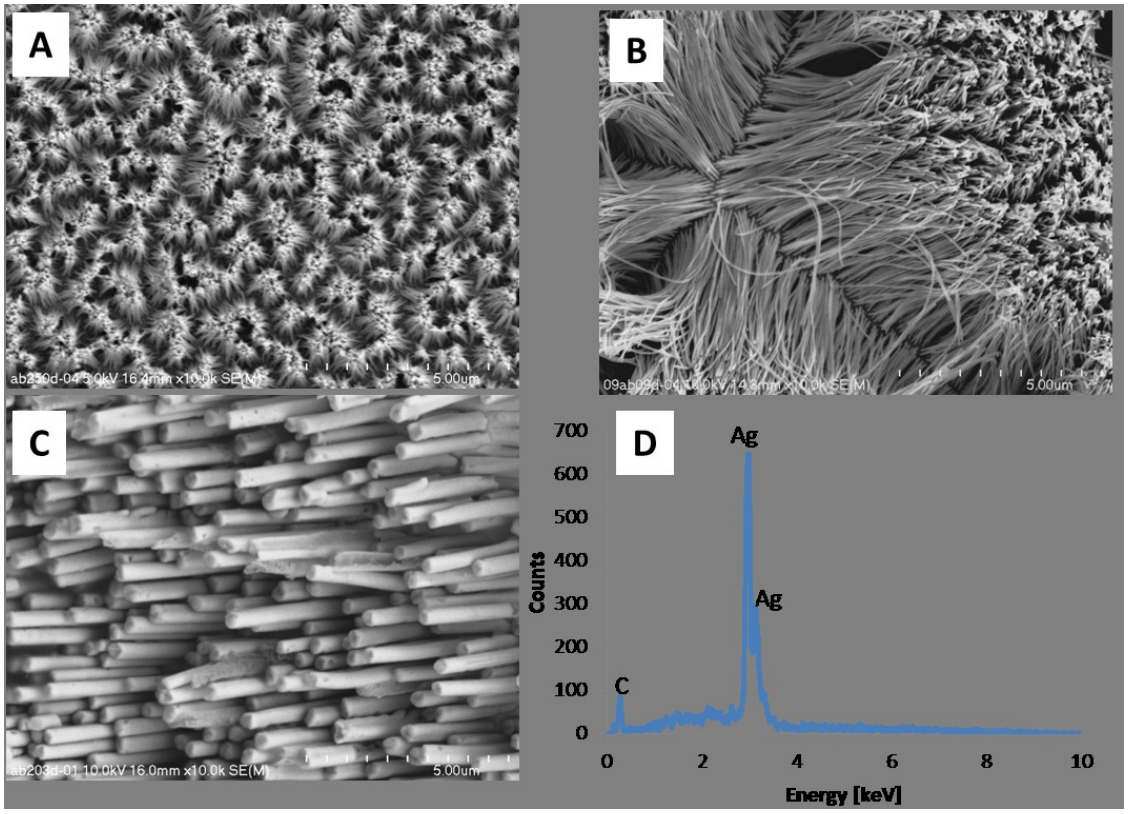

FIG. 3: FE–SEM images of free–standing silver nanowires obtained by DC electrode position inside AAO templates with diameters of about: 40 (A), 80 (B) and 300 nm (C) together with EDAX analysis (D).

FE–SEM images (Figure 3) of the free–standing silver nanowires liberated from the AAO templates show an uninterrupted silver nanowire structure up to approximately 1.0 µm (Figure 3A), 2.8 µm (Figure 3B) and 2.2 µm (Figure 3C) length. The average diameter of nanowires is approximately: 40, 80 and 300 nm for sulfuric, oxalic and phosphoric acid templates, respectively. Consequently, Ag nanowires have an aspect ratio of about 25, 35 and 7, respectively. To confirm the chemical composition of obtained Ag nanowires, the EDAX analysis was performed (Figure 3D). As can be expected, the spectrum showed that Ag nanowires are composed of silver. The spectrum display also carbon peaks as a result of the presence of the thin, conducting C layer attached to the bottom of the sample in order to improve its mechanical stability and electrical conductivity during SEM analysis. The PPy nanowires after dissolution of the AAO template in a NaOH solution are shown in Figure 4(A-C).

The fabricated PPy nanowires have a uniform diameter of about 80 – 85 nm and the length of 17.6 µm that gives an aspect ratio of about 207. In order to confirm the composition of PPy nanowires, IR analysis was performed in the range of 450 – 4000 cm^{-1} (Figure 4C). For the PPy nanowire spectrum, the bands at 2917 cm^{-1} are related to the carbonyl group C=O stretching. The broad band at 3420 cm^{-1} is attributed to the N-H stretching in pyrrole. The presence of the absorption band at 1620 cm^{-1} in the PPy spectrum is assigned to the axial deformation of C = C bond.

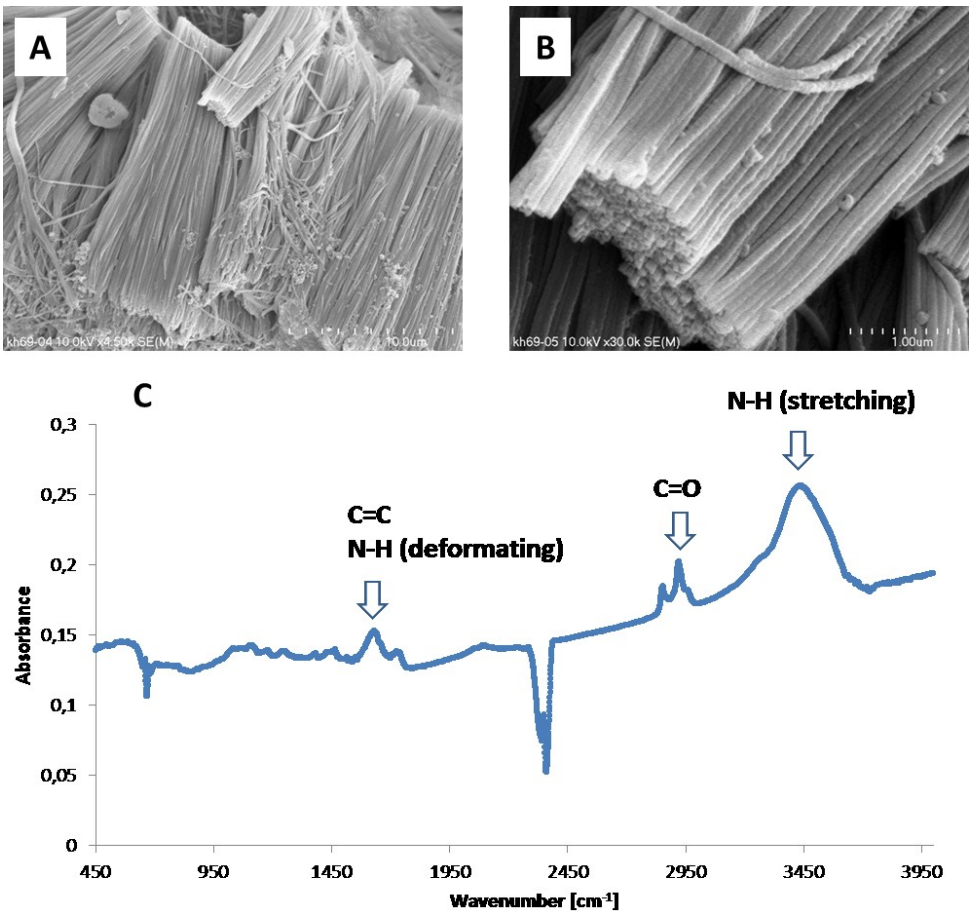

FIG. 4: FE-SEM images of the PPy nanowires after dissolution of the AAO template at different magnifications: 4500 (A) and 30000 (B) and its IR analysis.

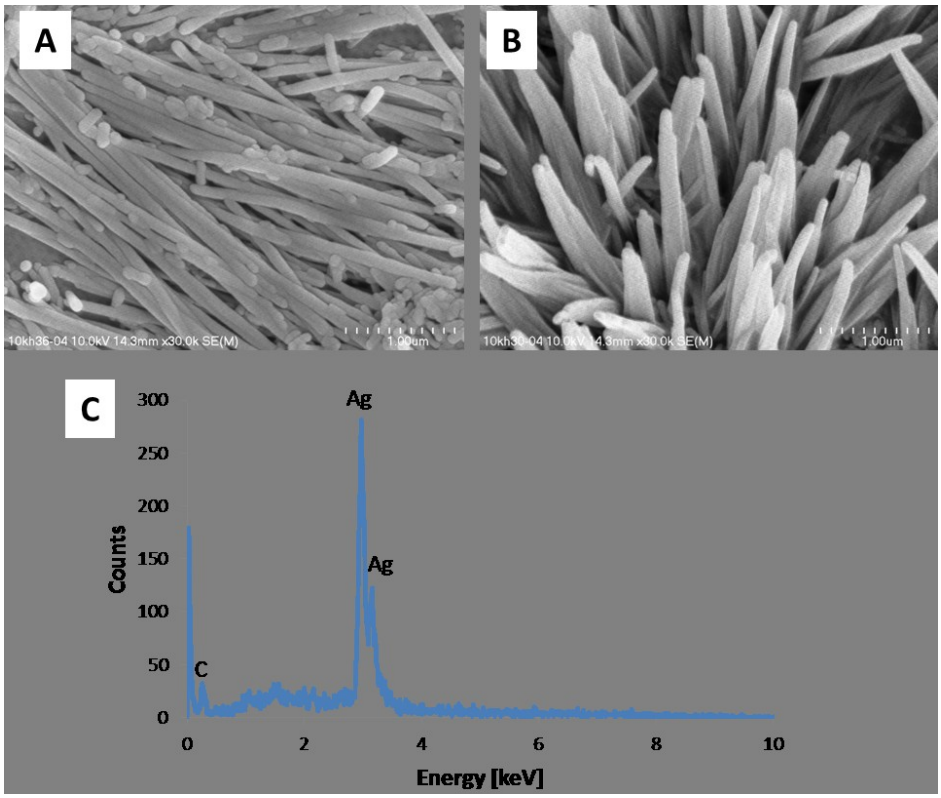

FIG. 5: FE–SEM micrographs of hybrid Ag (A) and PPy–Ag nanowires (B) with EDAX analysis of hybrid nanowires (C).

Fig. 5 shows Ag (A) and hybrid PPy–Ag (B) nanowires synthesized by a simple simultaneous cathodic electropolymerization of pyrrole and metal deposition inside the pores of AAO membrane after dissolution of the AAO template. It is easily to notice that silver nanowires have smoother surface than hybrid PPy–Ag. In the composite material, aggregation of nanowires is stronger and nanowires have more rough side–surfaces as shown in Figure 5B.

After dissolution of metallic part of hybrid PPy–Ag nanowires, performed in HNO_3 at 0 ^oC for 1 h, the obtained PPy nanowires have a diameter of about 65 nm (Fig. 6).

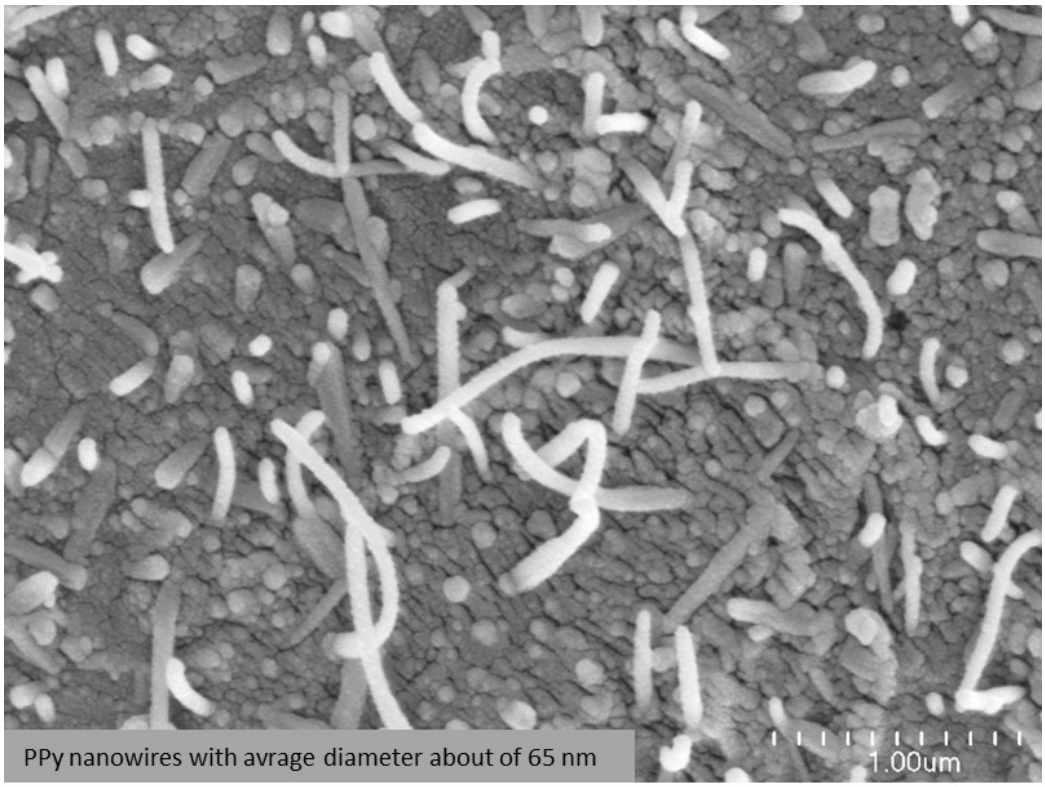

Fig. 6: PPy nanowires obtained after dissolution of silver part of hybrid PPy–Ag nanowires.

Conclusions

The following conclusions can be drawn:

- Through–hole AAO membranes with pore diameters from tens to few hundreds of nanometers can be easily fabricated by a simple two-step anodization of aluminum and subsequent pore–opening procedure.
- Using DC electrode position, anodic electropolymerization and cathodic polymerization accompanied by electrochemical deposition of metals, silver, polypyrrole (PPy) and polypyrrole–silver (PPy–Ag) nanowires were successfully prepared. The diameter of synthesized nanowires corresponds with the diameter of the used AAO templates.

Acknowledgments

This work was supported by the International PhD–studies programme at the Faculty of Chemistry / Jagiellonian University within the Foundation for Polish Science MPD Programme co–financed by the EU European Regional Development Fund. The research was carried out with the equipment purchased thanks to the financial support of the European Regional Development Fund in the framework of the Polish Innovation Economy Operational Program (contract no. POIG.02.01.00-12-023/08). The SEM imaging was performed in the Laboratory of Field Emission Scanning Electron Microscopy and Microanalysis at the Institute of Geological Sciences, Jagiellonian University, Poland.

References

[1] Bhushan, B. "Springer Handbook of Nanotechnology". 2nd Ed., B. Bhushan, (New York, 2007).

[2] Sulka, G.D. "Highly Ordered Anodic Porous Alumina Formation by Self-organized Anodising and Template-assisted Fabrication of Nanostructured Materials", In: Nanostructured Materials in Electrochemistry, edited by Ali Eftekhari, (Wiley–VCH, Weinheim, Germany, 2008), pp. 1–116.

[3] Atwan, M.H., Northwood, D.O.and Gyenge E.L., International Journal of Hydrogen Energy, 32(15) (2007) 3116.

[4] Ardizzone, S., Cappelletti, G., Mussini, P.R., Rondinini, S. and Doubova L.M., Journal of Electroanalytical Chemistry, 532(1) (2002) 285.

[5] Ardizzone, S., Cappelletti, G., Doubova, L.M., Mussini, P.R., Passeri, S.M. and Rondinini S., Electrochimica Acta, 48(25) (2003) 3789.

[6] Guo, X., Zhang, X–N. and Tong L-M., Chinese Science Bull., 55(24) (2010) 2649.

[7] Zong, R–L., Zhou, J., Li, Q., Du, B., Li, B., Fu, M., Qi, X-W. and Li, L–T., Journal of Physical Chemistry B, 108(43) (2004) 16713.

[8] Camargo, P.H.C., Cobley, C.M., Rycenga, M. and Xia Y., Nanotechnology, 20(43) (2009) 434020.

[9] Lee, W., Scholz, R. and Goösele, U., Nano Letters, 8(10) (2008) 3244.

[10] Lin, D–H., Jiang, Y–X., Wang, Y. and Sun, S–G., Journal of Nanomaterials, (2008) 1.

[11] Jang, J., Advances in Polymer Science, 199 (2006) 189.

[12] Prigodin, V.N. and Epstein, A J., Synthetic Materials, 125 (2002) 43.

[13] Gence, L., Faniel, S., Gustin, C., Melinte, S. and Bayot, V., Physical Review B, 76(11) (2007) 115415-01.

[14] Gence, L., Callegari, V., Faniel, S., Vlad, A., Dutu, C., Melinte, S., Demoustier-Champagne, S. and Bayot, V., Physica Status Solid A, 205(6) (2008) 1447.

[15] Wang, W., Li, W., Zhang, R. and Wang, J., Synthetic Metals, 160(21–22) (2010) 2255.

[16] Cui, L., Shen, J., Cheng, F., Tao, Z. and Chen, J., Journal of Power Sources, 196(4) (2011) 2195.

[17] Jing, S., Xing, S., Yu, L. and Zhao C., Materials Letters, 61(23-24) (2007) 4528.

[18] Gniadek, M., Donten, M. and Stojek, Z., Electrochimica Acta, 55(26) (2010) 7737.

[19] Li, B.T., Tang, L.M., Chen, K., Xia, Y. and Jin, X., Chinese Chemical Letters, 22(1) (2011) 123.

Volume 5, Number 1, 2012. pp. 9-14

Jordan Journal of Physics

ARTICLE

Fabrication and Characterization of $Fe_{100-x}Ni_x$ Nanoparticles in the Invar Region

F. H. Rawwagah[a], A-F. Lehlooh[a], S. H. Mahmood[b], S. Mahmoud[c], A-R. El-Ali[a], M. R. Said[a], I. Odeh[a] and **I. Abu-aljarayesh[a]**

[a] *Department of Physics, Yarmouk University, Irbid, Jordan.*
[b] *Department of Physics, The University of Jordan, Amman, Jordan.*
[c] *Department of Physics, Yarmouk University, Irbid, Jordan.*

Received on: 25/7/2011; Accepted on: 8/1/2012

Abstract: In this work, $Fe_{100-x}Ni_x$ nanoparticle systems in the invar region (x = 29, 32 and 37) were prepared by the method of chemical co-precipitation. X-Ray Diffraction (XRD) patterns confirmed the coexistence of both bcc and fcc phases for x = 29 and 32. However, only fcc phase was observed for x = 37. Scanning Electron Microscope (SEM) images indicated that the particle size is ~ 120-500 nm, and is almost independent of x. Mössbauer spectroscopy (MS) on the prepared nanoparticles indicated the development of a paramagnetic phase characteristic of the low-spin (antitaenite) fcc phase, in addition to the magnetic components characteristic of the bcc phase and the high-spin fcc phases. Since it is not possible to resolve the low- spin fcc phase from the high-spin fcc phase in XRD patterns, MS proves to be an effective tool for studying the prepared nanoparticle systems.

Keywords: Chemical co-precipitation; Mössbauer Spectroscopy; Superparamagnetic relaxations; γ' - (antitaenite) phase.

Introduction

Iron nickel alloys in the invar region (65 – 70 at. % Fe) are of special interest to scientists and engineers due to their interesting anomalous thermal and magnetic properties [1-10]. Invar alloys demonstrated several anomalies such as low thermal expansion coefficient at room temperature, instability of ferromagnetism, low Curie temperature and saturation magnetizations, large high field susceptibilities and relatively flat magnetization versus temperature. They also exhibited anomalies in their atomic volume, elastic modulus and heat capacity. The Invar (derived probably from Invariant) effect was discovered by Guillaume in 1897 [1]. The observed anomalously low thermal expansion of these alloys makes them of high dimensional stability under changing temperature. Therefore, they are widely used in precision mechanical systems in many different industries as well as opto-mechanical engineering applications. The coefficient of thermal expansion (CTE) of the Invar 36 alloy at room temperature is approximately 1×10^{-6} K^{-1}. Of course, like most mechanical properties, CTE varies with temperature. However, Invar's CTE is the lowest of any metal, and varies slowly with temperature which makes it suitable for some applications involving significant temperature changes. The low CTE of Invar alloys is very favorable for building different systems that require temperature invariant dimensions such as laser cavities. Longitudinal mode separation of a laser cavity depends very sensitively on the distance between the mirrors of the cavity. This distance must be maintained fixed with a tolerance of up to the wavelength of the laser (~ 0.5 μm for visible light lasers), which demands materials with near zero thermal expansion coefficient at room temperature.

Corresponding Author: S. H. Mahmood **Email**: s.mahmood@ju.edu.jo

In the Fe- rich region, Fe-Ni alloys exist in the α-phase (bcc), whereas in the Ni-rich region they exist in the γ-phase (fcc), and a mixture of the two phases was observed for alloys with intermediate concentrations [2,4,5]. In addition to these two ferromagnetically ordered phases, Mössbauer spectroscopy demonstrated the presence of a paramagnetic phase which was attributed to superparamagnetic relaxations or to a low spin γ' -phase [4, 5, 10-12]. However, the composition of the alloy at which this component appears and its relative abundance in the alloy were not identical in the literature, demonstrating the sensitivity of this component to the preparation method. The magnetic anomalies in Fe-Ni alloys prepared by chemical co-precipitation [4] and by arc melting [5] near the Invar 36 concentration were thus previously investigated by Mössbauer spectroscopy. In this concentration range, magnetic and structural phase transitions were observed, and the low spin component appeared. This component was attributed to superparamagnetic clusters [5] and partly to the low spin γ'-phase (antitaenite) [7].

This work is an effort to understand the magnetic behavior of FeNi alloys in the invar region in light of differences in reported experimental results. The apparent sensitivity of the paramagnetic phase to the method of sample preparation and experimental measurements, and the conflicting explanations concerning the appearance of such phase have motivated us to conduct the present investigation. Thus, in this work, we have prepared Fe-Ni nanoparticles using the chemical co-precipitation method, and investigated their structural and magnetic properties using X-ray diffraction, Electron Microscopy, and Mössbauer spectroscopy.

Experimental

The alloys $Fe_{71}Ni_{29}$, $Fe_{68}Ni_{32}$ and $Fe_{63}Ni_{37}$ were prepared using chemical co-precipitation. Proper amounts of Iron-oxide Fe_2O_3 powder for each sample were dissolved in a proper amount of Nitric acid (HNO_3) with the aid of heat. A proper amount of Nickel-acetate Ni $(CH_3CO_2)_2$ salt was dissolved in distilled water. The solution for each sample was then added at once to a clean beaker together to form a homogeneous mixture of the two solutions. A pH of ~ 7 for the new solution was reached by adding ammonia solution. The metal ions in the mixture were precipitated by adding a proper amount of Sodium oxide Na_2O solution. The precipitate was washed by distilled water several times until pH reading of ~7 was reached. The sample was then dried in air for ~12 hours at 100 ºC. The dry metal carbonate mixture was powdered and placed in a catalytic fixed bed flow reactor through which air was passed at a flow rate of 150 cm^3/min. and a temperature of 300°C for one hour. The produced homogeneous metal oxide mixture was then reduced in a hydrogen gas atmosphere at 300°C for 3 hours, and the resulting alloy powder was cooled to room temperature by an electric fan for about an hour, under helium atmosphere.

Scanning Electron Microscopy (SEM) was used to investigate the morphology of the particles and the particle size distributions for the prepared samples. X-ray diffraction for the powder samples is performed using a standard θ-2θ diffractometer with Co-K_α (λ = 1.79025 Å) radiation. Mössbauer Spectroscopy in transmission geometry was conducted using a standard constant acceleration Mössbauer spectrometer, and the spectra were collected over 512 channels. Isomer shifts were measured relative to the centroid of the α-Fe spectrum at room temperature, and the spectra were fitted using a software based on least squares analysis.

Results and Discussion

Scanning electron microscope (SEM) images for the samples $Fe_{100-x}Ni_x$ (x = 29, 32 and 37) show that the samples consist of uniform distributions of almost spherical particles with diameters ranging from ~ 120 – 500 nm (Fig. 1). The particle size distribution appears to be similar for the samples with x = 29 and 32 and finer for the sample with x = 37.

XRD patterns (Fig. 2) indicate that the sample with x = 29 consists of two phases; the α-bcc FeNi phase and the γ-fcc phase. The γ-phase increases with increasing Ni concentration until x = 37 where the sample becomes a pure fcc phase. The lattice parameter of the bcc phase is (2.85 ± 0.01) Å, while that of the fcc phase is (3.55 ± 0.01) Å. These are only slightly lower and higher than the lattice parameters for bcc Fe (2.87 Å) and fcc Ni (3.52 Å), respectively. The small difference in lattice parameters could be associated with the fact that Ni atom has a smaller size than Fe atom. In the concentration range of this study, the difference in lattice parameters for the three samples is within experimental uncertainty.

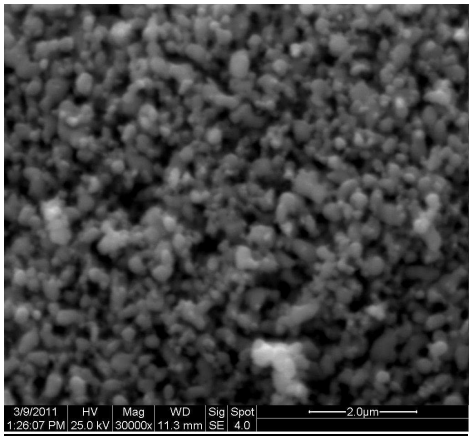

(a)

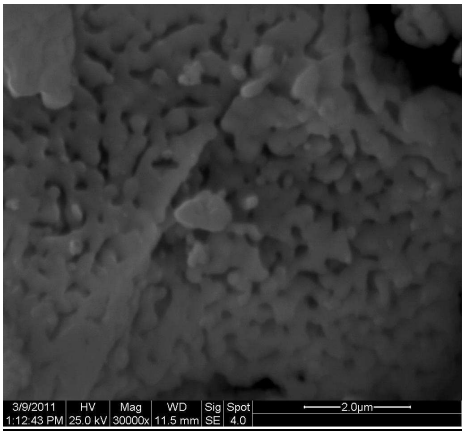

(b)

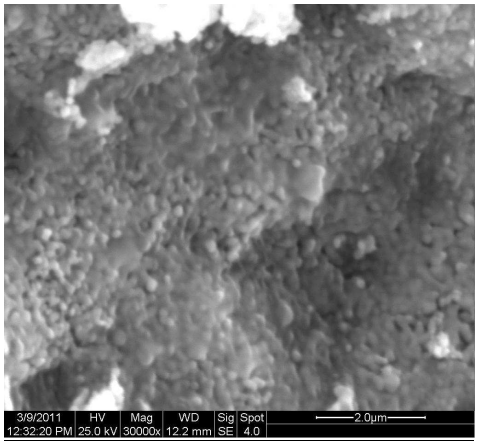

(c)

FIG. 1: SEM images for $Fe_{100-x}Ni_x$ with (a) x = 29, (b) x = 32 and (c) x = 37.

The crystallite size is measured from the broadening of the diffraction lines using the Scherrer equation:

$$D = \frac{K\lambda}{\beta \cos\theta}$$

Here, K is a constant (0.94), λ is the wave length of X-ray (1.79 Å) and β is the width of the diffraction peak at half maximum. The measured crystallite size for the samples is (35 ± 5) nm. The crystallinity of the samples does not appear to depend appreciably on the Ni concentration, which indicates that the entrance of Ni into the bcc Fe, or that of Fe into fcc Ni, does not influence the crystal structure appreciably.

Mössbauer spectra for the different samples are shown in Fig. 3 and the hyperfine parameters obtained from fitting the spectra with the appropriate components are listed in Table 1. The spectrum for the sample with x = 29 was fitted with two magnetic sextet components and a central singlet. The component with B_{hf} = 34.3 T is associated with the bcc FeNi phase, and that with B_{hf} = 29.2 T is associated with the fcc FeNi phase. These values are consistent with those reported earlier for these phases in alloys with x = 30 prepared by arc melting [5] and by chemical co-precipitation [7]. The central singlet with width of 0.82 mm/s and relative intensity of 15% is also consistent with that observed for the sample with x = 30 prepared by arc melting [5]. However, this singlet is appreciably broader than that with width of 0.40 mm/s observed in the sample prepared by co-precipitation. This broadening could be associated with superparamagntic relaxations in small particles. Such a relaxation in superparamagnetic clusters which results in broadening of the singlet was reported earlier [5, 13].

The spectrum for the sample with x = 32 was also fitted with two magnetic sextets corresponding to the bcc and fcc phases, and a broad central singlet that could be associated with superparamagnetic relaxations. The relative intensity corresponding to the fcc phase grows at the expense of the bcc phase (Table 1), which is consistent with the behavior of the relative intensities of the two phases in the XRD patterns (Fig. 2). However, the relative intensity of the singlet drops down to about half its value for the previous sample, which could be associated with a reduction of the proportion of the small superparamagnetic particles in this sample.

TABLE 1. Isomer shift (IS) in mm/s, hyperfine magnetic field (B_{hf}) in Tesla (T), relative intensity (I) and width (W) of the inner lines in mm/s of Mössbauer spectra for the $Fe_{100-x}Ni_x$ system.

	x = 29	*x = 32*	*x* = 37
IS_1	0.01	0.02	0.07
IS_2	0.00	0.02	0.06
IS_3 (Singlet)	-0.05	0.04	-0.03
B_{1hf}	34.3	34.2	30.0
B_{2hf}	29.2	29. 7	16.3
I_1	0.53	0.35	0.57
I_2	0.32	0.58	0.32
I_3 (Singlet)	0.15	0.07	0.13
W_1	0.27	0.25	0.34
W_2	0.71	0.43	0.58
W_3 (Singlet)	0.82	0.74	0.49

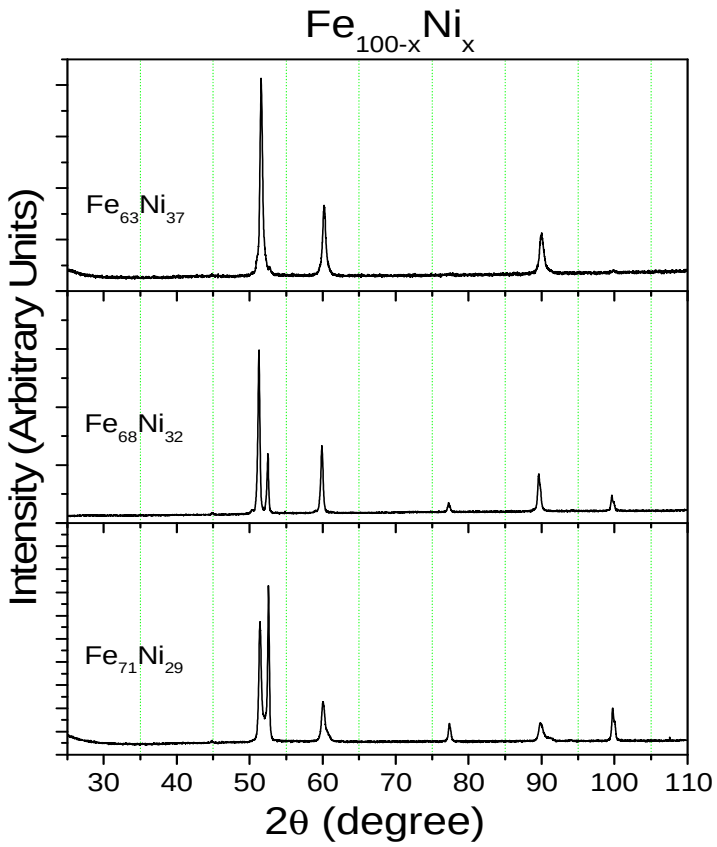

FIG. 2: XRD patterns of $Fe_{100-x}Ni_x$ nanoparticles.

The spectrum of the sample with *x* = 37 was fitted with two sextets with hyperfine fields of 30.0 T and 16.3 T, in addition to a relatively narrow central singlet with width of 0.49 mm/s. The two low field sextets were previously reported for the alloy with *x* = 35 prepared by arc melting [5], and were assigned to fcc phase. This assignment is consistent with the pure phase observed in the XRD pattern for this sample. The peaks of the magnetic component with B_{hf} = 16.3

T coalesce into a broad magnetic sextet. This component was shown in our previous work to be associated with superparamagnetic relaxations. Thus, this component in the present work could be attributed to superparamagnetic relaxations in nanoparticles associated with the finer particle size distribution observed in SEM image for this sample. A similar component was detected in a previous work [6]. The narrow singlet is consistent with that reported earlier for FeNi powders prepared by chemical co-precipitation [7]. The significant narrowing of the singlet component in the spectrum of this sample in comparison with that in the previous samples led us to trust that the origin of this component is different from that in the previous two samples. Thus, this component is assigned to the paramagnetic γ' - low spin (antitaenite) phase which was reported to develop in regions with $x < 30$. This component develops in fcc region of the alloy at composition commensurate with the bcc to fcc complete structural phase transition probably due to competition between the two structural phases, and reveals the coupling between the magnetic and structural properties. These results also reveal the sensitivity of the structural and magnetic phase transitions to composition of the alloy. Thus, an extension of the fcc phase to higher Ni concentrations would shift the stoichiometry at which the γ' - low spin phase develops. The different heat treatment used in this study could be responsible for the difference in the relative proportion of this component and the concentration at which it occurred.

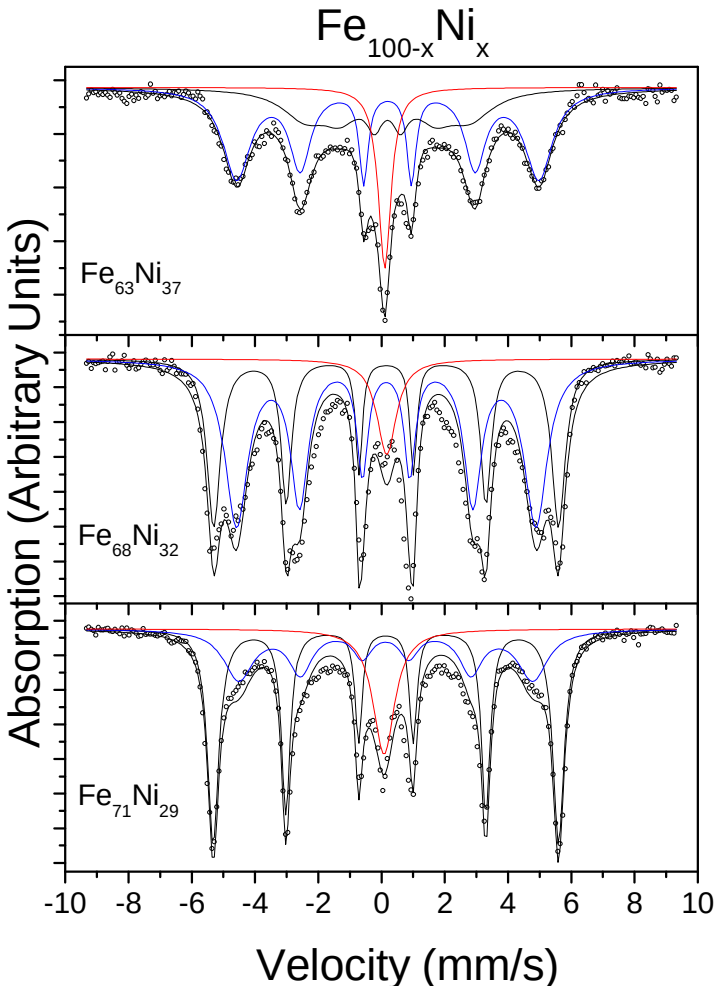

FIG. 3: Mössbauer spectra for the $Fe_{1-x}Ni_x$ system (x = 0.29, 0.32 and 0.37).

Conclusions

The method of chemical co-precipitation proved to be suitable for the preparation of invar FeNi nanoparticles with approximately uniform particle size distribution. The prepared nanoparticle systems demonstrated anomalous structural and magnetic phase transitions in a narrow range of elemental concentrations around the invar stoichiometry. The prepared FeNi nanoparticles by chemical co-precipitation demonstrated different magnetic properties and phase transitions than the bulk system prepared by arc melting [5]. The antitaenite phase developed in the concentration region around the invar stoichiometry (36 at.% Ni), and superparamagnetic relaxations associated with the nanoparticles were observed up to that concentration, while such relaxations were not observed in alloys with $x > 30$ prepared by arc melting as demonstrated by our previous work [5]. The variations of the magnetic phases and their relative proportions at different values of x could indicate the sensitivity of these phases to the preparation procedure and the particle size distribution.

Acknowledgement

This work is supported by a generous grant from the Scientific Research Support Fund (SRSF), Jordan.

References

[1] Guillaume, Ch.E., C. R. Acad. Sci. 125 (1897) 235.

[2] Valderruten, J.F., Pérez Alcázar, G.A. and Grenèche, J.M., J. Phys.: Condens. Matter, 20 (2008) 485204.

[3] Nakamura, Y., IEEE Trans. Magn. 12 (1976) 278.

[4] Mahmood, S.H., Rawwagah, F.H., Lehlooh, A-F. and Mahmoud, S., Abhath Al-Yarmouk: Pure Sci. & Eng. 4(1-B) (1995) 61.

[5] Lehlooh, A-F. and Mahmood, S.H., Hyperfine Iteractions, 139/140 (2002) 387.

[6] Shiga, M. and Nakamura, Y., J. Magn. Magn. Mater. 40 (1984) 319.

[7] Lehlooh, A-F., Abu-allaban, M., Williams, J.M. and Mahmood S.H., In: M.A. Khan, A. Ul Haq, Kh. Hussain and A.Q. Khan (eds), Proc. of the 5th Intern. Conf. on Adv. Mater., Islamabad, A.Q. Khan Res. Lab. Kahuta, (1997) 313.

[8] Rancourt, D.G., Smit, H.H.A. and Thiel, R.C., J. Magn. Magn. Mater. 66 (1987) 121.

[9] Rancourt, D.G., Hargraves, D., Lamarche, G. and Dunlap, R.A., J. Magn. Magn. Mater. 87 (1990) 71.

[10] Weiss, R.J., Proc. Phys. Soc. London, 82 (1963) 281.

[11] Rancourt, D.G. and Scorzelli, R.B., J. Magn. Magn. Mater. 150 (1995) 30.

[12] Rancourt, D.G. and Scorzelli, R.B., J. Magn. Magn. Mater. 174 (1997) 324.

[13] Ok, H.N. and Hans, M.S., J. Appl. Phys. 44 (1973) 1932.

Volume 5, Number 1, 2012. pp. 15-20

Jordan Journal of Physics

ARTICLE

Effect of the Addition of Microsilica on the Durability of Mortars Exposed To the Sodium Sulfate Attack

C. Nasser and **M. Meriam**

A/MIRA University, Béjaïa, Algeria.

Received on: 1/7/2011; Accepted on: 8/1/2012

Abstract: This article presents a detailed experimental study on the sulfate attack of mortars of self compacting concrete, and the effectiveness of employs microsilica and limestone fillers in the minimization of the damage resulting from such an attack. The test solution used to supply the sulfate ions and the cations was the sodium sulfate solution 4.5%. The solution saturated with lime was employed as the reference solution. The main variables investigated in the study were the type of cement and mineral addition. The expansion measured on prisms of mortar of (40x40x160) millimeters was employed to estimate their durability after exposure to the sodium sulfate solution attack during 91 days. Specimens of mortars were visually examined to assess the extent of deterioration due to the sulfate attack. The x-ray diffraction was used to evaluate the microstructural nature of the sulfate attack. The test results proved that the use of microsilica had a beneficial effect on the expansion due to the sodium sulfate attack. While mortars with limestone filler have undergoes degradation even with the use of cement resistant to sulfates.

Keywords: Microsilica; Limestone filler; Sodium sulfate attack; Mortars, Expansion.

Introduction

It has been recognized for a long time that the presence of sulfate ion in soils can cause severe damage to concrete structures. Until now, however, the exact definition of the mechanism of attack seems very difficult because of the complexity of its behavior. Indeed, many factors such as cement type, cation sulfate type, sulfate concentration and exposure period can affect the sulfate resistance [1, 2]. This attack was often been discussed in terms of chemical reaction between the hydrates in cement paste (C_3A and $Ca(OH)_2$) and the dissolved compounds, such as sodium sulfate in the attacking solution and by the reaction of SO_4^{2-} ions to form expansible products (ettringite and gypsum).

Several ideas were suggested to increase the resistance of concrete against the sulfate attack by decreasing porosity (contained high amount of cement or low water-cement ratio) or by improving resistance (cement resistant to sulfate or addition of pozzolanas).

Researchers have reported on the sulfate resistance imparted by microsilica, which is generally incorporated in concrete to improve its technological proprieties and its durability. This excellent resistance is related to the filling action of microsilica because of its fine particles size, and pore refinement process occurring due to the conversion of portlandite into secondary C-S-H gel, through strong pozzolanic reaction [1, 2].

The aim of this work is to develop a comparative evolution of the sodium sulfate 4.5% resistance and durability of microsilica mortar and limestone fillers mortar, with two different cements. An experimental device was thus developed to obtain conclusive results about the effect of use of mineral additions of different reactivity.

Corresponding Author: C. Nasser **Email**: nasser_chelouah@yahoo.fr

Experimental

Materials

In the tests reported in this paper, studies of expansion of mortars samples (4x4x16 (cm)) were carried out. Two cements were used, an artificial Portland cement CPJ CEM II/A 42,5 produced by Ain El Kebira and cement resistant to sulfates CPA CEM I/42,5 produced by Lafarge. The chemical compositions of cements used in this investigation are shown in Table 1.

Two mineral additions were employed, a microsilica with a density of 2.15 g/cm^3 and a limestone filler of density of 2.62 g/cm^3. Chemical compositions of these additions are illustrated in Table 2.

TABLE 1. Chemical and mineralogical composition of cements

	CEM I 42,5	CEM II/A 42,5
MgO (%)	1.7	0.17
SO_3 (%)	1.9	1.00
Loss on ignition (%)	1.5	0.24
Insoluble residue (%)	0.7	2.64
C_3S (%)	57.00	61.34
C_2S (%)	19.00	17.00
C_3A (%)	3.00	5.59
C_4AF (%)	14.00	11.93

TABLE 2. Chemical composition of additions

	Limestone filler	Microsilica
SiO_2 (%)	42.00	92.1
Al_2O_3 (%)	0.0	0.25
Fe_2O_3 (%)	0.0	0.79
CaO (%)	54.84	-
MgO (%)	0.1	-
SO_3 (%)	0.6	0.36
Na_2O (%)	0.02	0.17
K_2O (%)	0.1	0.96

The water/cement ratio of all the mixtures of mortar examined in this study was 0.5 and the water /cementitious materials ratio was 0.45. In order to obtain adequate workability for a mortar of self-compacting concrete, the use of a superplasticizer was indispensable.

MEDAFLUID SFR 122 chemical admixture was incorporated in the mortar mixture with a proportion. The superplasticizer was added to the mixing at a level of 1.5% by mass of total cement. River bed sand of density 2.5 g/cm^3, with a maximum size of 3 mm, was used as the fine aggregate in all mortar mixtures.

Exposure of mortar samples

The mortars were cast in prisms of (4x4x16 cm)). the mortar samples were cured in a saturated $Ca(OH)_2$ solution during 12 days. At the end of this period, some samples were remained in the preceding solution, employed as reference solution for control samples. Some samples were moved to sodium sulfate solution (Na_2SO_4) of 4.5 % concentration and kept continuously immersed for predetermined periods.

The sodium sulfate solution used for the immersion tests is renewed every 4 weeks to reduce the increase in pH due to the leaching of OH^- ions from the mortar specimens and cement paste (to avoid reaching the pH of saturated Ca $(OH)_2$ solution and to compensate for the loss of the concentration of the sulfate solution due to the process of degradation).

TABLE 3. Composition of mortars specimens

	MSCII (Kg/m^3)	MFCII (Kg/m^3)	MFCI (Kg/m^3)
CEM II	625	625	-
CEM I	-	-	625
Sand 0/3	1073	1073	1073
Limestone filler	-	69.5	69.5
Microsilica	69.5	-	-
Water	312.5	312.5	312.5
Superplasticizer	9.39	9.39	9.39

The deterioration of the mortar samples was studied by evaluating their expansions for predetermines periods (14, 21, 28, 56 and 90 days). At each age of test, three specimens of each type of mortar were placed on the comparator and their expansions were determined, and then their values were brought to an average. The morphological changes of the cement hydrates, due to the exposure to the sodium sulfate solution, were studied using the x-ray diffraction, which provides semi-quantitative information on the elementary composition of the mortar.

Results and discussions

Visual examination

A thorough visual examination was carried out every month on the mortars cured without

interruption in the sodium sulfate solution and saturated $Ca(OH)_2$ solution to evaluate the visible signs of degradation (material damages) and spalling on surfaces of mortar specimens.

No surface sign deterioration was detected on the mortar samples after 90 days of immersion in the test solutions. No sign of spalling was observed and no layer of white material was found deposited on the faces of the mortars, as shown in figs. 1 and 2; that confirms the results obtained by Dehwah (2007) [3]. This result is in agreement with that found by Wee et. *al* (2000), which concluded that a replacement of cement by 5 to 10% of microsilica played a key role in resisting sodium sulfate attack, indicating no signs of spalling after about 1 year of exposure to 5% Na_2SO_4 [4].

Fig. 1. Mortars preserved in the 4.5% sodium sulfate solution during 90 days.

Fig. 2. Mortars preserved in the saturated lime solution during 90 days

Day and Ward (1988) observed expansions of 1% and more, accompanied by the significant reductions of the mechanical properties of the samples without any surface sign degradation [5]. According to Hill *et. al* (2003), mortars preserved in the saturated $Ca(OH)_2$ solution (control solution) were not faded and the visual examination did not show any sign of degradation, which is in agreement with the results of our study [6].

Figs 1 and 2 show the results of the visual examination of mortar specimens subjected to sulfate attack after 90 days of immersion in the test solutions.

Morphological changes

The XRD patterns, shown in Figures 3, 4 and 5, were obtained for samples scraped from the surface of the mortar specimens conserved in the test solutions. The diffractogram, shown in figure 3, indicate a veritable difference between the two samples from the two solutions. Especially in MSC II (Na_2SO_4), an abundant presence of ettringite was detected. Indeed, three peaks were detected at 35.9°, 42.4° and 47,63° 2θ for ettringite, in addition to portlandite with weak peaks intensities and gypsum at 29.4° and 35.9° 2θ. On the other hand, as shown in figure 4, signs of degradation of mortars exposed to the sodium sulfate solution (graph MFCII(Na_2SO_4)) were observed, and this according to the concomitant presence of ettringite, thaumasite, portlandite and gypsum. Indeed, gypsum peaks were detected at 29.3° and 35.9° 2θ. A thaumasite peak at 50.6° 2θ was observed in figure 3. Ettringite and portlandite were present as several weak and average intensity peaks. Figure 5 shows resemblances of diffractograms MFCI(sulfate) and MFCI(lime) on the level of the portlandite peaks intensities and angles of their detections. This element showed important intensities at 18.06°, 34.09° and 50.7° 2θ. In addition to the portlandite, diffractogram $MFCI_{(Na2SO4)}$ shows a concomitant presence of ettringite at 32.1° 2θ, gypsum and thaumasite. Indeed, three gypsum peaks were detected at 2θ of 29.45°, 35.9° and 45.8°. Two peaks of thaumasite, one at 27.9° 2θ and another at 47.6° 2θ, were noted. The decrease in CSH during the reaction with the gypsum and limestone promotes the appearance of thaumasite. The XRD Data shows that the peaks of CSH are very low in sulfate solutions. In other XRD Data is not the case.

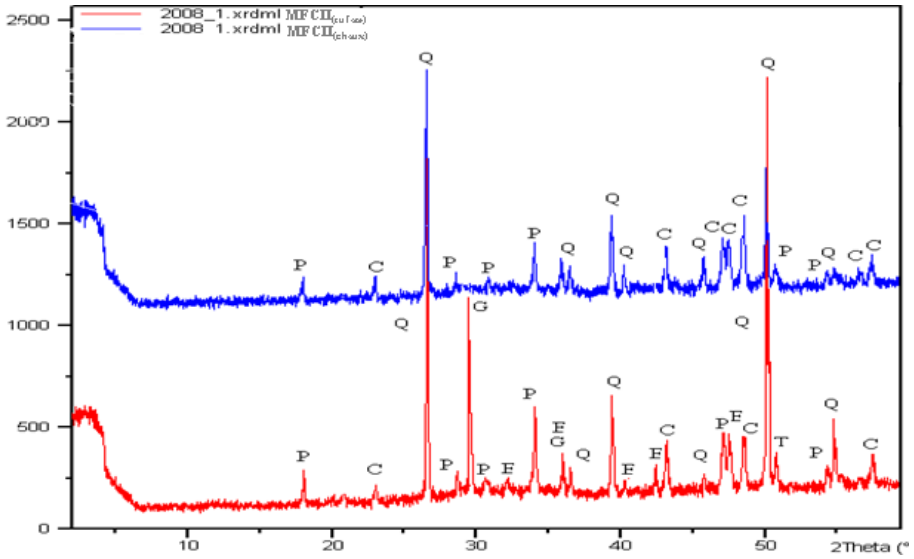

Fig. 3. XRD of mortars MSCII preserved in the solutions Na2SO4 and Ca(OH)2 during 90 days. (P = portlandite, C = calcite, Q = quartz, E = ettringite, T = thaumasite, G = gypsum).

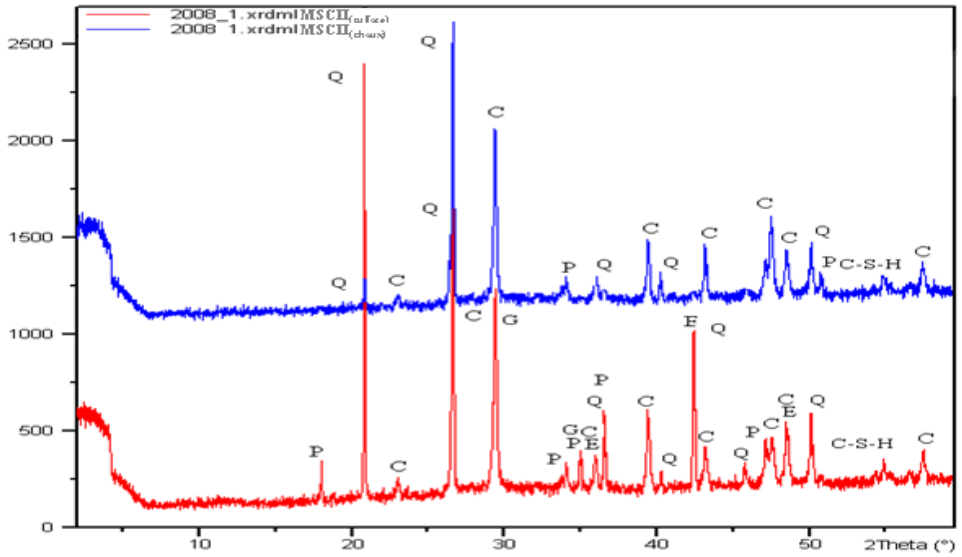

Fig. 4. XRD of mortars MFCII preserved in the solutions Na2SO4 and Ca(OH)2 during 90 J. (P = portlandite, C = calcite, Q = quartz, E = ettringite, T = thaumasite, G = gypsum, C-S-H = calcium silicate hydrated).

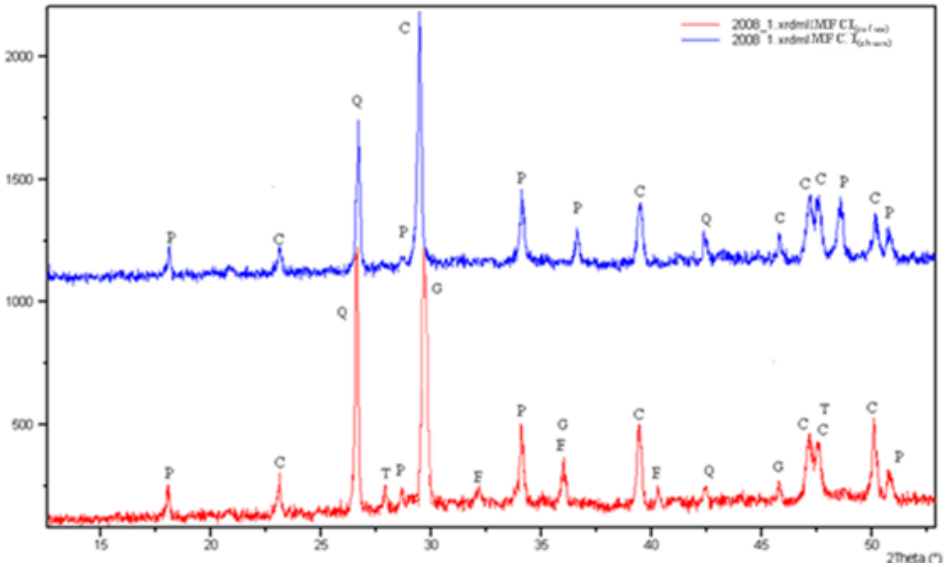

Figure 5: XRD of mortars MFCI preserved in solutions of Na2SO4 and Ca(OH)2 during 90 J (P= portlandite, C=calcite, Q= quartz, E=ettringite, T=thaumasite, G=gypsum).

Expansion

Fig. 6 shows the test results of expansion of the mortar specimens conserved in the sodium sulfate solution. The expansion of mortars MFCII (mortars with limestone filler and cement CEMII) is much more important. It is approximately 940 µm/m at 90 days, compared to mortars MSCII (mortars with microsilica) and MFCI (mortars with limestone filler and cement CEMI) which have expansions of 788 and 511 µm/m at 90 days respectively. According to these curves, we see well that mortar MFCI is most resistant to sodium sulfate.

This is due to the small quantity of the phase of calcium aluminate hydrates (C_3A) with the predominance of the clinker (the only component of this cement) which generates more calcium silicate hydrates. This result forms a compact concrete with a high resistance and durability. Mortar MSCII seems to be of important resistance to sodium sulfate, which is ensured by the fine particle size of microsilica which makes the unit very compact and impermeable to the aggressive solutions.

The prolonged hydration of the free lime which is in excess in mortars MFCII(sulfate) and MFCI(sulfate) (mortar with limestone filler) formed the portlandite which caused constraints by its crystalline growth, thereafter, an increase in volume. The low content of portlandite in MSCII(sulfate)

The introduction of microsilca in mortars can block the pores [7].

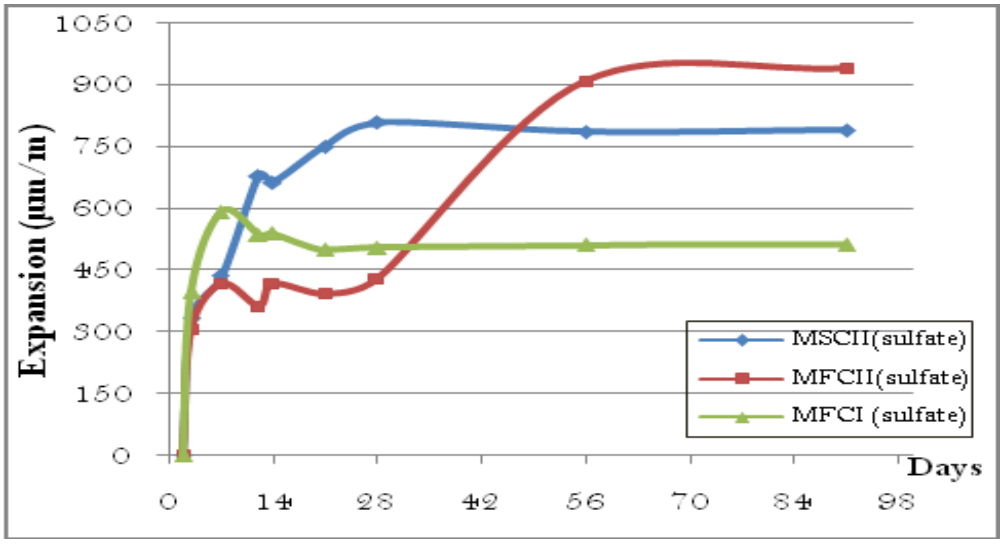

Fig. 6: Expansion of the mortars in the sodium sulfate solution.

According to Lachaud (1979), the portlandite is hydrated in MSCII(sulfate) and forms ettringite which does not cause an important expansion because of its weak specific surface and its weak adsorption capacity with respect to water [8].

Based on the small quantity of the portlandite (which is consumed by microsilica to form the C-S-H) in MSCII(sulfate), the ettringite formed is not expansible in spite of its high rate, this result agrees well with the results of Mehta (1973 a, b) which was observed, when the portlandite is in small quantity, the ettringite formed as coarse crystals of about 60 µm check labeling inside the figures with caption that have a weak specific surface and thus a weak adsorption and expansion capacity [9, 10].

Tian and Cohen (2000) showed in their study, that the formation of the gypsum by the external sulfate attack can cause a significant expansion even when the formation of the ettringite is excluded [11].

Even the mortar of cement CEMI (MFCI(sulfate)), which is supposed to be resistant to sulfates, marked a light swelling in the sodium sulfate solution. This expansion is appreciably slower and less severe than in MFCII(sulfate) mortar (cement CEMII). According to Eglinton (1998) and Lota (1995), the principal reason of the mortar resistance with respect to sulfates is due to the low quantity of calcium aluminate hydrates (C_3A) [12, 13].

Conclusions

This manuscript presented a detailed study of the process of degradation of the prisms of mortars in the environment of sodium sulfate, and evaluated the potential consequences of the use of mineral additions of different reactivity's, on the durability of the three compositions of mortar of self- compacting concrete.

The use of microsilica has a beneficial effect on the reduction of the expansion of the mortars in the aggressive solution, because of its strong pozzolanic reaction and the consumption of the calcium hydroxide.

However, the addition of limestone filler did not prevent the expansion, and the formation of thaumasite. Even the use of cement resistant to sulfates (CPA-CEM I / 42.5) did not eliminate the expansion; consequently, the addition of limestone filler is to be avoided in the sodium sulfate environments.

References

[1] Lee, S.T., Moon, H.Y. and Swamy, R.N., Cement and Concrete Composites, 27 (2005) 65.

[2] Zelié, J., Radovanovi, I. and Jozié, D., MTAEC9, 41(2) (2007) 91.

[3] Dehwah, H.A.F., Construction and Building Materials, 21 (2007) 29.

[4] Wee, T.H., Suryavanshi, A.K., Wong, S.F. and Anisur Rahman. K.M., Cement and Concrete Composites, 27 (2000) 65.

[5] Day, R.L. and Ward, M.A., MRS Symposia Proceedings, 113 (1988) 153. In Skalny. J., Marchand. J., Odler. I., 2002 – "Sulfate attack on concrete". (Spon Press Edition. Taylor and Francis Group. London and New York), 217p.

[6] Hill, J., Byars, E.A., Sharp, J.H., Lynsdale, C.J., Cripps, J.C. and Zhou, Q., Cement and Concrete Composites 25 (2003) 997.

[7] Hatimi, I.E., "Contribution à l'étude physico-chimiques de la consolidation des poussières de four de cimenterie par des cendres volantes", (Mémoire de maitrise en sciences appliquées. Université Sherbrooke (Québec). Canada, 1999). 198p.

[8] Lachaud, R., Annales de l'institut technique du bâtiment et des travaux publics, Paris, 3(70) (1979) 1.

[9] Mehta, P.K.. Cement and Concrete Research, 3 (1973a) 1. In Skalny J., Marchand J., Odler I., "Sulfate attack on concrete". Ed. (Spon Press, Taylor and Francis Group, London and New York, 2002) 217p.

[10] Mehta, P.K., Journal of the American Ceramic Society, 56 (1973b) 315. In Skalny J., Marchand J., Odler I., "Sulfate attack on concrete". (Edition Spon Press, Taylor and Francis Group, London and New York, 2002) 217p.

[11] Eglinton, M., "Resistance of Concrete to Destructive Agents". in P.C. Hawlett (ed.), (Lea's Chemistry of Cement and Concrete, Arnold, London, 1998) 300. In Skalny. J., Marchand. J., Odler. I., Sulfate attack on concrete. (Spon Press Edition, Taylor and Francis Group, London and New York, 2002) 217p.

[12] Lota, L.S., Pratt, P.L. and Bensted, J., A discussion of the paper: Cement and Concrete Research, 25 (1995) 1811. In Skalny. J., Marchand. J., Odler. I., Sulfate attack on concrete, (Spon Press Ed., Taylor and Francis Group, London and New York, 2002), 230p.

Volume 5, Number 1, 2012. pp. 21-26

Jordan Journal of Physics

ARTICLE

Metallic and Composite Micropoint Cathodes: Aging Effect and Electronic and Spatial Characteristics

M. S. Mousa[a], **A. Fischer**[a,b] and **K. O. Mussa**[a]

[a] *Department of Physics, Mu'tah University, Al-Karak, Jordan.*
[b] *Institut für Physik, Technische Universität Chemnitz, Chemnitz, Germany.*

Received on: 30/6/2011; Accepted on: 8/1/2012

Abstract: Composite micro-emitters consisting of a tungsten core coated with different dielectric materials were prepared. Various properties of these emitters were measured, including the current-voltage (IV) characteristics and spatial current distributions. We compared coated and uncoated tips and determined differences between both types. It could be proven that coated emitters are superior to uncoated ones in terms of the current stability and the emission current obtained for the same applied voltages. After these samples have been stored under atmospheric conditions for a period of 10 to 20 years from the first time being characterized, they were tested again. The IV characteristics and spatial current distributions in addition to stability measurements were recorded. Various similarities as well as some differences compared to the initial characterization have been found. It is interesting to note that after one and a half decades these composite emitters are still functioning effectively without being subjected to field desorption processes. The dielectric layers built on the tungsten cores were still in shape and stable. Some theoretical analysis of the tip properties and their change during storage time is included. Particular attention is paid to the deviations from the ideal Fowler-Nordheim (FN) behavior as well as the related slope and intercept correction factors.

Keywords: Field electron emission; Coated tips; Aging effects.

Introduction

As an electron source, the field emitter is particularly attractive due to its favorable emission properties and simple operating principle. In the past decades, there has been sustained interest in field emitters as high brightness electron sources for various technological devices. The most widely used material for such emitters is tungsten [1,2].

Metallic micropoint emitters have faced extra interest by the emergence of microfabrication technology, especially in the form of planar field emitter arrays (e.g. Refs. [3-7]) which were incorporated into devices such as flat-panel cathode luminescent display [8].

To avoid metallic tip degradation from the ion sputtering processes during emission and to obtain an electron source with long lifetime and high beam brightness, a wide range of composite micropoint cathodes has been manufactured. This involved coating the tungsten tips with a variety of dielectric materials [9-11].

A guidance to the interpretation of the measured electron emission characteristics is given by Forbes and Deane [12, 13], along with a detailed analysis of the transmission coefficients for the potential energy barrier.

The aim of this work was to try to analyze long-term stability of such composite microemitters. For this purpose, we considered three insulator coated tungsten tips, which have been manufactured and tested 10 to 20 years ago [2,14,15].

Corresponding Author: M. S. Mousa **Email**: mmousa@mutah.edu.jo

Thereafter, these tips have been stored under standard atmosphere conditions without any further operation until we now tested them again to study the aging effect on these composite emitters.

Experimental

The preparation procedures, under which the coated W-tips had been manufactured, are described in the original publications [2, 14, 15].

In all cases, we started with tungsten tips, electrochemically etched from a high purity 0.1 mm diameter wire. These tips had afterwards been coated by tetracyanoethylene (TCNE) [2], magnesium oxide (MgO) [14] and zinc oxide (ZnO) [15], respectively.

The analyses were essentially carried out in two evacuated field emission microscopes; one diffusion pumped system with an additional liquid nitrogen (LN_2) trap (vacuum system 1) and one turbo pumped system (vacuum system 2). In both systems, base pressures of less than 1×10^{-8} mbar have been reached after baking the system at a temperature of about 180 °C overnight. The cathode was mounted ~10 mm away from the conductive phosphorus screen (anode), and a current limiting resistor of 20 MΩ was used. The images presented were taken through the vacuum systems' windows by a standard digital camera.

Results

We deal with coated tungsten microemitters, where several coatings have been analyzed; namely TCNE, MgO and ZnO. These samples were coated fifteen years ago, tested, kept in the laboratory under atmospheric conditions and have been re-examined in this work to analyze the impact of aging.

The results presented include the IV characteristics, FN plots and emission images. We compare these results with those previously obtained.

TCNE Coated Microemitter

This type of coating presented one of the most successful metal-insulator composite emitters due to being the electron source that enabled the *in-situ* observation of the transition process from cold to hot emission process during field emission assisted vacuum deposition of polymers on tungsten tips [2]. The emission current obtained (in vacuum system 2) was stable and the emission image showed a bright spot which demonstrated temporal stability after the electron emission switch-on phenomenon. The values previously obtained were 7 µA at 1000 V applied.

The IV characteristics were recorded as shown in Fig. 1 (left) with the FN plot on the right side of the same figure. This result agrees with the results recorded 15 years ago with just a slight decrease in the current obtained. The emission images (shown in Fig. 2) recorded during the voltage increase astonishingly resemble the emission image presented in the original work [2]. Continuing the cycle showed the smooth curve of the IV and FN plots' characteristics for the voltage decrease (see Fig. 3).

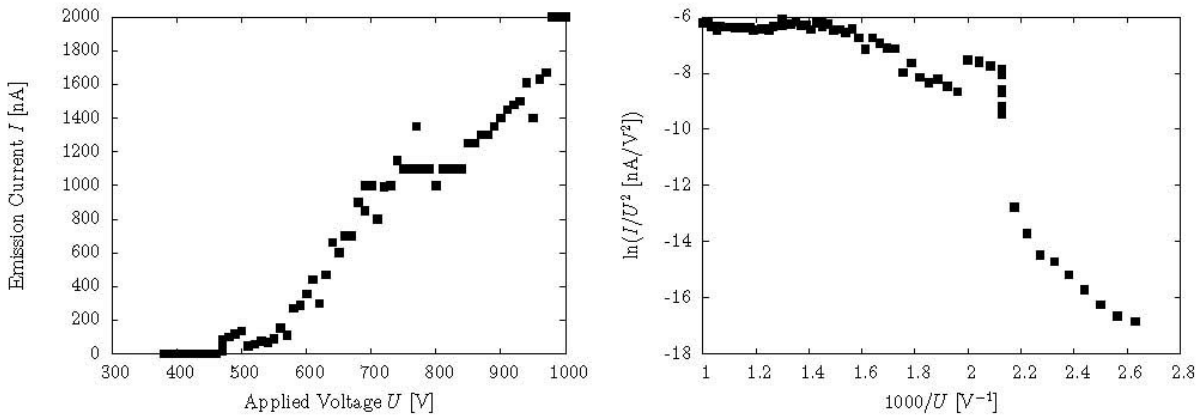

FIG. 1: The IV characteristics (left) and Fowler-Nordheim plot (right) of TCNE-coated tungsten tip during a further voltage increase.

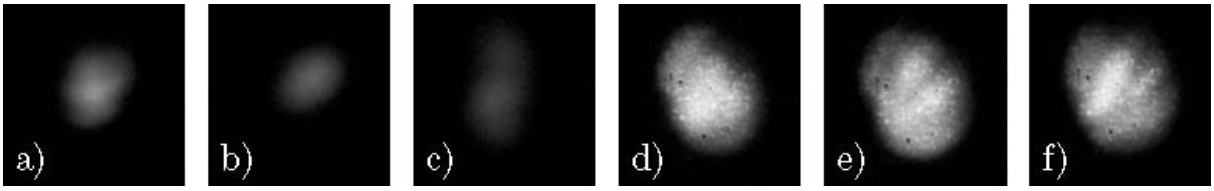

FIG. 2: Field emission images of TCNE-coated tungsten tip taken at 470 V (a,b), 510 V (c) and 980 V (d-f).

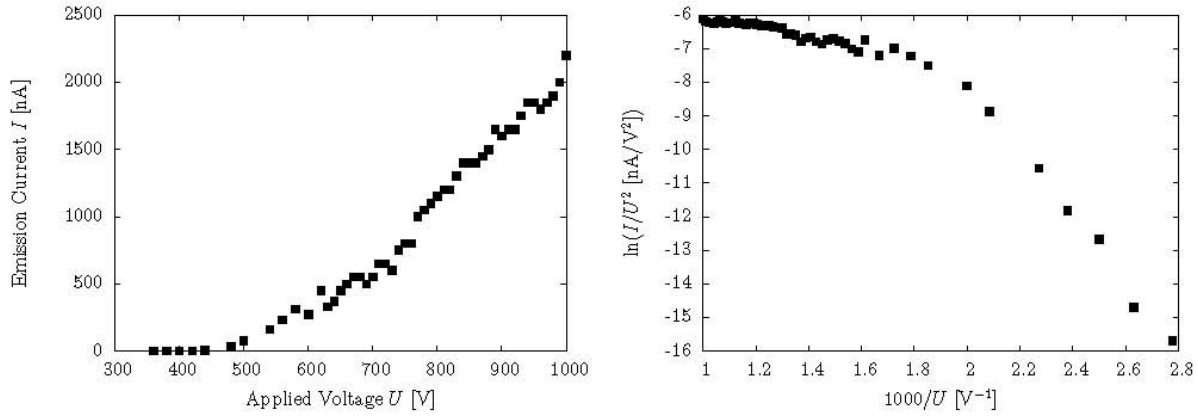

FIG. 3: The IV characteristics (left) and Fowler-Nordheim plot (right) of TCNE-coated tungsten tip during another voltage decrease.

MgO Coated Microemitter

In this section, the MgO coated tungsten emitter, that was examined 12 years ago with its characteristics published in [14] is now being re-examined (in vacuum system 1). The IV characteristics of this composite emitter (see Fig. 4, left) showed a switch on effect at 3340 V to an emission current of 17 μA which then increased gradually to 25 μA with increasing the applied voltage to 4700 V. The related FN plot is presented in the same Fig. 4 (right) with linear behavior obtained for lower fields. The emission images obtained from the MgO coated tungsten tip showed a single spot at low current and 1860 V. Increasing the voltage up to 2000 V showed emission from more than one sub-emission center that increased in number with increasing the voltage up to 2970 V. Increasing the voltage even more to 3340 V leads to the observation of a switch-on effect, thus producing a single spot image. Further increase of the voltage to 3800 V produced a more symmetric and concentrated emission spot, which is similar to that obtained during the original characterization process [14]. After increasing the voltage further to 4700 V, stability measurements were taken revealing limited stability compared to the original characterization. Subsequent decrease of the voltage produced the IV characteristics as shown in Fig. 6 with linear FN plot at the very low applied field region.

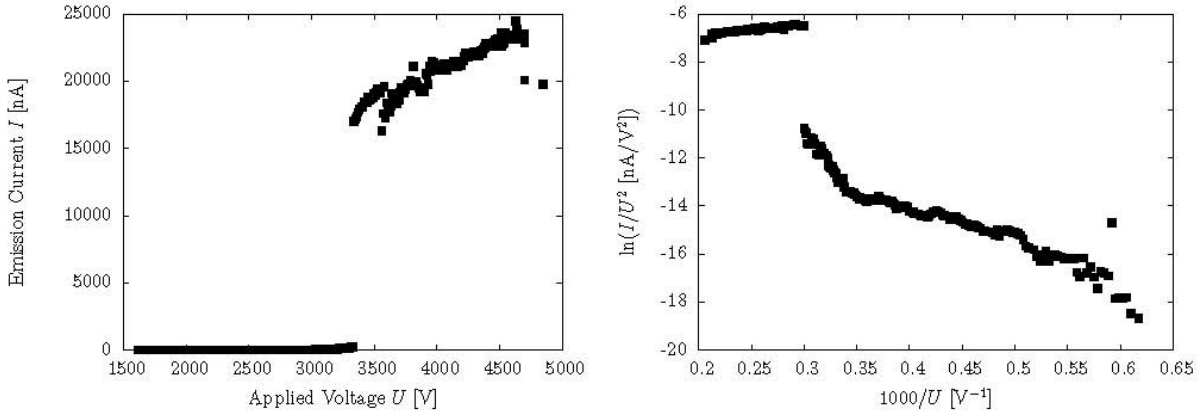

FIG. 4: The IV characteristics (left) and Fowler-Nordheim plot (right) of MgO-coated tungsten tip.

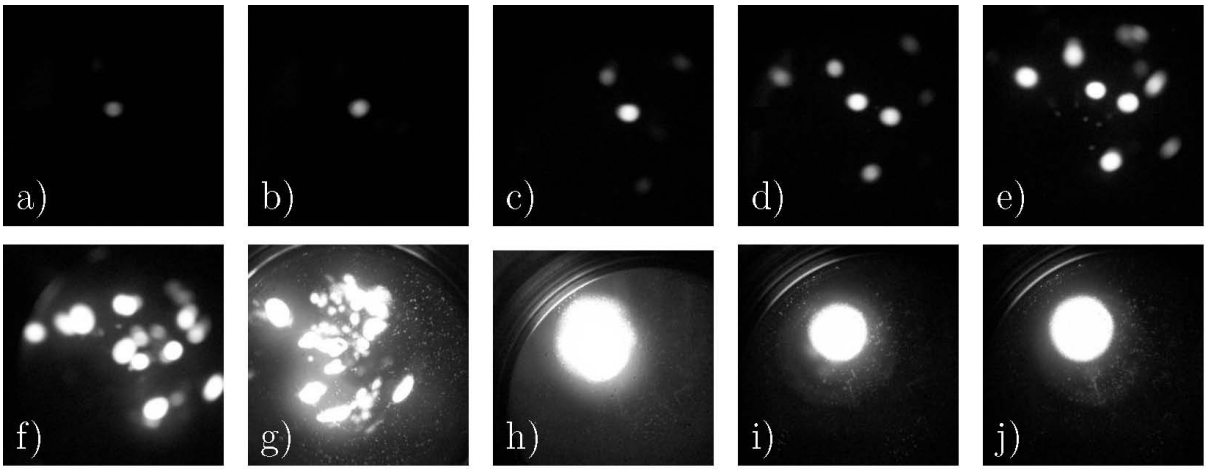

FIG. 5: Field emission images of MgO-coated tungsten tip taken at 1860, 1950, 1970, 2150, 2500, 2970, 3300, 3340, 3560 and 3800 V, respectively (a-j).

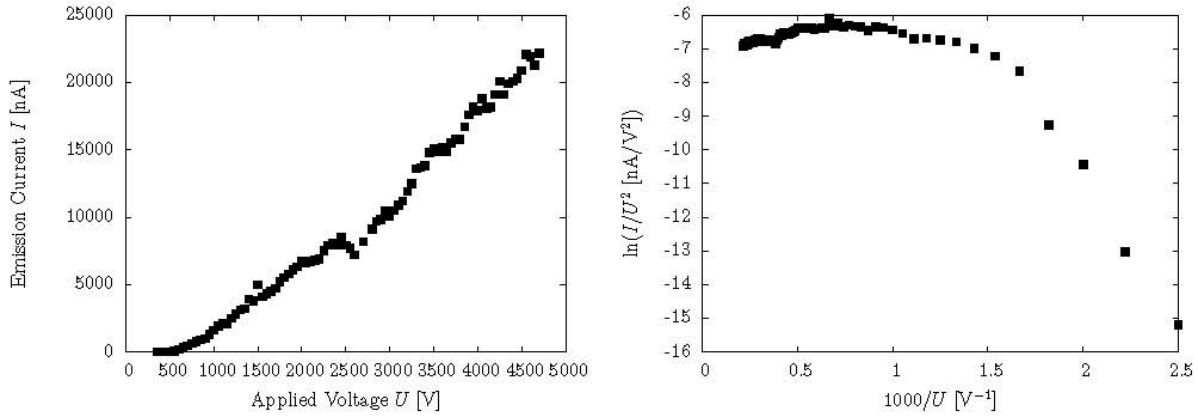

FIG. 6: The IV characteristics (left) and Fowler-Nordheim plot (right) of MgO-coated tungsten tip.

ZnO Coated Microemitter

In this section, the ZnO coated tungsten emitter, that was examined 20 years ago with its characteristics published in [15] is now being re-examined (in vacuum system 2). The IV characteristics obtained from the field emission process at the ZnO coated tungsten microemitter showed a smooth and regular increase of current with voltage (see Fig. 7, left) followed by a switch on from 3 to 6 μA at 3800 V. The emission current values were obtained at higher voltages than they were obtained originally [15], although linearity of the FN plot (see Fig. 7, right) is more obvious for a wider range of voltage. The emission images obtained from this composite emitter showed a striking similarity in the scattered multi-spot appearance compared to the original work at exactly the same voltage. Fig. 8 presents the spatial distributions of emission from ZnO coated tungsten tips showing the stability behavior of this type of electron source. The images demonstrate a limited stability measurement where we notice multiple emission sites randomly switching on and off. Each spot has a different energy distribution spectrum [10]. Subsequently decreasing the voltage showed a very smooth behavior (see Fig. 9).

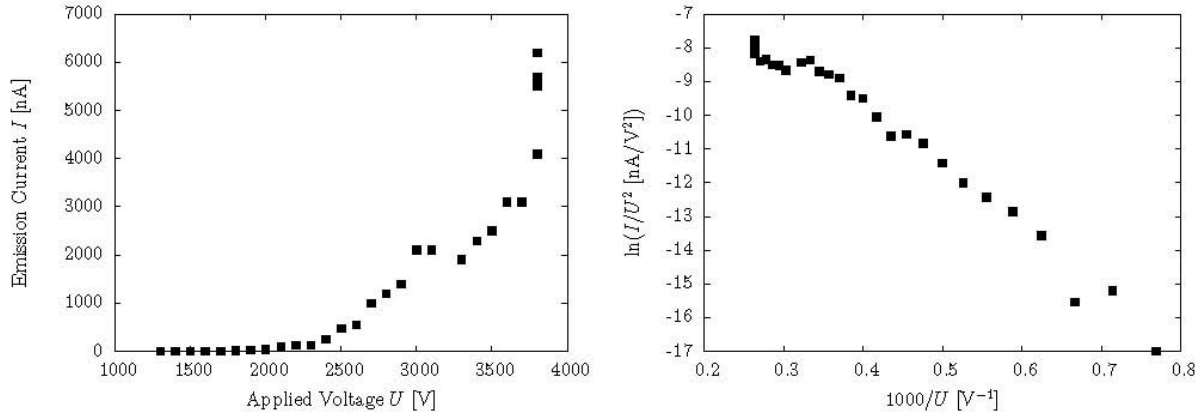

FIG. 7: The IV characteristics (left) and Fowler-Nordheim plot (right) of ZnO-coated tungsten tip.

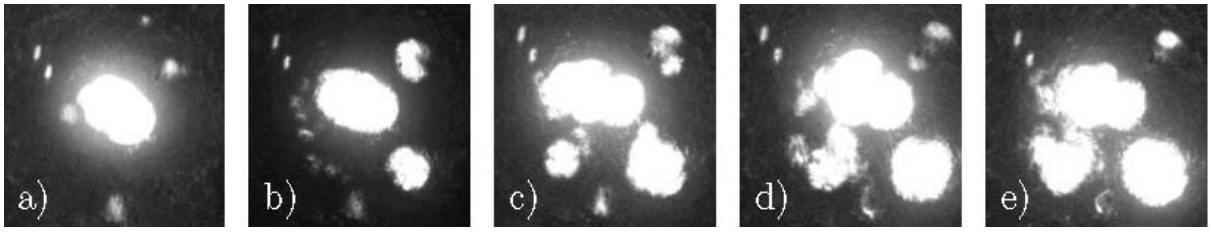

FIG. 8: Field emission images of ZnO-coated tungsten tip during stability measurement at 3800 V. The images were taken every 10 minutes reading an emission current of (a-e) 4.1, 5.7, 5.5, 6.2 and 5.6 μA.

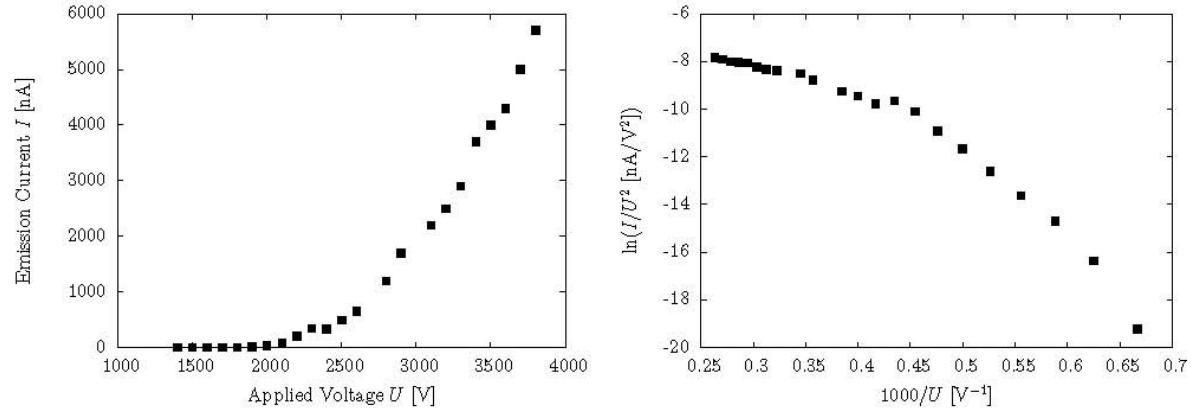

FIG. 9: The IV characteristics (left) and Fowler-Nordheim plot (right) of ZnO-coated tungsten tip.

Conclusions

Composite emitters, consisting of clean tungsten tips with known profile, coated with a variety of insulating materials, such as TCNE, MgO and ZnO were previously prepared and characterized. After about 10 to 20 years of keeping these samples under standard atmosphere conditions, they were tested again to study the strength of coating and the influence of aging. Results obtained by measuring the IV characteristics and emission images showed both striking similarities and marked differences between the characteristics obtained in both ages. One might have expected to find the tips highly degraded due to adsorption of corrosive substances present (at least in traces) within the standard atmosphere. Ultimately, experimental work reported here proves that the dielectric coating used in these experiments formed permanent structures on the tungsten core.

To highlight it once more, the coated tips showed outstanding long time stability by surviving about 15 years under standard atmosphere environment in fully operational condition. Thus, it might be worth systematically testing their capabilities under poor vacuum conditions.

Acknowledgements

Thanks are extended to the Alexander von Humboldt foundation for a Feodor Lynen fellowship and Mu'tah University for the hospitality.

References

[1] Crewe, A.V., Isaacson, M. and Johnson, D., Rev. Sci. Instrum., 40(2) (1969) 241.

[2] Mousa, M.S., Lorenz, K.L. and Xu, N.S., Ultramicroscopy, 79(1-4) (1999) 43.

[3] Busta, H.H., Zimmerman, B.J., Pogemiller, J.E., Tringides, M.C. and Spindt, C.A. J. Vac. Sci. Technol. B, 11(2) (1993) 400.

[4] Spindt, C.A., Holland, C.E., Rosengreen, A. and Brodie, I., J. Vac. Sci. Technol. B, 11(2) (1993) 468.

[5] Trujillo, J.T. and Hunt, C.E., J. Vac. Sci. Technol. B, 11(2) (1993) 454.

[6] Gray, H.F., J. Phys. Colloques, 50(C8) (1989) 67.

[7] Mousa, M.S., Holland, C.E., Brodie, I. and Spindt, C.A., Appl. Surf. Sci., 67(1-4) (1993) 218.

[8] Spindt, C.A., Surf. Sci., 266(1-3) (1992) 145.

[9] Latham, R.V. and Mousa, M.S., J. Phys. D: Appl. Phys., 19(4) (1985) 699.

[10] Mousa, M.S., Surf. Sci., 231(1-2) (1990) 149.

[11] Mousa, M.S., Surf. Interface Anal., 39(2-3) (2007) 102.

[12] Forbes, R.G. and Deane, J.H.B., Proc. R. Soc. Lond., Ser. A, 463(2087) (2007) 2907.

[13] Forbes, R.G. and Deane, J.H.B., J. Vac. Sci. Technol. B, 28(2) (2010) C2A33.

[14] Mousa, M.S. and Share', M.A., Ultramicroscopy, 79(1-4) (1999) 195.

[15] Mousa, M.S., Surf. Sci., 266(1-3) (1992) 110.

Volume 5, Number 1, 2012. pp. 27-31

Jordan Journal of Physics

ARTICLE

Characterizing a New Composite Material: Effect of NaOH Coating of Variable Thickness on the Properties of a Tungsten Microemitter

K. O. Mussa[a], **A. Fischer**[a,b] and **M. S. Mousa**[a]

[a] *Department of Physics, Mu'tah University, Al-Karak, Jordan.*
[b] *Institut für Physik, Technische Universität Chemnitz, Chemnitz, Germany.*

Received on: 30/6/2011; Accepted on: 8/1/2012

Abstract: Tungsten based microemitter tips have been prepared with various tip radii ranging from 30 to 100 nm. These tips were manufactured by electrochemical etching of a 0.1 mm diameter high purity (99.95%) tungsten wire at the meniscus of two molar NaOH solutions. Contrary to the standard procedure, the tips' surfaces have not been cleaned off NaOH solution by ultrasonic cleaning in distilled water. Only a coarse cleaning by dipping the electro-polished samples a few times in distilled water has been performed. Thus, a layer of NaOH remained on the surface, which acts like a coating. The thickness of this coating layer left on the core material depends on the number of dips of the sample in water after etching. This procedure produced composite microemitters which consisted of a tungsten core with three different thicknesses of coating – thick, medium or thin – consecutively produced by dipping the etched samples in water for one, six or twelve time(s). A conventional field emission microscope with a tip (cathode) – screen (anode) separation standardized at ~ 10 mm was used to characterize the electron emitters. The system was evacuated down to a base pressure of ~10^{-8} mbar when baked at up to ~180 °C overnight. This allowed measurements of typical Field Electron Emission (FE) characteristics; namely the current – voltage (IV) characteristics and the emission images on a conductive phosphorus screen (the anode).
Keywords: Nickel ferrite; Lattice parameters; Magnetic hysteresis; Cationic distribution.

Introduction

Due to its favorable emission properties and simple operating principle, the field emitter is particularly attractive as an electron source. In the past decades, there has been sustained interest in field emitters as high brightness electron sources for various technological devices. For applications, such as electron microscope sources, that require point-geometry emitters, the most widely used substrate material is tungsten [1,2]. Metallic micropoint emitters have faced extra interest by the emergence of microfabrication technology, especially in the form of planar field emitter arrays (e.g. Refs. [3-7]) which were incorporated into devices such as flat-panel cathode luminescent display [8].

To avoid metallic tip degradation from the ion sputtering processes during emission and to obtain an electron source with long lifetime and high beam brightness, a wide range of composite micropoint cathodes has been manufactured. This involved coating the tungsten tips with a variety of dielectric materials which was started in 1986 by Latham and Mousa [9]. Recently, several types of dielectric coating on tungsten were reviewed by Mousa [10]. A guidance to the interpretation of the measured electron emission characteristics is given by Forbes and Deane [11], along with detailed analysis of the transmission coefficients for the potential energy barrier.

Corresponding Author: A. Fischer **Email**: andreas.fischer@physik.tu-chemnitz.de

In this work, we consider the probably simplest way of coating microemitters which is utilizing NaOH. This material is deposited on the tips' surfaces by the standard etching process and usually washed off before any further processing. Here, we only coarsely wash the surface allowing a more or less thick layer of NaOH to remain on the surface and subsequently we analyze its properties as a coating material.

Experimental

The preparation of tungsten microemitters of a tip radius of less than 100 nm is generally performed by an electrolytic etching technique as described in the literature [2,9]. The tips here are produced from a 0.1 mm high purity tungsten wire by electrolytic etching at the meniscus of two molar sodium hydroxide (NaOH) solutions. According to the standard procedure, the tip would be cleaned directly after the etching by repeatedly immersing it in distilled water and finally subjecting it to ultrasonic cleaning.

Contrary to this standard procedure, we avoided the thorough cleaning leaving a layer of NaOH behind on the tips' surfaces. The thickness of this NaOH layer was influenced by partial cleaning through immersing the tips in distilled water for one, six or twelve time(s), respectively. The resulting layers will be referred to as thick, medium or thin in that order.

The analyses were essentially carried out using a field emission microscope. This system could be evacuated to a base pressure of about 10^{-8} mbar after baking at ~180 °C overnight. The cathode was mounted ~10 mm away from the phosphorus screen and a current limiting resistor of 20 MΩ was used.

Results

The emission characteristics obtained from three sets of etched tungsten tips – coated with NaOH layers of different thicknesses – show a generally interesting behavior. As the applied voltage is slowly increased, the emission current "switches on" from approximately zero (i.e., a very low value, usually a few nA) to a stable saturated value of 10 to 30 µA. By slowly reducing the voltage, the current decreases smoothly until it vanishes at a certain threshold voltage. For all samples, the IV plots (Fig. 1) show the usual exponential - like increase at low voltages (< 1000 V). At higher voltages, the current-voltage-relations turn into straight lines. This indicates that the emission current in this region is bounded by limited electron supply.

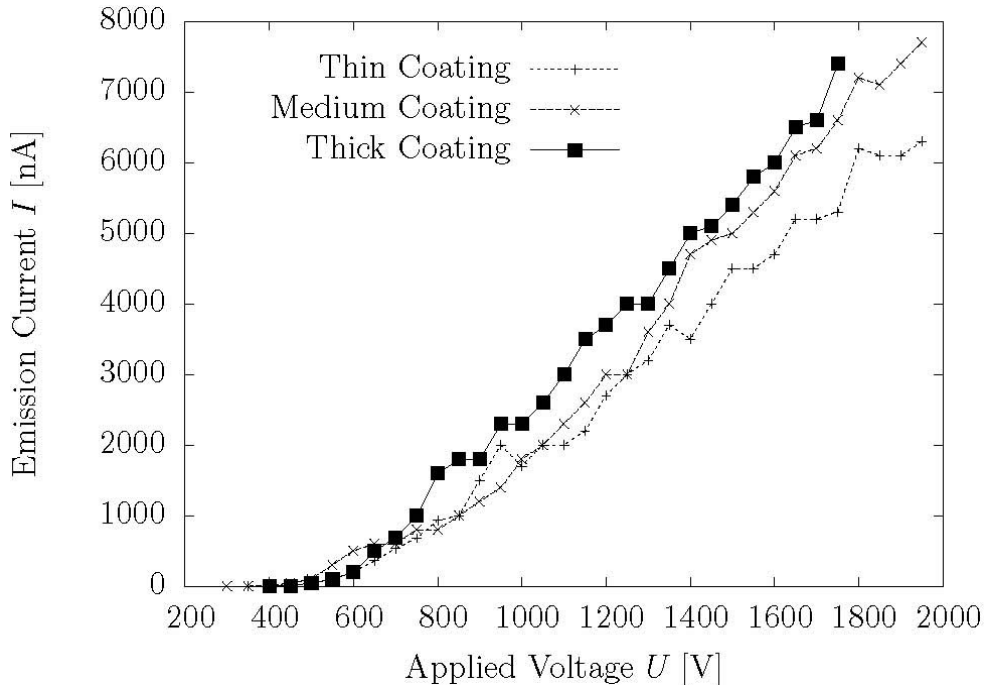

FIG. 1: The emission characteristics of micropoint cathodes coated with different layers of NaOH. The IV plots show the usual exponential - like increase at low voltages (< 1000 V). At higher voltages, the emission currents appear to be bounded by electron supply limits, resulting in rather straight current - voltage relations in this region. Comparing the three graphs, we find that the current increases with the thickness of the coating layer. Note that the data have been recorded during voltage decrease. (The connecting lines in the graphs are for eye-guidance only.)

Comparing the three graphs in Fig. 1, we find that the current (at a given voltage) generally increases with the thickness of the coating layer. Thus, the NaOH coating apparently enhances the electron emission at the surface.

The FN plots of the emission characteristics (Fig. 2) show a variety of effects. In the right hand part, the relation is mostly linear in all graphs indicating the usual field emission behavior. However, for higher electric field strengths (left of about 1.7 in 1000/U) the graphs bend and finally start decreasing slightly. This again indicates that the emission currents are bounded by an electron supply limit. The graphs of the tips coated with the medium or thick layer show a specialty. The two maxima found at about 0.8 and 1.3 for the thick coating as well as 0.7 and 1.7 for the medium coating (each in values of 1000/U) might imply field dependent structural reorganization of these NaOH layers. As the data have been recorded during voltage decrease, this effect was found to be reversible upon cycling the voltage.

Additionally, we find protective properties of the NaOH coating; i.e., all of the tips were able to serve rather high currents of up to 20 µA or more with good stability and without being blown out. In Fig. 3 the highest current recorded during these measurements (which is 28.7 µA) is shown.

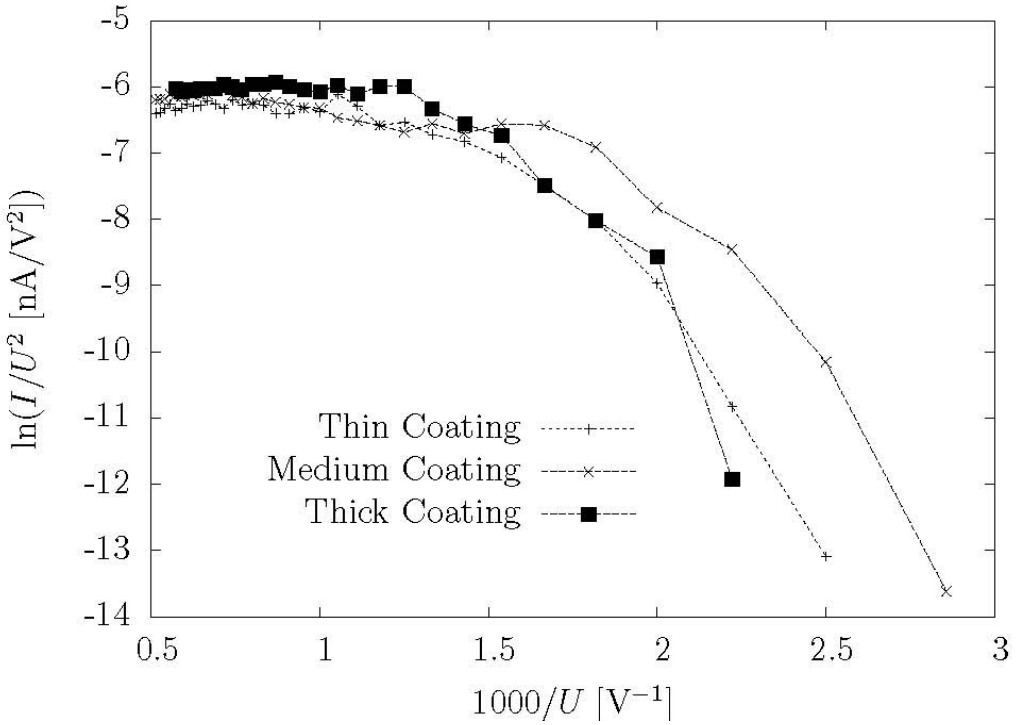

FIG. 2: The FN plots of the emission characteristics of the composite cathodes show several effects. In the right hand part of these plots, we find a mostly linear relation indicating the usual field emission behavior. However, at increasing field strengths the graphs bend (at about 1.7 in 1000/U) and finally start slightly decreasing, which indicates that the emission currents are bounded by an electron supply limit. The graphs of the tips coated with the medium or thick layer show two maxima (each found at about 0.8 and 1.3 for the thick coating as well as 0.7 and 1.7 for the medium coating), which might imply field dependent structural reorganization of these NaOH layers. Note that the data have been recorded during voltage decrease. (The connecting lines in the graphs are for eye-guidance only.)

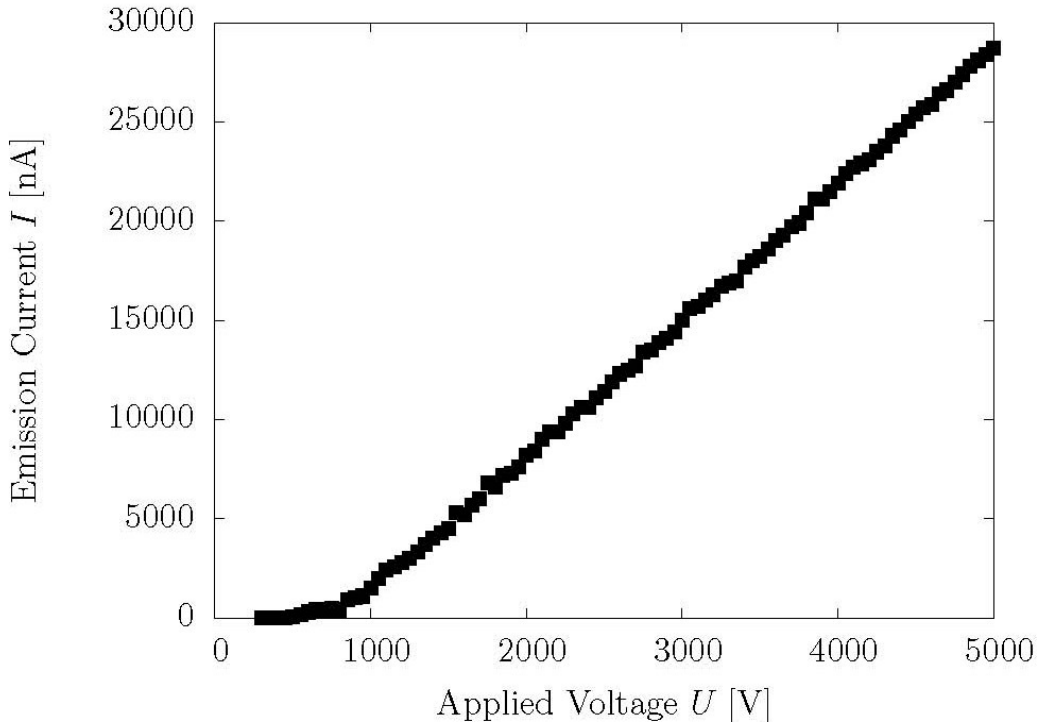

FIG. 3: The IV plots of the emission characteristics during the voltage decrease of another cycle for the emitter coated with a medium NaOH layer. Note that the tip could be operated at a maximum emission current of 28.7 μA without being destroyed.

Conclusions

Tungsten based microemitters have been prepared by electrolytically etching a 0.1 mm high purity tungsten wire at two molar NaOH solutions; i.e., using the same technique as employed by Müller in 1937. Contrary to the standard procedure, the tips' surfaces have not been cleaned off NaOH solution by ultrasonic cleaning in distilled water. Thus, a layer of NaOH remained on the surface, which provides a novel coating material.

The presence of emission current switch-on effects during initial voltage increase and the rather non-linear FN plots indicate the presence of a dielectric coating layer on the emitters' surfaces. The nature of the current saturation phenomenon with stable charge distribution on the emitters' surface is not fully understood. Amongst other possible explanations, it could indicate a new field emission mechanism. Further research will be needed to clarify this point. Nonetheless, it appears that such tips might provide an electron source with stable supply mechanism of saturated current for technological application.

All of the tips were able to serve rather high emission currents of up to 20 μA or more without being destroyed. This indicates protective properties of the NaOH layer on the tips' surfaces.

As a further step, it might be interesting to investigate the long-term storage stability of this coating material. This seems particularly relevant as – in a related investigation – we found that TCNE, MgO and ZnO coated tips can maintain their original properties while being stored under standard atmosphere conditions for more than a decade.

Acknowledgements

Thanks are extended to the Alexander von Humboldt foundation for a Feodor Lynen fellowship and Mu'tah University for the hospitality.

References

[1] Modinos, A., "Field, Thermionic and Secondary Electron Emission Spectroscopy". (Plenum Press, New York, London, 1984).

[2] Good, Jr, R.H. and Müller, E.W., "Field Emission". In Flügge, S., editor, Elektronen-Emission, Gasentladungen 1, volume 21 of Handbuch der Physik, pages 176-231. (Springer, Berlin, 1956).

[3] Busta, H.H., Zimmerman, B.J., Pogemiller, J.E., Tringides, M.C. and Spindt, C.A., J. Vac. Sci. Technol. B, 11(2) (1993) 400.

[4] Spindt, C.A., Holland, C.E., Rosengreen, A. and Brodie, I., J. Vac. Sci. Technol. B, 11(2) (1993) 468.

[5] Trujillo, J.T. and Hunt, C.E., J. Vac. Sci. Technol. B, 11(2) (1993) 454.

[6] Gray, H.F., J. Phys. Colloques, 50(C8) (1989) 67.

[7] Mousa, M.S., Schwoebel, P.R., Brodie, I. and Spindt, C.A., Appl. Surf. Sci., 67(1-4) (1993) 56.

[8] Spindt, C.A., Surf. Sci., 266(1-3) (1992) 145.

[9] Latham, R.V. and Mousa, M.S., J. Phys. D: Appl. Phys., 19(4) (1985) 699.

[10] Mousa, M.S. Surf. Interface Anal., 39(2-3) (2007) 102.

[11] Forbes, R.G. and Deane, J.H.B., Proc. R. Soc. Lond., Ser. A, 467(2134) (2011) 2927.

Volume 5, Number 1, 2012. pp. 33-42

Jordan Journal of Physics

ARTICLE

Adsorption of Thorium(IV) and Uranium(VI) onto Azraq Humic Acid, Jordan

A. K. Mohammad and **F. I. Khalili**

Department of Chemistry, University of Jordan, Amman 11942, Jordan.

Received on: 20/6/2011; Accepted on: 8/1/2012

Abstract: Humic Acid (HA) is an important constituent of soil organic matter that was the subject of several environmental studies. In this work, the adsorption isotherms of Thorium (IV) and Uranium(VI) onto Azraq Humic acid (AZHA) were studied at different temperature and pH values. The results indicate that Thorium(IV) has higher adsorptivity than Uranium(VI). The increasing of pH resulted in higher adsorptivity of Thorium(IV) and Uranium(VI). In contrast to transition metals and lanthanides, such as Ni(II), Cu(II), Zn(II), Cd(II), Hg(II), Gd(III), Ce(III) and Yb(III), the adsorption was entropy driven, while the adsorption of actinides on HA was found to be exothermic and so enthalpy driven. This leads to the hypothesis that Thorium(IV) and Uranium(IV) are encapsulated in the interior of HA helix with their water of hydration because the interior is full with water. However, transition metals and lanthanides are adsorbed on the exterior of HA helix.

Keywords: Humic acid; Adsorption; Thorium(IV) and Uranium(VI) metal ions; Adsorption isotherms; Enthalpy; Entropy.

Introduction

Azraq Oasis is located in the eastern desert of Jordan 100 km east of Amman and has a total area of about 26 km², where there is a plenty of plants, water, animal and bird life and warm weather. These are the best conditions for the formation and the development of humic acid (HA) [1, 2]. For this reason, Azraq Oasis is considered as a national park and a natural laboratory. It is a laboratory for studying soils, aquifers, erosion, bird migration and planting. It is also a laboratory for studying birds and the distinctive human culture of the Bedouins. Also, there is a potential pollution from the increasing traffic on the highways passing through Azraq to Iraq and Saudi Arabia. This is why Azraq is an important place to be studied [3].

Humic substances (HA's), the major organic constituents of soil and sediments, are widely distributed over the earth's surface, occurring in almost all terrestrial and aquatic environments. It arises from the chemical and biological degradation of plant and animal residues and from synthetic activities of microorganisms. The products so formed tend to associate into complex chemical structures that are more stable than the starting materials. Important characteristics of humic substances are: their ability to interact with metal ions, hydrous oxides, clay minerals and organic compounds such as alkanes, fatty acids, dialkylphthalates, pesticides, … etc.

HA's are amorphous, dark-colored, acidic, predominantly aromatic, hydrophilic, chemically complex and polyelectrolyte-like materials that range in molecular masses from a few hundreds to several thousands of Dalton's [4]. HA exists in soil and aquatic systems in either dissolved or particulate (solid) state.

The complexation of dissolved HA from Azraq with metal ions (pH > 4) has been studied extensively [5]. However, previous studies on adsorption of metal ions on solid HA (pH < 4)

Corresponding Author: F. I. Khalili **Email**: fkhalili@ju.edu.jo

are restricted to few measurements of % metal uptake by HA. Recently, the adsorption isotherms of transition and Lanthanide metals ions: Ni(II), Cu(II), Zn(II), Cd(II), Hg(II), Gd(III), Ce(III) and Yb(III) on solid AZHA (at pH < 4) were studied in order to achieve better understanding of interaction of metal ions with HA. In addition, the effect of environmental factors such as pH, temperature and ionic strength on adsorption capacity of HA have been studied [6, 7]. One of the important results drawn from these works was about the nature of interaction between transition metals, Lanthanides and HA surface. The results indicate that there is a significant covalent (specific adsorption) interaction in addition to electrostatic (nonspecific adsorption) interaction between transition metals and HA surface. Thorium and uranium metals have different chemistry and higher oxidation states (IV and VI), respectively than transition metals(II) and lanthanides(III). The present work's aims are:

1. Studying the adsorption isotherms of Uranium(VI) and Thorium(IV) metal ions on solid AZHA at pH =1.0, 2.0 and 3.0 at 25 ^{o} C, 35^{o} C and 45^{o} C to give a better understanding of the nature of adsorption of metal ions on HA.
2. Comparing the chemistry of transition metals and lanthanides interaction with HA with that of uranium and thorium.

Experimental

Materials and methods

All reagents used in this study were of analytical grade. $Th(NO3)_4.5H_2O$ is from Riedel DeHaën Chemical company Inc., $UO_2(NO_3)_2.6H_2O$ and $NaClO_4$ are from Merck, EDTA and PAR (4-(2-Pyridyl azo)resorcinol(I)) indicator are from Park, Sodium fluoride from RiedelDeHaën, Triethanolamine from Peking's Reagent, Sulphosalicylic acid and 35% Hydrochloric acid from Analatical Rasayan. Arsenazo(III) indicator from BDH Chemicals Ltd. Sartorius PP-25 pH meter model was used for pH measurements. The analytical balance used is from Shimadzu and its type is AW120, its readability: 0.1 mg. Shaking of samples was done using Memmert shaker equipped with a thermostat. UV-VIS spectrophotometer from Spectroscan model 80DV with software UV Win5 v5.0.5. Centrifuge model ALC PK130 was used.

Preparation of stock solutions

Stock solutions 2500 ppm of the two metal ions were prepared by dissolving specific amounts of the nitrate salt of UO_2(II) and Th(IV) in 0.1 M $NaClO_4$and then adjusted to the desired pH. The stock solutions were used to prepare solutions with different concentrations. The dilution is achieved by using 0.1 M $NaClO_4$ and 0.1 M $HClO_4$ solutions with different pH 1.0, 2.0 and 3.0 (to keep the ionic strength and the pH constant for all the different concentrations prepared).

Adsorption experiments

Batch adsorption was carried out using pyrex glass flasks. An accurate mass of batch adsorption was prepared using pyrex glass flasks. An accurate mass of 0.05 g of Azraq Humic acid (AZHA) measured to the nearest 0.1 mg was shaken with 50.0 mL of metal ion solution at different concentrations, in a thermostatted shaker for 24 h (which had been found sufficient to ensure equilibrium) at 25.0, 35.0 and 45.0 ^{o}C and at pH = 3.0, 2.0 and 1.0. A 15 mL amount of the solution was centrifuged at 4000 rpm to separate solid humic from the solution then the supernated solution was taken and analyzed by spectrophotometer. A calibration curve was determined using standard samples prepared from metal nitrate in 0.1 M $NaClO_4$ prior to measurements. Then, the adsorption isotherms were obtained.

Spectrophotometric determination of Thorium(IV) ions

The spectrophotometric determination of thorium(IV) ions in the aqueous solution was carried out as follows: Transfer of 1.00 mL of Arsenazo(III) indicator to a 20.0 mL of 9.0 M hydrochloric acid solution and add 1.00 mL of the aqueous test solution. Dilute the volume to 50.0 mL by addition of water. Absorption measurement was carried out using a (1.0 cm) quartz cell within one hour of sample preparation at a wavelength of 630 nm [8].

Spectrophotometric determination of Uranium(VI) ions

The spectrophotometric determination of Uranium(VI) ions in aqueous solution was carried out as follows: Transfer of 2.00 mL of PAR indicator to a solution containing 5.00 mL of the complexing solution, 5.00 mL of the buffer solution and 4 mL of the aqueous test solution in 50.0 mL volumetric flask and diluting

to 50.0 mL by water. Absorption measurement was carried out using a (1.0 cm) quartz cell within one hour of sample preparation at a wavelength of 530 nm [9].

Results and discussion

Rate of metal ion sorption by Humic Acid

The rate of metal ions uptake by AZHA was determined at different times (0.25, 0.5, 1.0, 2.0, 4.0, 6.0, 12.0, 18.0 and 24.0 h), with three concentrations (10, 25 and 50 ppm) at different pH and temperature values.

The percentage of metal ion loading by AZHA expressed as percentage uptake was calculated (Eq.1), where:

$$\% \text{ Metal uptake} = C_i - C_e / C_i * 100$$

C_i: Initial metal concentration (ppm).

C_e: The residual concentration of metal ion in solution at equilibrium in (ppm).

The results of these experiments are shown in Tables (1-2) and for example in Fig. 1.

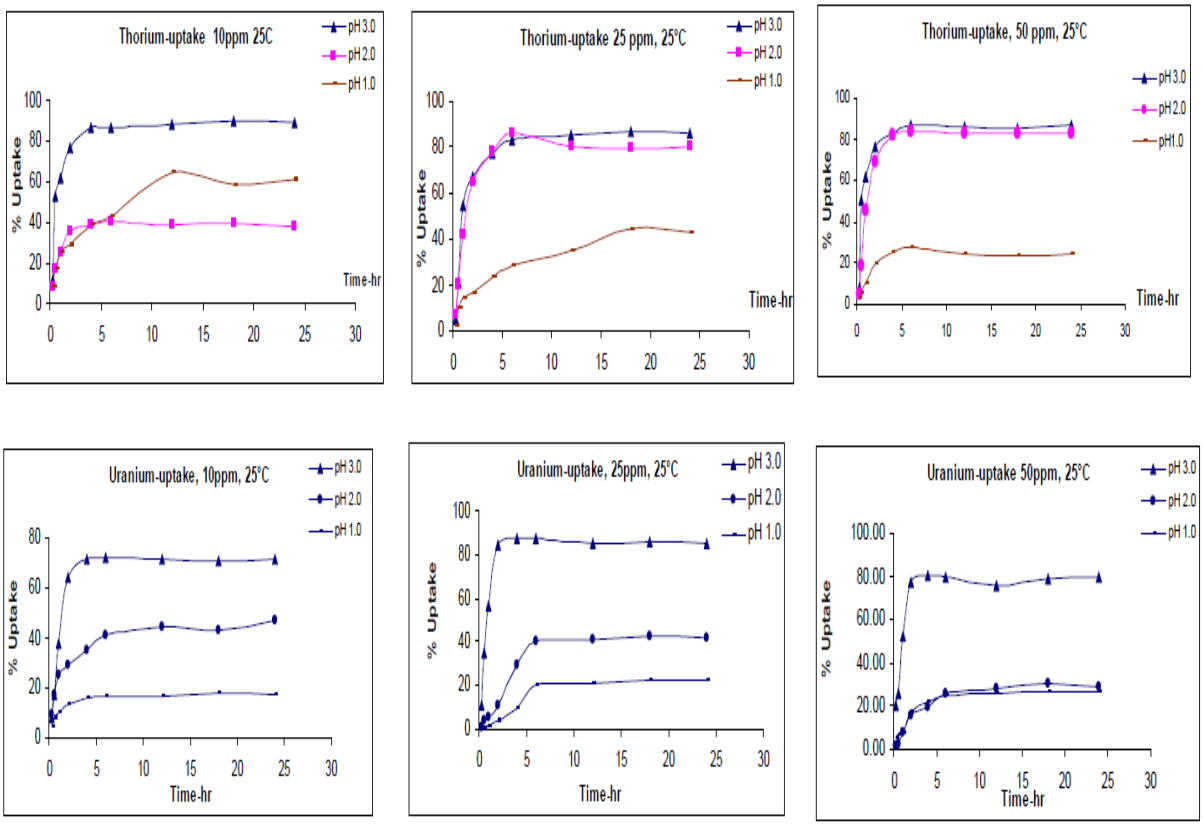

FIG. 1: Thorium(IV) and Uranium(VI) % uptake by HA at pH 1.0, 2.0 and 3.0, at T= 25°C and initial metal concentration of 10ppm.

As shown in Fig. 1 and Tables 1-2, there is an increase in the rate of adsorption as the pH increases. This is due to the deprotonation of carboxyl sites in the humic acid (HA), which causes humic acid strands to disaggregate due to the repulsion of negative charges and increases the number of sites on HA available for interaction with positively charged metals ions.

TABLE 1. Thorium(IV) uptake by HA at pH 1.0, 2.0 and 3.0, from an initial concentration of 10, 25 and 50 ppm and T= 25 °C.

Time (hr)	Conc. of 10 (ppm) at pH 1.0	Conc. of 25 (ppm) at pH 1.0	Conc. of 50 (ppm) at pH 1.0	Conc. of 10 (ppm) at pH 2.0	Conc. of 25 (ppm) at pH 2.0	Conc. of 50 (ppm) at pH 2.0	Conc. of 10 (ppm) at pH 3.0	Conc. of 25 (ppm) at pH 3.0	Conc. of 50 (ppm) at pH 3.0
0.25	8.0	1.8	3.3	8.0	7.60	5.2	11.2	5.2	8.3
0.50	17.0	10.5	6.0	17.0	20.1	18.6	53.3	21.2	50.8
1	25.8	14.8	10.7	25.8	42.4	45.5	62.0	55.0	62.0
2	28.8	16.5	19.6	35.3	65.2	69.2	76.5	67.0	76.1
4	39.2	23.2	25.6	39.2	78.4	81.9	87.1	77.6	83.2
6	42.9	28.4	27.3	40.3	86.0	83.3	86.7	82.9	87.4
12	64.7	34.8	24.7	38.8	80.0	83.1	88.6	85.1	86.3
18	59.0	44.4	23.4	39.7	79.5	83.3	90.3	86.9	85.5
24	61.0	42.8	24.1	37.7	80.2	83.1	89.3	86.0	87.0

TABLE 2. Uranium(VI) uptake by HA at pH 1.0, 2.0 and 3.0, from an initial concentration of 10, 25 and 50 ppm and T= 25 °C.

Time (hr)	Conc. of 10 (ppm) at pH 1.0	Conc. of 25 (ppm) at pH 1.0	Conc. of 50 (ppm) at pH 1.0	Conc. of 10 (ppm) at pH 2.0	Conc. of 25 (ppm) at pH 2.0	Conc. of 50 (ppm) at pH 2.0	Conc. of 10 (ppm) at pH 3.0	Conc. of 25 (ppm) at pH 3.0	Conc. of 50 (ppm) at pH 3.0
0.25	4.6	0.0	5.4	9.0	0.8	1.4	8.0	10.8	20.3
0.50	7.9	0.4	7.3	17.0	3.6	2.6	17.0	35.0	25.5
1	10.1	1.6	8.0	25.0	5.2	7.8	37.5	56.6	52.7
2	28.8	4.0	17.3	29.0	10.8	15.8	64.3	84.4	77.3
4	13.3	9.2	21.5	35.0	29.2	19.8	71.6	87.3	80.8
6	15.8	20.4	24.6	41.0	40.4	26.0	72.1	87.8	79.3
12	16.5	21.2	26.1	44.0	40.8	28.4	71.2	85.4	76.2
18	17.6	22.4	26.4	43.0	42.8	30.2	70.9	86.2	79.2
24	17.2	22.8	26.9	47.0	42.0	29.2	71.4	85.3	80.0

Adsorption isotherms

The adsorption isotherms were determined for Thorium(IV) and Uranium(VI) at different pH values (1.0, 2.0 and 3.0) and temperatures (25 ^{o}C, 35 ^{o}C and 45 ^{o}C). The adsorption isotherms results were analyzed by using the following linearized Langmuir [10] and Freundlich isotherm [11] equations:

Langmuir isotherm:

$$c/q = 1/(qm\ K_L) + (1/qm)\ c \quad (1)$$

Freundlich isotherm:

$$\log q = \log K_F + (1/n) \log c \quad (2)$$

Therefore, a plot of c/q versus c gives a straight line of slope (1/qm) and intercept 1/(qm K_L), and a plot of log q versus log c gives a straight line with a slope 1/n and intercept log K_F as shown in Tables (3-4) and Figures(2-3) for example. Where K_L parameter is related to the strength of the adsorbed ion– adsorbent binding (i.e. Thorium(IV) ions–HA), qm is the saturation adsorption capacity, K_F is a parameter related to the adsorption capacity and n is a measure of adsorption intensity [12, 13].

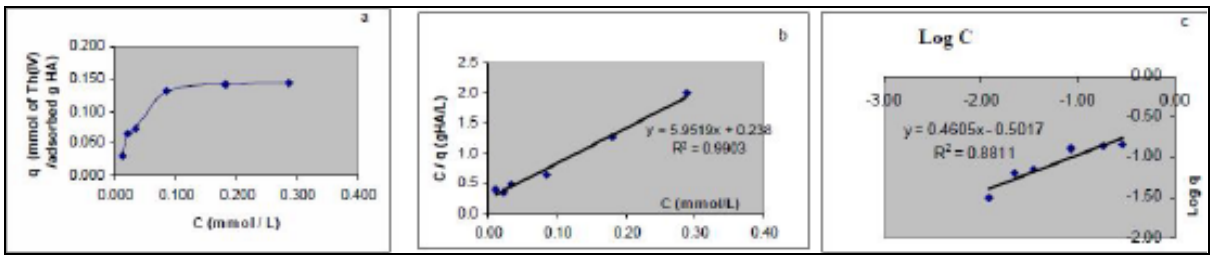

FIG. 2: Plots of (a) adsorption isotherm of Thorium(IV), (b) linearized Langmuir, (c) linearized Freundlich at pH = 1.0 and T= 25 ^{o}C.

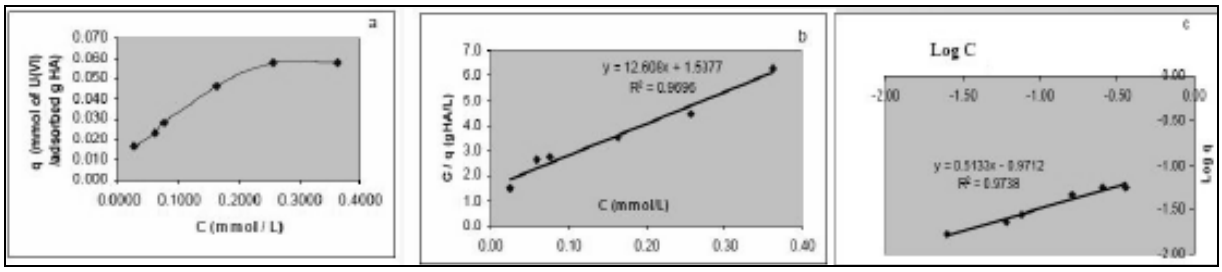

FIG. 3: Plots of (a) adsorption isotherm of Uranium(VI), (b) linearized Langmuir, (c) linearized Freundlich at pH = 1.0 and T = 25 ^{o}C.

TABLE 3. The R^2, qm, K_L, K_F and n values obtained from Langmuir and Freundlich plots for Thorium (IV).

T(^{o}C)	Langmuir model			Freundlich model		
	R^2	qm (mmol/g)	K_L (L/mmol)	R^2	K_F	n
pH=1.0, 25	0.990	0.168	25.0	0.984	0.315	2.172
35	0.969	0.117	23.3	0.947	0.168	2.778
45	0.982	0.108	20.8	0.881	0.144	2.904
pH=2.0, 25	0.927	0.425	20.0	0.945	1.345	1.558
35	0.985	0.354	51.5	0.957	1.089	1.961
45	0.984	0.324	41.8	0.953	0.901	1.959
pH=3.0, 25	0.927	0.824	17.8	0.990	4.933	1.230
35	0.975	0.896	17.1	0.999	5.049	1.240
45	0.924	0.934	15.1	0.982	5.244	1.208

The estimated parameters of the adsorption isotherms, calculated from the intercepts and slopes of the corresponding linear plots for Thorium(IV) and Uranium(VI) adsorption onto HA at different temperatures, together with their correlation coefficients (R^2), are given in Tables (3-4) at different pH values (1.0, 2.0 and 3.0). The correlation regression coefficients (R^2) have been determined for each isotherm. Their values are very good for Freundlich and Langmuir models. The applicability of Langmuir equation is an indication of the homogeneous sites of interaction utilized by metal ions that have almost the same heat of adsorption. The correlation regression coefficient (R^2) has been determined for each isotherm. In general, the Freundlich correlation coefficients are higher than the Langmuir correlation coefficients; consequently, it would appear that the Freundlich equations give a better representation of experimental isotherm data as shown in the previous Tables (3-4). This suggests that the HA contain both homogeneous and heterogeneous surfaces with more heterogeneous sites.

TABLE 4. The R^2, qm, K_L, K_F and n values obtained from Langmuir and Freundlich plots for Uranium(VI).

T(°C)	Langmuir model			Freundlich model		
	R^2	qm (mmol/g)	K_L (L/mmol)	R^2	K_F	n
pH=1.0, 25	0.970	0.079	8.20	0.974	0.107	1.948
35	0.965	0.067	7.86	0.991	0.0844	2.037
45	0.973	0.066	7.09	0.930	0.0950	1.726
pH=2.0, 25	0.870	0.351	4.83	0.958	0.664	1.277
35	0.871	0.331	3.33	0.980	0.489	1.255
45	0.942	0.283	3.26	0.990	0.381	1.313
pH=3.0, 25	0.954	0.335	9.37	0.943	0.734	1.478
35	0.944	0.455	4.88	0.993	0.813	1.317
45	0.978	0.627	2.84	0.997	0.997	1.187

The estimated parameters of the adsorption isotherms, calculated from the intercepts and slopes of the corresponding linear plots for Thorium(IV) and Uranium(VI) adsorption onto HA at different temperatures, together with their correlation coefficients (R^2), are given in Tables (3-4) at different pH values (1.0, 2.0 and 3.0). The correlation regression coefficients (R^2) have been determined for each isotherm. Their values are very good for Freundlich and Langmuir models. The applicability of Langmuir equation is an indication of the homogeneous sites of interaction utilized by metal ions that have almost the same heat of adsorption. The correlation regression coefficients (R^2) have been determined for each isotherm. In general, the Freundlich correlation coefficients are higher than the Langmuir correlation coefficients; consequently, it would appear that the Freundlich equations give a better representation of experimental isotherm data as shown in the previous Tables (3-4). This suggests that the HA contain both homogeneous and heterogeneous surfaces with more heterogeneous sites.

Depending on the values of qm and n in Tables (3-4), the adsorption of Thorium(IV) has higher adsorptivity and is more favorable than Uranium(VI) metal ions onto AZHA at the same pH and temperature [14, 15]. This may be due to that it has larger ionic radius (small hydrated radius) and charge than Uranium(VI) in the uranyl ion (UO_2^{2+}) and this causes stronger electrostatic interaction.

Comparing adsorptivity

To compare the chemistry of transition metals, Cu(II) and Ni(II) [6] and lanthanides, Gd(III), Ce(III) [7] interaction with HA with that of Uranium and Thorium, the following trends were observed:

At pH=3.0, 25 °C

Ce > Th > Gd > Cu > U > Ni

qm = 0.951 0.824 0.798 0.451 0.455 0.336

At pH=3.0, 35 °C

Ce > Gd > Th > Cu > U > Ni

qm = 1.15 0.928 0.896 0.489 0.455 0.380

At pH=2.0, 35 °C

Ce > Gd > Th > U > Cu > Ni

qm = 1.08 0.787 0.354 0.331 0.182 0.251

At pH=2.0, 25 °C

Ce > Gd > Th > U > Ni > Cu

qm = 0.828 0.561 0.425 0.351 0.234 0.163

Table (5) shows the ionic radius for the above mentioned ions. Interestingly, the adsorptivity of metal ions (qm) on AZHA was found to be directly proportional to the ionic radius (for example, Figures (4-5)). This is due to the decrease of hydration energy (ΔHh) as the ionic radius increases [16]. Increasing the hydration energy due to the increase in the hydration shell makes it more difficult for metal ions to discharge the water of hydration and bond to HA surface.

TABLE 5. Chemical properties of metal ions.

Metals	Th(IV)	U(VI)	Ce(III)	Gd(III)	Cu(II)	Ni(II)
Coordination number	8	7	7	7	6	6
Ionic radius (Å)	1.19	0.97	1.21	1.14	0.87	0.83

The adsorptivity is highest for the metal ion that has the largest radius as shown in Figures (4- 5). This can be explained by that in aqueous medium the metal ions exhibit strong hydrolysis and a distinct lowering of pH is noted when the salts of these elements are dissolved in water. The formation of aqua complex $[M(OH_2)_m]^{n+}$ takes place (where m is larger than six, perhaps eight or nine). The aqua complex, having m H_2O molecules surrounding the central ion, has a definite structure and the cloud of water molecules (hydration shell) has different geometry than the rest of the water. Thus, when say $M(NO_3)_n$ salts are dissolved in water, there will be very little attraction between $[M(OH_2)_m]^{n+}$ and the solvated NO_3^- ion. Unless the other ions or ligands have a strong structure-breaking influence, the sheath of water molecule will protect the metal ions from influence of other anions or ligands. When complexes are formed, the approach of a ligand will interfere with the hydration shell and the ordered geometry will break down [17]. So, metal ions with smaller radius will be surrounded by a stronger hydration shell than those with larger radius. This makes the bonding with HA more difficult, and the adsorptivity decreases. The adsorptivity (qm) values have no correlation with the charge density (charge/radius) of the metal ions. It is worthy to mention that the charge of metals ions is not the limiting factor in determining the adsorptivity of metal ions. This leads to the assumption that electrostatic interaction is not the predominant factor that determines adsorptivity.

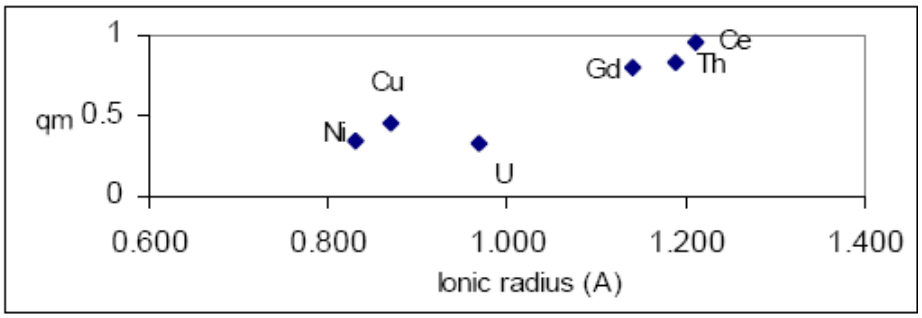

FIG. 4: The relation between qm determined from Langmuir plots and the ionic radius of metal ions at pH = 3.0 and T = 25 ^oC.

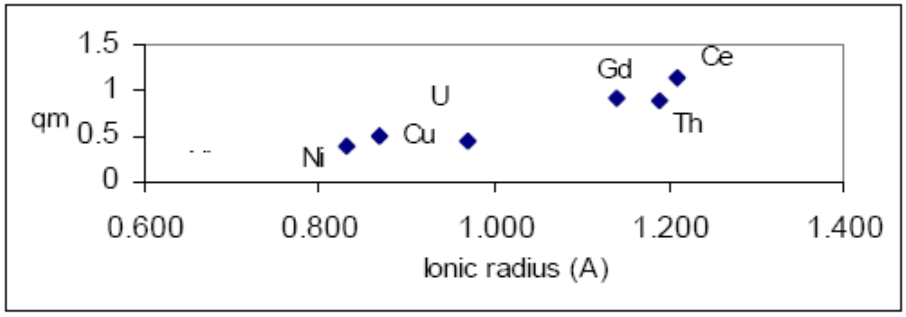

FIG. 5: The relation between qm determined from Langmuir plots and the ionic radius of metal ions at pH = 3.0 and T = 35 ^oC.

From Figures (4-5), the metal ion that has a large ionic radius has small hydrated radius, it will have better fitting into the hypothetical cylindrical structure of humic acid, and qm will increase.

The effect of pH

Generally, as pH increases, adsorption increases. This is noticed by the increased values of qm with increasing pH, as we can see in Tables (3-4) and Figure (6) which represents the values of qm for Thorium(IV) and Uranium (VI) metal ions at different pH values. As the pH increases from 1.0 to 3.0, the degree of dissociation of carboxylate groups increases (pK_a 4.19) and the negative charge on HA increases, which will lead to more electrostatic interaction with metal ions. Thus, it seems that there are other binding sites like carbonyl, alcohol and thiol groups which become important at this pH range, so the active sites of HA become more exposed to metal ion interaction.

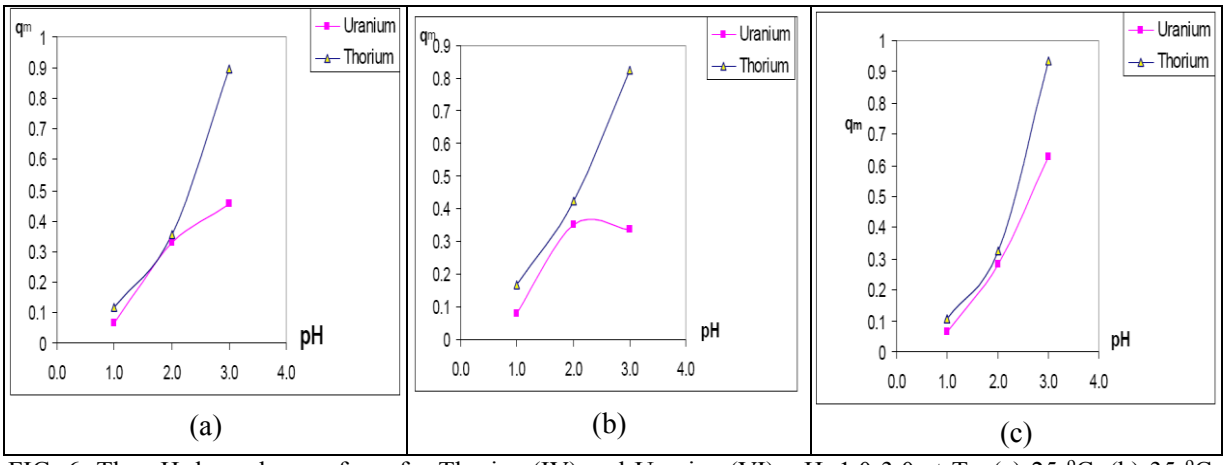

FIG. 6: The pH dependence of qm for Thorium(IV) and Uranium(VI), pH=1.0-3.0 at T= (a) 25 °C, (b) 35 °C, (c) 45 °C.

The effect of temperature

From Langmuir equation, K_L values were calculated at different temperatures. From the data in Tables 3- 4, the relation between ln K_L and 1/T was plotted at pH = 1.0 and 3.0 as shown in Figures (7- 8) below, and from the van't Hoff equation, ΔH and ΔS were calculated for Th(IV) and U(VI) as shown in Table (6). However, from Table (6), and Figs. (7- 8), the adsorptivity process is enthalpy driven for Uranium(VI). On the other hand, the adsorptivity process is enthalpy and entropy driven for Thorium(IV). It is clear that qm values decrease with increasing temperature at pH = 1.0 and pH = 2.0.

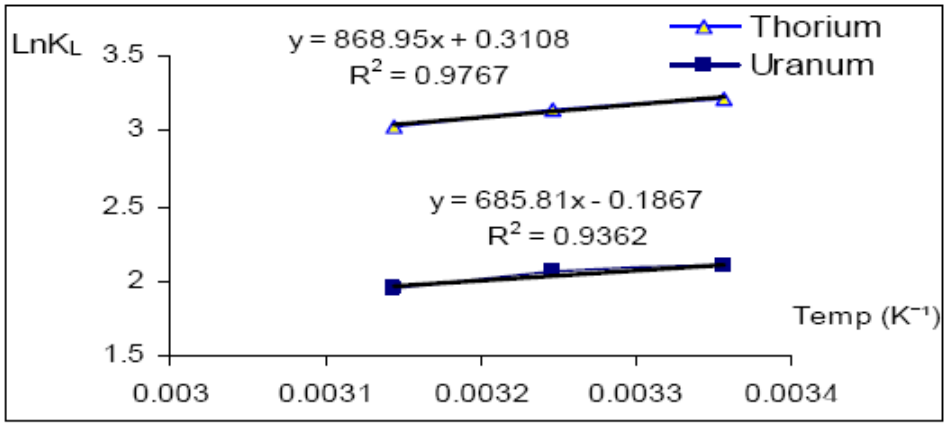

FIG. 7: The relation between ln K_L and 1/T, where T = (298K, 308K and 318K) at pH = 1.0.

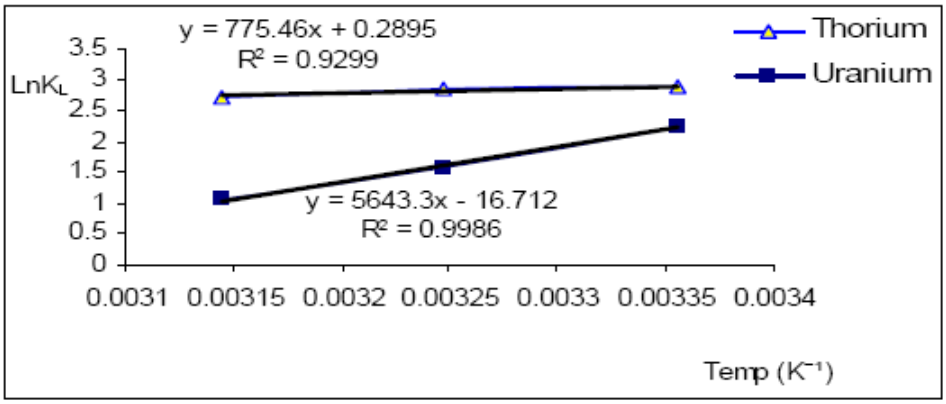

FIG. 8: The relation between ln K_L and 1/T, where T = (298K, 308K and 318K) at pH 3.0.

This indicates that the interaction between metal ions with HA is exothermic. This is in contrast to that observed in the case of transition elements [6] and lanthanides [7], which have been found to have an entropy driven interaction with HA. This indicates that the discharge of water of hydration is not important in the case of actinides due to the high charge on the metal ions.

This leads to the hypothesis that Thorium(IV) and Uranium(VI) are encapsulated in the interior of HA helix with their water of hydration because the interior is full with water [18]. However, Copper(II), Nickel(II) and Gadolinium (III) are adsorbed on the exterior of HA helix as shown in Fig. 9.

TABLE 6. Enthalpy and entropy values for the adsorption of Thorium(IV) and Uranium(VI) onto AZHA.

Metals	pH = 1.0		pH = 3.0	
	Th(IV)	U(VI)	Th(IV)	U(VI)
$\Delta H(kJmol^{-1})$	-7.224	-5.701	-6.447	-46.918
$\Delta S(J\ K^{-1}mol^{-1})$	2.584	-1.552	2.407	-138.9

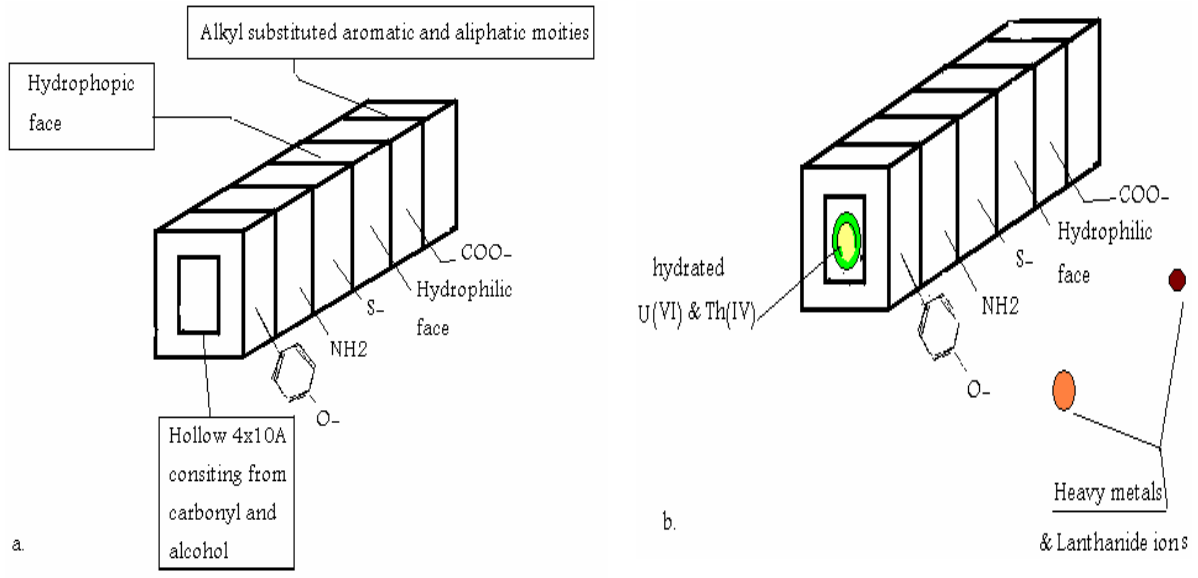

FIG. 9: Part a. Schematic view of the secondary structure of a HA strand [18]. Part b. Suggestion for loaded HA strand with different metal ions.

Conclusion

- The adsorptivity of metal ions (transition, lanthanide and actinide) on HA is directly proportional to the ionic radius of metals ion. Large size metal ions like Cerium(II), Thorium(IV) and Uranium(VI) fit the large hollow interior (4 x 10 Å) of the rod like structure of helical strand of HA, Fig. 7 [18].
- As pH increases, the adsorptivity (qm) of metal ions increases.
- The order of adsorptivity onto AZHA for Thorium(IV) is greater than for Uranium(VI).

References

[1] Khalili, F., Dirasat: Pure Sciences, 14 (1987) 151.

[2] Khalili, F., J. Iraqi Chem. Soc., 13 (1988) 71.

[3] Swaileh, K.M., Mesmar, M.N. and Ismail, N.S., Hydrobiologia, 286(3) (1994) 167.

[4] Schnitzer, M., "Soil Organic Matter", (Elsevier Scientific Publishing Company, New York, 1978).

[5] Baker, H. and Khalili, F., Analytica Chimica Acta, 497 (2003) 235.

[6] El-Eswed, B. and Khalili, F., J., Colloid Interface Sci., 299(2) (2006) 497.

[7] Nabtiti, T.K. and Khalili, F., Proc. of ICCE-2009, Thailand: Special Issue of Research Journal of Chemistry and Environment, (2010) P. 383.

[8] Savvin, S.B., Talanta, 8 (1961) 673.

[9] Neas, R.E. and Guyon, J.C., Analytical Chemistry, 44 (1972) 799.

[10] Langmuir, I., Journal of American Chemical Society, 40(9) (1918) 1361.

[11] Freundlich, H., Trans. Faraday Soc., 28 (1932) 195.

[12] Paduraru, C., Bilba, D., Sarghie, I. and Tofan, L., J. Serb. Chem. Soc., 70(10) (2005) 1205.

[13] Mckay, G. and Porter, J.F., J. Chem. Tech. Biotechnol., 69 (1997) 309.

[14] Fendorf, S.E. and Li, G., Environ. Sci. Technol., 30 (1996) 1614.

[15] Lee, D.C., Park, C.J., Yang, J.E., Jeong, Y.H. and Rhee, H.I., Biotechnol., 54 (2000) 445.

[16] Hunt, J.P. "Metal Ions in Aqueous Solutions". 2nd Ed., (Benjamin Inc, New York, 1965).

[17] Sinha, S.P., "Complexes of the Rare Earths".1st ed., (Pergamon Press, London, 1966).

[18] Davies, G., Fataftah, A., Cherkasskiy, A., Ghabbour, E.A., Radwan, A., Jansen, S.A., Kolla, S., Paciolla, M.D., Sen, Jr.L.T., Buermann, W., Balasubramanian, M., Budnick, J. and Xing, B., J. Chem. Soc., Dalton Trans. (1997) 4047.

Volume 5, Number 1, 2012. pp. 43-52

Jordan Journal of Physics

ARTICLE

Indoor and Outdoor Heavy Metals Evaluation in Kindergartens in Amman, Jordan

R. Z. Al Bakain[a], **Q. M. Jaradat**[b] and **K. A. Momani**[a]

[a] *Department of Chemistry, Mu'tah University, Al-Karak, Jordan.*
[b] *Department of Chemistry, Yarmouk University, Irbid, Jordan.*

Received on: 31/7/2011; Accepted on: 8/1/2012

Abstract: Selected heavy metals and water-soluble cations and anions in street, playground and indoor dust samples in the kindergartens (KGs) of Amman area-Jordan were determined by using flame atomic absorption spectrometer and ion chromatography. To achieve this aim, dust samples were collected from 38 different KGs at 4 different sites during summer season. It was found that the average total levels of Cu, Zn, Pb, Fe and Mn in street dust were 23.45, 188.47, 148.05, 8829.68 and 67.73 mg/kg, respectively. While for outdoor dust samples, the levels were 4.63, 127.38, 18.48, 8361.10 and 57.83 mg/kg, and finally, for indoor dusts were 23.51, 262.78, 71.33, 5566.14 and 51.28 mg/kg, respectively. The anions; F^-, Cl^-, NO_3^- and SO_4^{2-} and the cations; Na^+, K^+, Ca^{2+} and Mg^{2+} were analyzed by ion chromatography (IC). The results showed that there were high levels of these ions in all dust samples. The physiochemical properties; pH, moisture and organic matter content were also determined. The accuracy of results for heavy metals was examined by analysis of a standard reference material (SRM). Pearson coefficient was used to measure the correlation between the ions and the heavy metals in all the sites. ANOVA was also used to study the relation between the type of site and the heavy metals content.

Keywords: Heavy metals; Indoor, outdoor and street dust; Kindergartens; Major ions; Amman-Jordan.

Introduction

Heavy metals are natural constituents of the earth-crust and emitted to the environment by different ways; combustion of fossil fuel and road traffics, tears of tires, corrosion of building materials, automobile bodies, brake lining, industry and human activities, then settled in soil, water, air, dust and sediments. [1, 2-6]. Increasing industrialization has been accompanied throughout the world by the extraction and distribution of mineral substances from their natural deposits. Many of these substances have undergone chemical changes through technical processes, and finally dispersed in solutions, by way of effluent, sewage, dumps, dust, into the water, the earth and the air and thus into the food chain [1]. Thus, the threat posed by heavy metals to human health and the environment has risen sharply over the past decades, so there is arising public health interest in possible effects of heavy metals on the human health. Many investigations were carried out to determine the levels of heavy metals in different sites and materials worldwide, including: road side sediment [7], soil and vegetation [8], street dust and soils [9], human blood [10], indoor air [11], children hair [12], sewage sludge [13], sediment core [14], air [15], human teeth [16] and food [17].

Heavy metals can inter human bodies through many ways; the common modes of intake of external materials are inhalation of air into the lungs, ingestion of food, water and at times non–food items into the gastrointestinal system and transfer through the skin, also intravenous,

Corresponding Author: R. Z. Al Bakain **Email**: ramia.bakain@yahoo.com

intramuscular and vaginal routes. Food is digested in the stomach by enzyme hydrolysis to produce small molecules which are absorbable. The pH values of the stomach fluids are around 1 to 3 due to the presence of HCl. The digested materials move into the duodenum and the small intestine, where the pH is around 6 to 7. The materials on the surface of the gastrointestinal tract may be absorbed into the walls and into the blood stream.

Identification the toxicity and the percentage of heavy metals in the location we live in is important, especially on children who are more likely to ingest quantities of dust than adults with their habit of placing dirty fingers and objects of all kinds into their mouths (mouth- to -hand) activity [1], so they are more susceptible to intake of toxin than adults [18]. Preschool children under the age of five are particularly vulnerable to heavy metal poisoning because of development and behavioral consideration. The maximal brain growth and differentiation are found in the first few years of life.

In this study, Amman had been chosen, the capital of the Hashemite Kingdom of Jordan, located in the center of Jordan. It is the densest city with a population of about 2.2 millions and consists of two main parts: (the new Amman = the west) and (the old Amman = the east). The environment of Amman is influenced by natural emissions due to the geological location as well as man-made sources, such as vehicle emissions, industrial waste and emissions. Therefore, in this study we intend to:

- Evaluate the levels of heavy metals (Zn, Cu, Pb, Fe and Mn) in the dust of 38 different kindergartens.
- Measure the levels of the cations: Ca^{2+}, Mg^{2+}, NH_4^+, Na^+ and K^+, and the anions: NO_3^-, F^-, Cl^-, PO_4^{3-}, Br^- and SO_4^{2-} in street dust and compare them with those in outdoor and indoor dusts.

Experimental conditions

Sampling sites

Thirty eight KGs from sixteen sites were chosen as sampling sites in Amman. These sites represent different possible sources of pollution with different: geological type of area, cleaning mode, heating system, age of building, presence of gas stations around and road type. The sampling sites are illustrated in Fig. 1. The first set of sampling sites An; A1-A10 were: Wadi Al-Seer, Sweifieh, Abdoun, 7th and 8th circles with medium and steady traffic are free from industries with new house structure compared to the others. The second set Bn; B1-B10 were: Al-Ashrafiye, Hai-Nazal (east and west) and Jabal Al-Taj, with almost old structure buildings placed close to each others, nearby roads and dense inhabitants in the same neighborhood. The third set Cn; C1-C10 were: Marka region, Tabarbour and North Al-Hashimi, an area with high traffic density. Sampling sites number four Dn; D1-D8 were the downtown regions: Al-Hussein, Al-Abdalli, Al-Shmeisani and Al-Weibdeh, that are located in the center of the city, near high traffic routes, with high density vehicular traffic and large traffic stations with diesel-powered buses.

Sample collection procedure

Samples of indoor, outdoor and street dusts were collected during summer season prior to rain season to avoid washing of the heavy metals. Indoor dust samples were collected from the classrooms by using electrical vacuum, with clean and pre-washed paper bags, and then kept in polyethylene bags until the time of analysis. Outdoor dust samples were collected from the playgrounds and the entrance by gently sweeping the surface with a clean broom. The collected dust was transferred to a plastic scoop with the aid of a nylon brush and placed into pre-washed bags until the time of analysis. Finally, street dust samples were collected from the nearest street to each KG in the same way used for outdoor dust sample collection.

Sample pretreatment

Moisture and organic matter content

Moisture content was determined by weighing around 1.0 g of the dust samples, and then heated in an oven at 105ºC for 12 hours. The weight loss was calculated based on the difference between the final and the initial weights. The same samples were transferred into a furnace at 550º C for 4 hours, in order to determine the organic matter content, which was then calculated gravimetrically based on the weight difference.

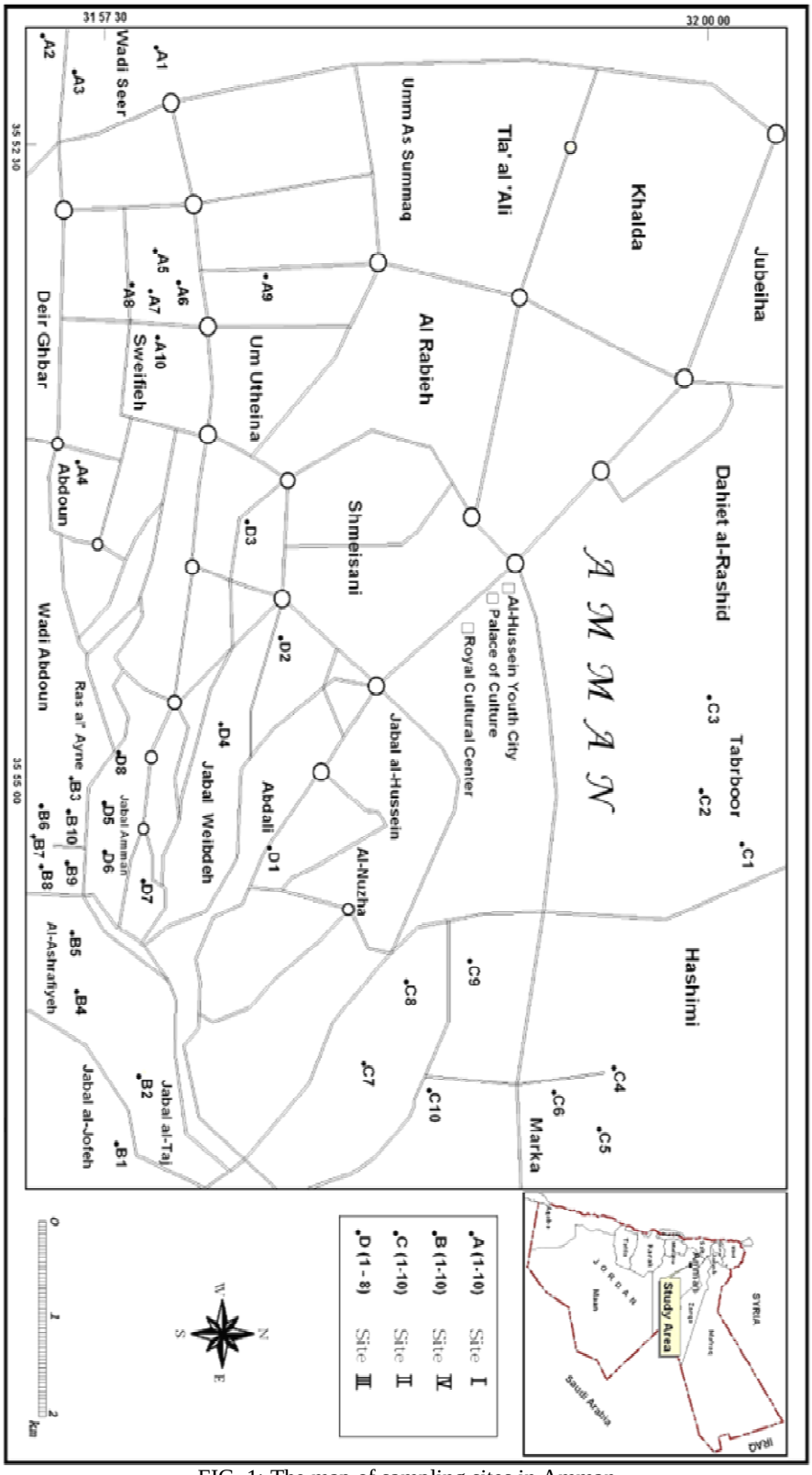

FIG. 1: The map of sampling sites in Amman.

pH measurement

The pH values of the water extract of dust samples were determined in milli-Q water (1: 2.5 wt/v) using polypropylene test tubes, with pH-meter (WTW, PH 523, Weilheim, Germany) after being calibrated at pH 4 and 7 buffer solutions at room temperature.

Water soluble anions and cations

Extraction of anions and cations was carried out by adding 15 ml of water to 0.7 g of dust sample. Then the mixture was heated at 95º C for 2 h by using test tube heater, sonicated for 30 minutes in ultrasonic bath at 50º C, filtered, diluted with water, then transferred into polyethylene sample bottles and stored at 4°C until the time of analysis. Blank solutions were then prepared in the same way as employed for the real samples.

Acid-extractable fraction of heavy metal

Extraction of heavy metals in dust samples was carried out by weighing around 0.7 g of dry sample. 15 ml of concentrated HNO_3 (high purity) was added in 50 ml polypropylene test tubes, heated for 2 h at 95º C in a water bath, sonicated for 30 minutes in ultrasonic bath at 50º C, then centrifuged for 15 min at 1000 rpm. The sample was diluted with 1% HNO_3. Blank solutions were prepared in the same way as employed for the real samples.

Chemicals and instrumentation

All glassware and test-tubes used were initially cleaned with soap, washed thoroughly with tap water, rinsed with distilled water and socked in 10% HNO_3 (v/v) overnight, respectively. Centrifuge (MSF, Mior35, England), Furnace (Nebertherm, N5/RL, Germany), oven (Mipo/5/SS/EC, England), water bath shaker (D-3162, Kottermann laboratechchnike, 3047, West Germany) and Ultrasonic bath (Quantrex 210H) were used.

All the reagents were of analytical grade purity, HNO_3 assay 65% (Scharleau). Determination of anions and cations was carried out on DIONEX (DX-100), USA, Ion chromatographic system (IC). 250 × 4.0 mm ID, DIONEX AS4A-SC and 250 × 4 mm ID, DIONEX CS12 columns, with mobile phases of (1.8 mM Na_2CO_3 + 1.7 mM $NaHCO_3$**)** and **(**20 mM Methanosulfonic acid), respectively, were used for anion and cation measurements.

Determination of heavy metals was carried out using flame atomic absorption spectrometer (FAAS) (Varian 55B). The manufacturer's recommended procedures were followed throughout this work.

Running conditions for the analysis of ions

A standard mixture of six anions: F^-, Cl^-, Br^-**,** NO_3^-**,** PO_4^{3-} and SO_4^{2} with the following concentrations: 200, 300, 1000, 1000, 1500 and 1500 ppm, respectively of standard stock solution (Dionex, California) was used to prepare our standard solutions, based on the following concentrations of fluoride: 1, 2, 4, 8 and 16 ppm. A standard mixture of five cations: Na^+, NH_4^+, K^+, Mg^{2+} and Ca^{2+} of 2000, 4000, 2000, 2000 and 10000 ppm, respectively, of standard stock solution (Dionex, California) was used to prepare standard solutions based on the following concentrations of sodium: 1, 2, 4, 8, 16, 20, 30 and 40 ppm.

Validity and quality control

To estimate the analytical precision and accuracy of analytical results, reagent blanks, replicate samples and standard reference materials (SRM) were used. Blanks were prepared in a similar manner to that of the real samples and were analyzed before each measurement. All extractions and analyses were made with duplicates (n = 2) for quality assessment, and the average results were reported. Analysis of SRM was conducted by tested analytical method and comparison of the results obtained with the certified values. In this study, SRM (soil 7) was subjected to the extraction (duplicate trials) and then the results were reported as the percent of recovery for Fe, Cu, Pb, Zn and Mn.

Results and discussion

Physico-chemical properties of street, outdoor and indoor dust samples

Moisture (Mois), organic matter content (OM) and pH are some of the common physical and chemical soil properties that can influence the presence of metals in the environment. They were determined for the street, outdoor and indoor dust samples.

pH is a test for measuring binding strength and potential mobility of heavy metals in soil [19-21]. It has an influence on the form and other parameters affecting the concentration,

mobility, transformation and the presence of organic matter [21]. Changes in pH results in a transfer of elements from one phase to another may thus influence the mobility of heavy metals in the soil [9]. Metal solubility increases at low pH values [10]. For example, Pb precipitates when pH $>$ 7 [22-24]. The results in this study showed that pH values in the KG soil samples were neutral to sub-alkaline values for all the sampling sites (pH > 7). There was no significant difference in pH values in all the studied sites (An, Bn, Cn and Dn). For street, outdoor and indoor dust samples, the average values of pH at all the sites were 7.64, 7.54 and 7.19, with ranges of 7.00 – 9.26, 6.62 – 10.04 and 5.65 – 10.88, respectively. The reason behind this is that the nature of soil in Jordan is almost calcareous (high carbonate content,) which enhances the pH values [25]. $CaCO_3$ provided a buffer against the mobilization of heavy metals such as Pb [22]. The highest value of pH in street dust samples was in A4 due to the new constructions that were built during sample collection. For outdoor samples, the highest value of all sites was for B1, and for indoor samples it was for A10 due to the intensive daily cleaning in these kindergartens with detergents that are almost alkaline. On the other hand, the lowest pH value for street, outdoor and indoor dust pH samples was for B9, B7 and D4, respectively. This was referred to traffic emissions that emit acidic oxides as (SO_2) leading to lower the pH values [26].

The moisture content of the different types of samples is presented in Table 1. No wide variations in moisture content values were shown between inside, outside KGs and street dust samples. The highest overall average was found for the inside samples (1.88%), and the lowest was for outside samples (0.76%). This could be related to the lack of sunlight and lower temperature inside the kindergartens which decrease the evaporation rates.

TABLE 1. Physiochemical properties: organic content and moisture for street, outdoor and indoor samples with their standard deviations.

	OM%		Mois%		OM%		Mois%		OM%		Mois%	
KG	In	S.D.	In	S.D.	Out	S.D.	Out	S.D.	Street	S.D.	Street	S.D.
An	14.98	7.28	0.83	0.20	2.72	2.79	1.01	1.38	5.12	2.53	0.86	0.75
Bn	46.39	6.06	4.25	4.00	3.97	3.14	0.46	0.34	12.22	4.49	1.08	0.71
Cn	N.A	N.A	N.A	N.A	4.76	5.24	0.95	1.11	8.72	2.64	0.86	1.27
Dn	5.34	1.84	0.56	0.30	4.77	5.40	0.63	0.69	13.81	11.54	0.90	0.94
Mean	22.24	5.06	1.88	1.50	4.06	4.14	0.76	0.88	9.97	5.30	0.92	0.92
Min.	3.77		0.22		0.65		0.03		1.63		0.11	
Max.	56.16		11.40		15.29		3.87		32.92		4.47	

The average organic matter content in all the sites in street, outdoor and indoor dust samples was 9.97%, 4.06% and 22.24%, respectively, as illustrated in Table 1. The order was similar to that for the moisture content, indoor > street > outdoor. This might be due to the high organic contamination inside the KGs because of the paints and food residues, while for street samples; it might be due to the high traffic volume and car emission. The order of values in all the sites for street dust samples was Dn > Bn > Cn > An, for outdoor samples the order was Dn > Cn > Bn > An and for indoor samples it was Bn > An > Dn, while Cn was not analyzed due to low sample amount. Site Dn has the highest values in the street and outdoor samples due to the high traffic density in these sites. For indoor samples, Bn showed the highest values due to the usage of oil for heating in most of the KGs in these sites and also as a result of the high food residues that fall down from children with low cleaning rate.

Water soluble anions and cations

For anions, PO_4^{3-} and Br^- were not detected in all dust samples, while for cations, $NH_4^+$was not detected as shown in Table 2. The table indicated that SO_4^{2-} was the dominant anion in street and outdoor dust samples which might be due to the type of motor vehicles, mainly diesel powered buses and trucks. For indoor dust samples, Cl^- was the highest due to table salt (NaCl) and the food residues that fall down. The highest value for cationic species in all the sites of street and outdoor dust samples was for Ca^{2+}. This outcome could be due to the type of soil which exists in

the studied sites with calcareous nature. For indoor dust samples, Na^+ was the highest, due to the children food components such as chips, biscuits and table salt of high levels of sodium that falls down. Site Bn showed the highest concentration of SO_4^{2-} due to the type of motor vehicles used, mainly diesel powered bus and trucks [27]. However, F^- in street dust is attributed to dust from phosphate raw materials carried by automobiles and from natural soil [27] since the crude oil used in Jordan is of relatively high sulfur content ranging from 2-8% [27].

TABLE 2. The average concentrations for cations and anions (mg/kg) in all sites.

		K^+	Na^+	NH_4^+	Mg^{2+}	Ca^{2+}	NO_3^-	F^-	Br^-	Cl^-	PO_4^{3-}	SO_4^{2-}
An	**Indoor**	830	5291	274	246	1980	469	326	50	3258	114	2305
	S.D	**590**	**3215**	**185**	**340**	**2141**	**303**	**373**	**18**	**2762**	**65**	**2273**
	Outdoor	86	409	35	133	705	360	17	12	523	102	700
	S.D	**91**	**408**	**11**	**135**	**406**	**334**	**9**	**7**	**734**	**53**	**555**
	Street	373	616	73	101	1741	173	29	17	800	97	1357
	S.D	**379**	**251**	**24**	**59**	**984**	**55**	**9**	**10**	**200**	**51**	**632**
Bn	**Indoor**	2293	5611	1303	511	1539	623	810	N.D	5479	168	3170
	S.D	**631**	**1739**	**748**	**103**	**485**	**409**	**394**	**N.D**	**1605**	**113**	**1965**
	Outdoor	271	449	165	123	1128	417	34	N.D	382	612	761
	S.D	**91**	**408**	**11**	**135**	**406**	**334**	**9**	**N.D**	**734**	**53**	**555**
	Street	817	1227	381	390	1842	80	42	N.D	1427	N.D	1519
	S.D	**733**	**718**	**252**	**174**	**895**	**27**	**19**	**N.D**	**629**	**N.D**	**735**
Cn	**Indoor**	1713	5555	1356	348	1036	91	1113	154	5921	274	2104
	S.D	**1003**	**1525**	**783**	**129**	**451**	**53**	**847**	**89**	**2138**	**158**	**774**
	Outdoor	230	611	183	159	770	320	25	N.D	679	135	643
	S.D	**200**	**400**	**99**	**109**	**360**	**369**	**11**	**N.D**	**517**	**63**	**468**
	Street	291	981	272	154	1171	240	29	0	1325	N.D	1046
	S.D	**125**	**338**	**86**	**124**	**481**	**154**	**15**	**0**	**695**	**N.D**	**430**
Dn	**Indoor**	868	3216	185	214	1896	575	373	N.D	1933	287	2670
	S.D	**735**	**2608**	**76**	**162**	**1656**	**414**	**470**	**N.D**	**1618**	**117**	**2939**
	Outdoor	272	447	247	86	826	496	30	7	589	145	653
	S.D	**551**	**493**	**121**	**42**	**749**	**543**	**17**	**3**	**852**	**90**	**805**
	Street	471	922	273	215	1546	242	91	58	1355	71	1427
	S.D	**372**	**907**	**143**	**146**	**805**	**191**	**179**	**20**	**1183**	**118**	**1004**

NO_3^- might come from the type of fuel used, mainly diesel powered buses and trucks [27], so results showed high values of NO_3^- for street and outdoor dust samples in the site Dn due to the high traffic density when it is compared with the other studied sites. The normal range of NO_3^- in the atmosphere is 0.1-10 $\mu g/m^3$ [27]. To conclude, the high levels of water soluble anions and cations were mostly due to their associations in soluble natural compounds [28-29]. Furthermore, the use of local water for washing floors might be a source of cations and anions since it is full with ions.

Total heavy metals evaluation

In order to assess the accuracy of the results obtained by the analytical method used in this study, two methods were used; blank solution and standard reference materials (SRM). SRM soil 7 was subjected to the same extraction (triplicate trials) of the real samples. The recovery of heavy metals in soil 7 for Zn, Pb, Cu, Mn and Fe was 97.4%, 117 %, 115 %, 90% and 103.2%, respectively as shown in Table 3.

The results in Fig. 2 showed the average concentration of heavy metals in different street, outdoor and indoor dusts samples. Street dusts in sites An have the highest concentration levels for Pb, Fe and Mn, while Dn showed the highest levels of Cu and Zn. KGs in An sites are located on the major streets or nearby crowded major streets at about 20-50 m, so Pb sources come from automobile emissions [9, 21, 30], while Fe and Mn in street dusts come from metal corrosion, such as of the bodies of automobiles [31-32]. The highest content of Cu and Zn was found in Dn sites. This may be due to the presence of a bus station near these KGs with high traffic density, since Zn exists in the automobile door panels, carburettors and pumps, where Cu can be found in buses (bars, windings in motor and generator). This may increase the levels of Cu and Zn [33].

TABLE 3. Analysis of heavy metals (mg/kg) for SRM- soil -7.

Element	DL*	Certified value	Measured value	Recovery%
Fe	0.30	25700	26521	103.2
Cu	0.002	11	12.7	115
Pb	0.006	60	70.2	117
Zn	0.002	104	101.3	97.4
Mn	0.03	630	566	90

DL*: is the minimum detection limit of 6 samples (mg/L).

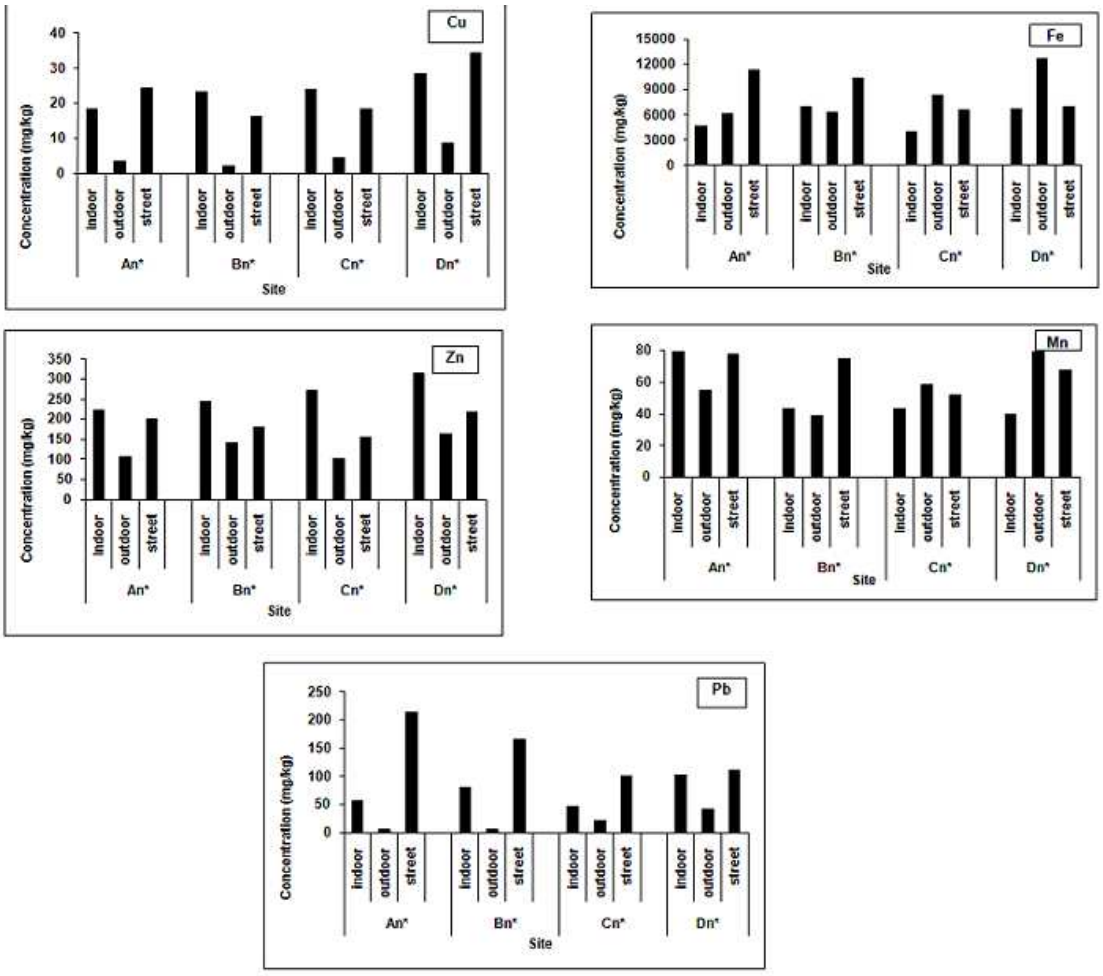

FIG. 2: The average total concentrations (mg/kg) of heavy metals in all sites, An: (A1 to A10), Bn: (B1 to B10), Cn: (C1 to C10) and Dn: (D1 to D8), for street, outdoor and indoor dust samples.

For outdoor dust samples, Dn showed the highest levels for all heavy metals due to the high traffic density with a bus station [33].

For indoor dusts, Dn has high contents for Cu, Zn and Pb due to high traffic density and bus stations. While for Mn; An showed the highest levels due to high corrosion of automobile bodies since the majority of KGs in An sites are located along the major streets.

Enrichment factor for street dust

The enrichment factor (EF) for heavy metals gives an indication of the degree of pollution of the dust by these metals in Amman city. Iron was used as a reference element because it is a crust – dominated element [21]. The enrichment factor was computed in accordance with the formula reported by Mason [34].

$$EF = \frac{[\ C_x / C_{Fe}\ ]_{dust}}{[\ C_x / C_{Fe}\ ]_{crust}}$$

where:

$[\ C_x / C_{Fe}\ ]_{dust}$: the ratio of the concentration of the metal being determined (C_x) to that of Fe (C_{Fe}) in the dust samples.

$[\ C_x / C_{Fe}\ ]_{crust}$: the ratio of the concentration of metal X to that of Fe in the earth crust.

Enrichment factors less than 2.0 are not considered significant, because such small enrichment may arise from differences in the composition of local soil material and reference soil used in EF calculations. The three contaminated categories recognized were based on the enrichment factor values as: ($EF < 10$) less enriched, ($10 < EF < 100$) intermediately enriched and ($EF > 100$) highly enriched. Enrichment factor values for heavy metals in all sites for street, outdoor and indoor dust samples are summarized in Table 4.

TABLE 4. Enrichment factor values for heavy metals in street dust samples.

	Cu	Zn	Pb	Mn
Indoor	0.48	11.52	7.30	0.53
Outdoor	3.99	35.35	48.55	0.37
Street	2.60	16.01	63.44	0.42

The results indicated that the highest enrichment factors observed in dust samples were for Pb and Zn due to the presence of the anthropogenic sources of these metals, such as traffic in street and outdoor sites. For indoor samples, the transfer of these metals from outside, in addition to some sources present inside, might be the reasons of the high EF. Mn was less enriched in all samples which is an indication of crustal contributions [35].

Statistical analysis

Pearson correlation coefficient between anions and cations was computed in all sites (indoor, outdoor and street) to measure the degree of correlation between the ion concentrations. High correlation coefficients were found between (Cl^- vs. Na^+), (K^+ vs. Mg^{2+}), (NH_4^+ vs. K^+), (F^- vs. K^+), (Cl^- vs. K^+), (NO_3^- vs.Ca^{2+}), (Cl^- vs. F^-) and (Br^- vs. F^-) with correlations of (0.69, 0.65, 0.60, 0.64, 0.51, 0.74, 0.66 and 0.53), respectively. This may suggest that each pair of ions has the same source/s, e.g. in this study high levels of Cl^- and Na^+ were found in indoor dusts, which may be due to their same source which is: table salt. While for street dusts, the high levels of ions may be due to high dissolved salt deposited on the surface from the vaporization of water.

Pearson correlation between heavy metals in each site (indoor, outdoor and street) dusts was calculated, which showed that there are no correlation between heavy metals in indoor dusts, where for outdoor dusts there are high correlations between (Zn vs. Pb) and (Fe vs. Pb) as follows: (0.62) and (0.51), respectively. This may suggest that these pairs have the same source which is: automobiles [36]. The street dusts have also high correlations between (Fe vs. Pb) and (Pb vs. Cu) as follows: (0.45) and (0.47), which indicates that automobiles are the common source of these heavy metals [36].

Also, Pearson correlation coefficients were calculated between heavy metal contents of sites (indoor vs. outdoor), (indoor vs. street) and (outdoor vs. street), which showed that there were correlations between Mn and Mn in indoor and each of street (0.38) and outdoor dusts (0.38), also between Pb indoor and outdoor dusts (0.41). These results may be due to the common source of these heavy metals in streets, which is automobiles [32] that may influence the environment of indoor and outdoor KGs.

(One-way ANOVA) followed by (Post Hoc Test, Tukey HSD) were used to study the relation between the types of sites (indoor, outdoor and street dusts) of KGs and heavy metal contents. It was shown that there were differences between heavy metal contents with changing the type of site, except for Mn.

The relation between the student's number inside KGs and heavy metal contents was determined by T-Test. No relation was found between Cu, Pb, Zn and Mn concentrations with number of students inside KGs: 0.416, 0.063, 0.611 and 0.729. Where for Fe concentrations, there is a significant relation between Fe levels and number of students inside KGs (0.001).

Conclusions

Based on the results of the current study, the following conclusions were obtained:

1- Average pH values for street, outdoor and indoor dust samples were neutral to sub-alkaline due to the type of soil in Jordan which is calcareous.

2- Moisture contents for street, outdoor and indoor dust samples were lower due to the evaporation rate that decreases the moisture content.

3- Organic matter was found in a high value for indoor dust samples due to high organic contamination.

4- For cation analysis, high levels of Ca^{2+} were found for outdoor and street dust samples due to the calcareous nature of soil in Jordan. For indoor dust, Na^{+} had the highest levels due to table salt and food stuff which contain high contents of Na^{+}.

5- For anion analysis, SO_4^{2-} had the highest levels in outdoor and street dust samples due to traffic emissions. Where for indoor dust samples, Cl^{-} had the highest level due to table salt.

References

[1] http://www.caobisco.com/english/pdf/Metals.pdf (1996).

[2] Duffus, J.H., Pure Appl. Chem., 74 (2002) 793.

[3] Jaradat, Q.M., Masadeh, A., Zaitoun, M.A. and Maitah, B.M., Soil & Sediment Contamination, 14 (2005) 449.

[4] Harte, J., Hldren, C., Schneider, R. and Shirley, C., "Toxic A to Z", 1st, (University of California Press, Oxford, England, 103, 1991), 244-246, 333-335.

[5] Moore, J.W. and Ramamoorthy S., "Heavy Metal in Natural Waters", 1st, (Springer-Verlag, New York, USA, 29, 1984) 78.

[6] Brady, J.E., "General Chemistry", 3ed, (John Willey & Sons, New York, 1982) 646.

[7] Lee, P-K., Yu, Y-H., Yun, S-T. and Mayer, B., Chemosphere, 60 (2005) 672.

[8] Abulude, F.O., Electron. J. Environ. Agric. Food Chem. 4(2) (2005) 863.

[9] Al-Khasman, O.A., Atmos. Environ., 38 (2004) 6803.

[10] Mahajan, R.K. and Walia, T.P.S., J. Health Allied Scs., 4 (2005) 1.

[11] Komarniciki, G.J.K., Environ. Pollut., 136 (2005) 47.

[12] Chlopicka, J., Zagrodzki, P., Zachwieja, Z., Krośniak, M. and Folta, M., Analyst, 120 (1995) 943.

[13] Pérez Cid, B., Lavilla, I. and Bendicho, C., Analyst, 121 (1996) 1479.

[14] Jha, S.K., Acharya, R.N., Reddy, A.V.R., Manohar, S.B., Nair, A.G.C., Chavan, S.B. and Sadssivan, S., J. Environ. Monit., 4 (2002) 131.

[15] Momani, K.A., Jiries, A.G. and Jaradat, Q.M., Turk. J. Chem., 24 (2000) 231.

[16] Nowak, B., Analyst, 120 (1995) 747.

[17] Dauwe, T., Janessens, E., Bervoets, L., Blust, R. and Eens, M., Environ. Pollut., 131 (2004) 373.

[18] Elik, A., Communic. Soil Sci., Plant Anal., 34 (2003) 145.

[19] Sukreeyapongse, O., Holm, P.E., Strobel, B.W., Panichsakpatana, S., Magid, J. and Hanson, H.C.B., J. Environ. Qual., 31 (2002) 1901.

[20] Murphy, A.P., Coudert, M. and Barker, J., J. Environ. Monit., 2 (2000) 621.

[21] Tokalioglu, Ş. and Karatal, Ş., Turk. J. Chem., 27 (2003) 333.

[22] Sipos, P., Németh, T. and Mohai, I., Environ. Geochem. Health, 27 (2005) 1.

[23] Hlavay, J., Polyák, K., Molnar, Á. and Mészáros, E., Analyst, 123 (1998) 859.

[24] Chuan, M.C., Shu, G.Y. and Liu, J.C., Water, Air, Soil Pollut., 90 (2004) 543.

[25] Jaradat, Q.M. and Momani, K.A., Turk. J. Chem., 23 (1999) 209.

[26] Al-Momani, I.F., Atmos. Environ., 37 (2003) 4507.

[27] Jaradat, Q.M., Momani, K.A. and Jiries, A.G., Turk. J. Chem., 21 (1997) 92.

[28] Momani, K.M., Jaradat, Q.M., Jbarah, A.Q., Omari, A.A. and Momani, I.F., J. Environ. Monit., 4 (2002) 900.

[29] Jaradat, Q.M., Momani, K.A., Jbarah, A.Q. and Massadeh, A., Environmental Research, 96 (2004) 139.

[30] Godin, P.M., Environ. Pollut., (series B), 10 (1985) 97.

[31] Arslan, H., Soil. Environ. Sci., 19(3) (2001) 439.

[32] Divrikli, U., Soylak, M., Elci, L. and Dogan, M., Soil. Environ. Sci., 21(2) (2003) 351.

[33] Goodarzi, F., Sanei, H., Lbonte, M. and Duncan, W.F., J. Environ. Monit., 4 (2002) 400.

[34] Mason, B.J., "Introduction to Geochemistry", 3rd Ed, (John Wiley, New York, 1966).

[35] Momani, I.F., Contamin., 16 (2007) 1.

[36] Tüzen, M., Soil. Environ. Sc., 21(3) (2003) 513.

Authors Index

Subject Index

طرائق البحث (التجريبية / النظرية): يجب أن تكون هذه الطرائق موضحة بتفصيل كاف لإتاحة إعادة إجرائها بكفاءة، ولكن باختصار مناسب، حتى لا تكون تكرارا للطرائق المنشورة سابقا.

النتائج: يستحسن عرض النتائج على صورة جداول وأشكال حيثما أمكن، مع شرح قليل في النص ومن دون مناقشة تفصيلية.

المناقشة: يجب أن تكون موجزة وتركز على تفسير النتائج.

الاستنتاج: يجب أن يكون وصفا موجزا لأهم ما توصلت إليه الدراسة ولا يزيد عن صفحة مطبوعة واحدة.

الشكر والعرفان: الشكر والإشارة إلى مصدر المنح والدعم المالي يكتبان في فقرة واحدة تسبق المراجع مباشرة.

المراجع: يجب طباعة المراجع بأسطر مزدوجة ومرقمة حسب تسلسلها في النص. وتكتب المراجع في النص بين قوسين مربعين. ويتم اعتماد اختصارات الدوريات حسب نظام Wordlist of Scientific Reviewers.

الجداول: تعطى الجداول أرقاما متسلسلة يشار إليها في النص. ويجب طباعة كل جدول على صفحة منفصلة مع عنوان فوق الجدول. أما الحواشي التفسيرية، التي يشار إليها بحرف فوقي، فتكتب أسفل الجدول.

الرسوم التوضيحية: يتم ترقيم الأشكال والرسومات والرسومات البيانية (المخططات) والصور، بصورة متسلسلة كما وردت في النص.

تقبل الرسوم التوضيحية المستخرجة من الحاسوب والصور الرقمية ذات النوعية الجيدة بالأبيض والأسود، على ان تكون أصيلة وليست نسخة عنها، وكل منها على ورقة منفصلة ومعرفة برقمها بالمقابل. ويجب تزويد المجلة بالرسومات بحجمها الأصلي بحيث لا تحتاج إلى معالجة لاحقة، وألا تقل الحروف عن الحجم 8 من نوع Times New Roman، وألا تقل سماكة الخطوط عن 0.5 وبكثافة متجانسة. ويجب إزالة جميع الألوان من الرسومات ما عدا تلك التي ستنشر ملونة. وفي حالة إرسال الرسومات بصورة رقمية، يجب أن تتوافق مع متطلبات الحد الأدنى من التمايز (1200 dpi Resolution) لرسومات الأبيض والأسود الخطية، و 600 dpi للرسومات باللون الرمادي، و300 dpi للرسومات الملونة. ويجب تخزين جميع ملفات الرسومات على شكل (jpg)، وأن ترسل الرسوم التوضيحية بالحجم الفعلي الذي سيظهر في المجلة. وسواء أرسل المخطوط بالبريد أو عن طريق الشبكة (Online)، يجب أرسال نسخة ورقية أصلية ذات نوعية جيدة للرسومات التوضيحية.

مواد إضافية: تشجع المجلة الباحثين على إرفاق جميع المواد الإضافية التي يمكن أن تسهل عملية التحكيم. وتشمل المواد الإضافية أي اشتقاقات رياضية مفصلة لا تظهر في المخطوط.

المخطوط المنقح (المعدّل) والأقراص المدمجة: بعد قبول البحث للنشر وإجراء جميع التعديلات المطلوبة، فعلى الباحثين تقديم نسخة أصلية ونسخة أخرى مطابقة للأصلية مطبوعة بأسطر مزدوجة، وكذلك تقديم نسخة إلكترونية تحتوي على المخطوط كاملا مكتوبا على Microsoft Word for Windows 2000 أو ما هو استجد منه. ويجب إرفاق الأشكال الأصلية مع المخطوط النهائي المعدل حتى لو تم تقديم الأشكال إلكترونيا. وتخزن جميع ملفات الرسومات على شكل (jpg)، وتقدم جميع الرسومات التوضيحية بالحجم الحقيقي الذي ستظهر به في المجلة. ويجب إرفاق قائمة ببرامج الحاسوب التي استعملت في كتابة النص، وأسماء الملفات على قرص مدمج، حيث يعلَم القرص بالاسم الأخير للباحث، وبالرقم المرجعي للمخطوط للمراسلة، وعنوان المقالة، والتاريخ. ويحفظ في مغلف واقٍ.

الفهرسة: تقوم المجلة الأردنية للفيزياء بالإجراءات اللازمة لفهرستها وتلخيصها في جميع الخدمات الدولية المعنية.

حقوق الطبع

يُشَكِّل تقديم مخطوط البحث للمجلة اعترافاً صريحاً من الباحثين بأنّ مخطوط البحث لم يُنْشَر ولم يُقَدَّم للنشر لدى أي جهَة أخرى كانت وبأي صيغة ورقية أو إلكترونية أو غيرها. ويُشترط على الباحثين ملء أنموذج يَنُصُّ على نقْل حقوق الطبع لتُصبح ملكاً لجامعة اليرموك قبل الموافقة على نشر المخطوط. ويقوم رئيس التحرير بتزويد الباحثين بإنموذج نقل حقوق الطبع مع النسخة المُرْسَلَة للتنقيح. كما ويُمنع إعادة إنتاج أيِّ جزء من الأعمال المنشورة في المجلّة من دون إذن خَطِّيٍّ مُسْبَق من رئيس التحرير.

إخلاء المسؤولية

إن ما ورد في هذه المجلة يعبر عن آراء المؤلفين، ولا يعكس بالضرورة آراء هيئة التحرير أو الجامعة أو سياسة اللجنة العليا للبحث العلمي أو وزارة التعليم العالي والبحث العلمي. ولا يتحمل ناشر المجلة أي تبعات مادية أو معنوية أو مسؤوليات عن استعمال المعلومات المنشورة في المجلة أو سوء استعمالها.

معلومات عامة

المجلة الأردنية للفيزياء هي مجلة بحوث علميّة عالمية مُحكمة تصدر عن اللجنة العليا للبحث العلمي، وزارة التعليم العالي والبحث العلمي، عمان، الأردن. وتقوم بنشر المجلة عمادة البحث العلمي والدراسات العليا في جامعة اليرموك، إربد، الأردن. وتنشر البحوث العلمية الأصيلة، إضافة إلى المراسلات القصيرة Short Communications، والملاحظات الفنية Technical Notes، والمقالات الخاصّة Feature Articles، ومقالات المراجعة Review Articles، في مجالات الفيزياء النظرية والتجريبية، باللغتين العربية والإنجليزية.

تقديم مخطوط البحث

تُرسَل نسخة أصلية وثلاث نسخ من المخطوط، مُرْفَقَةً برسالة تغطية من جانب الباحث المسؤول عن المراسلات، إلى رئيس التحرير:

أ.د. ابراهيم أبو الجرايش،
رئيس التحرير، المجلة الأردنية للفيزياء،
عمادة البحث العلمي والدراسات العليا،
جامعة اليرموك، إربد، الأردن.
هاتف : 111 11 72 2 962 00 / فرعي: 2075
فاكس : 121 11 72 2 962 00
بريد إلكتروني : jjp@yu.edu.jo

تقديم المخطوطات إلكترونيًا: اتبع التعليمات في موقع المجلة على الشبكة العنكبوتية.

ويجري تحكيمُ البحوثِ الأصيلة والمراسلات القصيرة والملاحظات الفنية من جانب مُحكّمين اثنين في الأقل من ذوي الاختصاص والخبرة. وتُشَجِّع المجلة الباحثين على اقتراح أسماء المحكمين. أما نشر المقالات الخاصّة في المجالات الفيزيائية النَشِطَة، فيتم بدعوة من هيئة التحرير، ويُشار إليها كذلك عند النشر. ويُطْلَب من كاتب المقال الخاص تقديم تقرير واضح يتسم بالدقة والإيجاز عن مجال البحث تمهيداً للمقال. وتنشر المجلةُ أيضاً مقالات المراجعة في الحقول الفيزيائية النشطة سريعة التغيُّر، وتشَجِّع كاتبي مقالات المراجعة أو مُستَكتبيها على إرسال مقترحٍ من صفحتين إلى رئيس التحرير. ويُرْفَق مع البحث المكتوب باللغة العربية ملخص (Abstract) وكلمات دالة (Keywords) باللغة الإنجليزية.

ترتيب مخطوط البحث

يجب أن تتم طباعة مخطوط البحث ببنط 12 نوعه Times New Roman، وبسطر مزدوج، على وجه واحد من ورق A4 (21.6 × 27.9 سم) مع حواشي 3.71 سم ، باستخدام معالج كلمات ميكروسوفت وورد 2000 أو ما اسْتَجَد منه. ويجري تنظيم أجزاء المخطوط وفق الترتيب التالي: صفحة العنوان، الملخص، رموز التصنيف (PACS)، المقدّمة، طرق البحث، النتائج، المناقشة، الخلاصة، الشكر والعرفان، المراجع، الجداول، قائمة بدليل الأشكال والصور والإيضاحات، ثَمَّ الأشكال والصور والإيضاحات. وتُكْتَب العناوين الرئيسة بخطٍ **غامق**، بينما تُكْتَب العناوين الفرعية بخطٍ *مائل*.

صفحة العنوان: وتشمل عنوان المقالة، أسماء الباحثين الكاملة وعناوين العمل كاملة. ويكتب الباحث المسؤول عن المراسلات اسمه مشارا إليه بنجمة، والبريد الإلكتروني الخاص به. ويجب أن يكون عنوان المقالة موجزا وواضحا ومعبرا عن فحوى (محتوى) المخطوط، وذلك لأهمية هذا العنوان لأغراض استرجاع المعلومات.

الملخص: المطلوب كتابة فقرة واحدة لا تزيد على مائتي كلمة، موضحة هدف البحث، والمنهج المتبع فيه والنتائج وأهم ما توصل إليه الباحثون.

الكلمات الدالة: يجب أن يلي الملخص قائمة من 4-6 كلمات دالة تعبر عن المحتوى الدقيق للمخطوط لأغراض الفهرسة.

PACS: يجب إرفاق الرموز التصنيفية، وهي متوافرة في الموقع http://www.aip.org/pacs/pacs06/pacs06-toc.html.

المقدمة: يجب أن توضّح الهدف من الدراسة وعلاقتها بالأعمال السابقة في المجال، لا أن تكون مراجعة مكثفة لما نشر (لا تزيد المقدمة عن صفحة ونصف الصفحة مطبوعة).

Subscription Form

Jordan Journal of PHYSICS

An International Peer-Reviewed Research Journal

Published by the Deanship of Research & Graduate Studies, Yarmouk University, Irbid, Jordan

Name: ..... الأسم:

Specialty: ..... التخصص:

Address: ..... العنوان:

P.O. Box: ..... صندوق البريد:

City & Postal Code: ..... المدينة/الرمز البريدي:

Country: ..... القطر:

Phone: ..... رقم الهاتف:

Fax No: ..... رقم الفاكس:

E-mail: ..... البريد الإلكتروني:

No. of Subscription: ..... عدد الإشتراكات:

Method of Payment: ..... طريقة الدفع:

Amount Enclosed: ..... المبلغ المرفق:

Signature: ..... التوقيع:

Cheques should be paid to Deanship of Research and Graduate Studies - Yarmouk University.

I would like to subscribe to the Journal
For

- ☐ One Year
- ☐ Two Years
- ☐ Three Years

One Year Subscription Rates

	Inside Jordan	Outside Jordan
Individuals	JD 8	€ 40
Students	JD 4	€ 20
Institutions	JD 12	€ 60

Correspondence

Subscriptions and Sales:

Prof. Ibrahim O. Abu-AlJarayesh
Deanship of Research and Graduate Studies
Yarmouk University
Irbid – Jordan
Telephone: 00 962 2 711111 Ext. 2075
Fax No.: 00 962 2 7211121

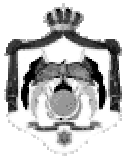

المملكة الأردنية الهاشمية

جامعة اليرموك

المجلة الأردنية

للفيزياء

مجلة بحوث علمية عالمية محكّمة

العدد الخاص

المجلد (5)، العدد (1)، 2012م / 1433هـ

المجلة الأردنية

للفيزياء

مجلة بحوث علمية عالمية محكّمة

المجلد (5)، العدد (1)، 2012م / 1433هـ

المجلة الأردنية للفيزياء: مجلة بحوث علمية عالمية محكّمة أسستها اللجنة العليا للبحث العلمي، وزارة التعليم العالي والبحث العلمي، الأردن، وتصدر عن عمادة البحث العلمي والدراسات العليا، جامعة اليرموك، إربد، الأردن.

ترسل البحوث إلى العنوان التالي:

الأستاذ الدكتور إبراهيم عثمان أبو الجرايش
رئيس تحرير المجلة الأردنية للفيزياء
عمادة البحث العلمي والدراسات العليا، جامعة اليرموك
إربد ، الأردن
هاتف 7211111 2 962 00 **فرعي** 2075

E-mail: *jjp@yu.edu.jo*
Website: *http://Journals.yu.edu.jo/jjp*